Technische Universität München
TUM School of Natural Sciences

Synthesis, Characterization and Catalytic Performance of Copper-Based Catalysts in the Butyraldehyde Hydrogenation

Max Johannes Hiller

Vollständiger Abdruck der von der TUM School of Natural Sciences der Technischen Universität München zur Erlangung eines

Doktors der Naturwissenschaften (Dr. rer. nat.)

genehmigten Dissertation.

Vorsitz: Priv.-Doz. Dr. Friedrich Esch

Prüfer*innen der Dissertation:

1. Prof. Dr. Klaus Köhler
2. Hon.-Prof. Dr. Richard W. Fischer

Die Dissertation wurde am 03.04.2023 bei der Technischen Universität München eingereicht und durch die TUM School of Natural Sciences am 12.05.2023 angenommen.

“And when I close my eyes tonight
To symphonies of blinding light
God, bless us everyone
We're a broken people living under loaded gun”

— Linkin Park

Die vorliegende Arbeit entstand im Zeitraum vom 15.07.2019 bis 31.03.2023 an der Fakultät für Chemie und am Zentralinstitut für Katalyseforschung (CRC) der Technischen Universität München.

Mein besonderer Dank gilt meinem akademischen Lehrer

Prof. Dr. Klaus Köhler

für die hervorragende Betreuung dieser Arbeit,
seine uneingeschränkte Unterstützung,
sein Vertrauen und die damit verbundenen Freiräume in der
Gestaltung und Bearbeitung der Aufgabenstellung,
sowie sein großes Interesse am Gelingen der Arbeit.

DANKSAGUNG

Bei meinem akademischen Lehrer **Prof. Dr. Klaus Köhler** möchte ich mich für die Aufnahme in seinen Arbeitskreis sowie die sich hieraus ableitende Möglichkeit, meine Dissertation unter seiner Beaufsichtigung anzufertigen, bedanken. Ich möchte mich für die große wissenschaftliche Freiheit, die ergiebigen Diskussionen sowie das mir entgegengebrachte Vertrauen bedanken. Auch für die stets angenehme und humorvolle Art möchte ich mich bedanken.

Bei **Prof. Dr. Richard W. Fischer** möchte ich mich für die Begutachtung meiner Arbeit bedanken und darüber hinaus auch für die Betreuung der Industriekooperation mit der Clariant Produkte (Deutschland) GmbH im Rahmen des Forschungsprojekts Hydrotech. Zudem danke ich Clariant für die finanzielle Unterstützung des Forschungsprojekts.

Bei allen Kollegen des Industriepartners Clariant möchte ich mich bedanken für die angenehme Zusammenarbeit, die fruchtvollen Diskussionen, die Durchführung der regelmäßigen Meetings sowie die Bereitschaft zu problemlösungsorientiertem Handeln. Ich möchte insbesondere erwähnen: **Dr. Christoph Dörfelt, Dr. Huiquing Song, Dr. Frank Grossmann, Dr. Roman Bobka** und **Dr. Andreas Reitzmann**.

Bei all meinen ehemaligen sowie aktuellen Kollegen möchte ich mich für die stets angenehme Zusammenarbeit, den (nicht-) wissenschaftlichen Austausch sowie die wunderbare gemeinsame Zeit bedanken. Gedanke sei **Dr. Patrick Bretzler, Dr. Tobias Bruhm, Dr. Oliver Thomys, Andrea Abram, Dr. Hannah Augenstein, Franz Bannert, Lea Kopietz, Jasper (Lingdi) Kong, Patrick Schlachta** und **Jinjin Tie**.

Ein besonderer Dank gilt hierbei **Dr. Oliver Thomys** für die Hilfe mit allen apparativen Problemen, nützliche Ideen und Tipps hinsichtlich der Katalysatorpräparation sowie als ausgezeichneter Ansprechpartner bei jeglichen Fragen aus dem Gebiet der anorganischen Chemie. Auch wenn wir des Öfteren nicht einer Meinung waren, möchte ich mich dafür umso mehr für die vielen aufreibenden, aber auch inspirierenden Diskussionen bedanken. Bei **Dr. Patrick Bretzler** möchte ich mich für jegliche Hilfe zu instrumenteller Analytik bedanken, ferner aber auch für mannigfaltige Unterstützung auch über die Chemie hinaus sowohl während als auch nach unserer gemeinsamen Zeit am Arbeitskreis Köhler. Des Weiteren möchte ich **Dr. Thomas Burger** danken für die hilfsbereite Unterstützung bei Fragen rund um Geräte in der Zentralanalytik. Ein ganz besonderer! Dank gilt **Andrea Abram** für die Messung unzähliger ICP-Proben (und die dadurch nötige stetige Wartung des Gerätes), für die Durchführung der Katalysatortests in der Flüssigphase sowie als Ansprechpartner bei IT-Problemen jeglicher Art. Zudem bedanke ich mich für die großartige Hilfe bei der Erstellung und für das Korrekturlesen des Manuskripts. Gedankt sei auch die stets akkurate Meldung des Restkaffee- sowie Milchbestandes. **Franz Bannert** danke ich für die Hilfe beim Erstellen von PI-Diagrammen.

Des Weiteren möchte ich mich bei all meinen Studierenden bedanken, die mit ihren Abschluss- sowie Forschungsarbeiten zu dieser Arbeit beigetragen haben: **Tobias Weng, Simon Nickl,**

Alexander Spears, Lisa Kreimer, Marcel Klotz, Tijana Pecirep und **Isabel Jüngling**. Insbesondere möchte ich hierbei **Lisa Kreimer** danken die durch Ihre unermüdliche Ausdauer und akribische Arbeit einen Meilenstein in der Inbetriebnahme der ILS-601 Testanlage gesetzt hat. **Isabel Jüngling** möchte ich danken für den gewissenhaften und akkuraten Umbau der Einzeltestanlage sowie die sich hieraus ermöglichten Charakterisierungen von gebrauchten Katalysatoren.

Darüber hinaus möchte ich einigen ganz besonderen Kollegen der (erweiterten) Heizgruppe danken, über die Jahre sind hier bei unzähligen Runden am Kicker, an der Tischtennisplatte oder auf dem Badmintonfeld wunderbare Freundschaften entstanden. Bedanken möchte ich mich bei **Martin Tschurl** (alias Tschurli), **Tobias Hinke** (alias Hassan III.), **Kevin Bertrang** (alias Bert), **Carla Courtois** (alias Kurz), **Flora Siegele** (alias Flörlie) und **Sebastian Pios** (alias Grubi bzw. Grubenklaus).

Zudem sei Frau **Renate Schuhbauer-Gerl** gedankt für die Hilfe bei allerlei „bürokratischer Hürden“.

Bei **Ulrike Ammari, Petra Ankenbauer,** und **Bircan Dilki** möchte ich mich für die Durchführung von Elementaranalysen bedanken. **Dr. Eliza Gemel** möchte ich danken für die Instandhaltung der Geräte in der Zentralanalytik im CRC sowie die große Freiheit hinsichtlich verschiedener „spezieller“ Messmethoden sowie Umbauten an Geräten. Bei **Jürgen Kudermann** möchte ich mich für Durchführung der GC-MS Messungen bedanken.

Dem kompletten Team der AC-Vorbereitung, **Richard Wetzel, Sara Garofalo, Thomas Miller** und **Tobias Kubo** möchte ich danken für den schnellen und unkomplizierten Verleih und Austausch von Werkzeug und Chemikalien und insbesondere für die hilfsbereite und oft nötige Unterstützung im Grundpraktikum sowie der kompetenten Durchführung des Praktikums.

Ferner möchte ich allen Mitarbeitern der Feinmechanik sowie der E-Werkstatt für die (schnelle) und stets gewissenhafte Ausführungen von Reparaturen, Modifikationen und Neugestaltungen jeglicher Art danken. Namentlich danken möchte ich **Patrick Gieb** und **Marc Schönberger**.

Den Kollegen von *Swagelok* möchte ich danken für die kompetente Beratung hinsichtlich Anlagenbauteilen aller Art sowie die schnelle Auftragsabwicklung. Bei den Kollegen von *ILS* (allen Voran **Michael Pagels**) sowie *Pro Control* möchte ich mich für die Unterstützung bei der Inbetriebnahme der Testanlage ILS-601 bedanken.

Bei einer ganz besonderen Freundin, **Jennifer Keller**, möchte ich mich für die herzliche Unterstützung über die letzten Jahre danken. Du trägst einen Anteil zu dieser Arbeit bei.

Meinen Eltern **Eva Breindl-Hiller** und **Eugen Hiller** möchte ich für die finanzielle und persönliche Unterstützung über die Jahre des Studiums und während der Promotion danken.

Zuletzt möchte ich mich noch bei meiner Partnerin **Dr. Elisabeth Groß** für die tatkräftige Unterstützung während der Promotion sowie für die gemeinsame Zeit neben der Promotion danken. Ohne dich hätte diese Arbeit nicht so gelingen können. Ich blicke gespannt und mit freudiger Erwartung auf den nächsten gemeinsamen Lebensabschnitt mit dir.

ABSTRACT

Solid copper-metal oxide catalysts are widely used in organic hydrogenation reactions. This thesis investigates copper catalysts used for the hydrogenation of butyraldehyde. Copper-zinc oxide, copper-aluminum oxide and copper aluminate spinel catalysts are synthesized by co-precipitation, thermal treatment and reductive activation. Structure-activity relationships are gained by detailed characterization of these catalysts including *in situ* techniques relating these findings to the catalytic performance in the butyraldehyde hydrogenation. A copper loading between 20 to 30 % and a precipitation pH between 7 to 9 are beneficial to obtain highly active catalysts with high copper dispersion. Aurichalcite is the main precursor phase of these catalysts. The direct reductive activation of the precursor and of an oxycarbonate intermediate is possible and results in increased activity. A design of experiments approach revealed that fast precipitation and short aging time are beneficial. Copper-zinc oxide catalysts are less long-term stable in gas-phase hydrogenation in comparison to copper aluminate spinel catalysts. The deactivation is caused by the formation of inactive zinc(II)-butyrate species, which is induced by the strong adsorption of butyric acid impurities at zinc sites. Copper aluminate spinel catalysts are less selective than copper-zinc oxide catalysts in liquid-phase hydrogenation due to acid-catalyzed side reactions.

KURZZUSAMMENFASSUNG

Kupfer-Metalloxid-Feststoffkatalysatoren werden in vielfältiger Form für organische Hydrierungsreaktionen verwendet. In dieser Arbeit werden Kupferkatalysatoren für die Hydrierung von Butyraldehyd untersucht. Kupfer-Zinkoxid- und Kupfer-Aluminiumoxid- sowie Kupferaluminat-Spinell-Katalysatoren werden durch Kofällung, thermische Behandlung und reduktive Aktivierung synthetisiert. Struktur-Aktivitäts-Beziehungen werden durch detaillierte Charakterisierung dieser Katalysatoren einschließlich *in-situ*-Techniken ermittelt und mit der katalytischen Aktivität bei der Hydrierung von Butyraldehyd verglichen. Eine Kupferbeladung zwischen 20 und 30 % und ein Fällungs-pH-Wert zwischen 7 und 9 sind vorteilhaft, um hochaktive Katalysatoren mit einer hohen Kupferdispersion zu erhalten. Aurichalcit ist die wichtigste Vorläuferphase dieser Katalysatoren. Die direkte reduktive Aktivierung des Vorläufers und auch des Oxycarbonat-Intermediates ist möglich und führt zu einer erhöhten Hydrieraktivität. Eine statistische Versuchsplanung ergab, dass schnelle Ausfällung und kurze Alterung von Vorteil sind. Kupfer-Zinkoxid-Katalysatoren sind bei der Gasphasenhydrierung im Vergleich zu Kupferaluminatspinell-Katalysatoren weniger langzeitstabil. Die Desaktivierung wird durch die Bildung inaktiver Zink(II)-butyrat-Spezies verursacht, die durch starke Adsorption von Buttersäureverunreinigungen an Zink-Plätzen unterstützt wird. Kupferaluminatspinell-Katalysatoren sind bei der Flüssigphasenhydrierung weniger selektiv als Kupfer-Zinkoxid Katalysatoren, da sie säurekatalysierte Nebenreaktionen verursachen.

TABLE OF CONTENTS

LIST OF ABBREVIATIONS

a.u.	arbitrary uni	
AU	Aurichalcite ($(Cu,Zn)_5(CO_3)_2(OH)_6$)	
BET	Brunauer-Emmett-Teller	
BJH	Barrett-Joyner-Halenda	
CHNS	Carbon-hhydrogen-nitrogen-sulfur (residual gas analysis)	
DoE	Design of experiments	
EA	elemental analysis	
GC	Gas chromatography	
GE	Gerhardite ($Cu_2(NO_3(OH)_3$)	
GHSV	Gas hourly space velocity	h^{-1}
HPLC	High-performance liquid chromatography	
HT	High-temperature	
HZ	Hydrozincite ($Zn_5(CO_3)_2(OH)_6$)	
ICDD	International Centre for Diffraction Data	
ICP	Inductively coupled plasma	
ILS	Integrated lab solutions	
IR	Infrared (spectroscopy)	
KPG	Core drawn precision glassware (German Kerngezogenes Präzisions-Glasgerät)	
LHSV	Liquid hourly space velocity	
m/z	Mass to charge ratio	
MS	Mass spectrometry	
OES	Optical emission spectroscopy	
pH	potential of hydrogen	
PI	Pipe and instrumentation (diagram)	
REACH	Registration, Evaluation, Authorization and Restriction of Chemicals	
RT	Room temperature	
RWGS	reverse water-gas shift reaction	
SMSI	Strong metal–support interaction	
STU	Single-test unit	
t	Time	s
T	Temperature	K
TCD	Thermal conductivity detector	
TGA	Thermogravimetric analysis	
TPD	Temperature-programmed desorption	
TPR	Temperature-programmed reduction	
TUM	Technical University of Munich	

UHV	Ultra-high vacuum	
wt.-%	Weight percentage	%
XPS	X-ray photoelectron spectroscopy	
XRD	X-Ray diffraction	
(Zn-)MA	(Zinc-)Malachite ($(Cu,Zn)_2(OH)_2CO_3$)	
ΔG	Gibbs free energy	$Jmol^{-1}$
ΔH	Reaction enthalpy	$Jmol^{-1}$

1

Introduction and Objectives

1.1 Catalysis and hydrogenation reactions

Catalysis is a process in which a substance, called a catalyst, increases the rate of a chemical reaction without itself being consumed in the reaction. In general, this is done by lowering the activation energy needed for the reaction. The catalyst does not undergo a chemical change itself.[1] During the reaction, the catalyst reacts with one or more reactants and forms an active intermediate which subsequently reacts to the product. By this, the catalyst is released and can undergo the next catalytic cycle. Catalysts work by providing an alternative pathway for the reaction with a lower activation energy. This lower activation energy allows that the reaction occurs faster.[2-3] Around 90 % of all commercially produced chemical products involve the use of a catalyst.[4]

In general, catalysis can be divided in three groups: homogeneous, heterogeneous and biocatalysis. The main differences between these types of catalysis are the nature of the catalyst and the reaction environment. Homogeneous catalysis involves a catalyst that is in the same phase as the reactants. This means that the catalyst and the reactants are either both in the gas-phase or both in a liquid-phase. Mostly, the substrates and the catalyst are in the liquid-phase.[5] A typical example for a homogeneously catalyzed process is the hydroformylation (also called oxo synthesis) to produce aldehydes. This reaction is mostly catalyzed by metal organic cobalt or rhodium complexes (see also chapter 1.4.1).[6-7] Heterogeneous catalysis, on the other hand, involves a catalyst that is in a different phase than the reactants. For example, a solid catalyst may be used in a gas-phase reaction or a liquid-phase reaction. Heterogeneous catalysis is often used in large scale industrial processes because the solid catalysts can be easily separated from the reaction mixture. On the other hand, homogeneously catalyzed reactions are often more selective.[8-10] A typical example for a heterogeneously catalyzed process is the ammonia synthesis over a solid iron catalyst.[11] This process consumes around 1-2 % of the world energy supply.[12] The last group, biocatalysis, involves the use of enzymes as catalysts. Biocatalysis occurs mostly in an aqueous solution and under mild reaction conditions, making it a highly attractive method for organic synthesis. Biocatalysis has become an important tool in the production of pharmaceuticals, fine chemicals, and biofuels.[13-14] Around 80 % of all catalyzed processes are heterogeneously catalyzed while only around 17 % are homogeneously catalyzed. The remaining 3 % belong to the group of biocatalysis.[15]

Metals or metal oxides are the predominant types of heterogeneous catalysts. These catalysts can be divided into two groups, unsupported, bulk catalysts and supported catalysts. While bulk catalysts consist only (mainly) of the active species, supported catalysts are the active species immobilized on an inert support.[16-17] Mainly, temperature stable oxides like alumina, silica or zeolites are used as typical support material.[18] An example for a bulk catalyst is the Ostwald process, the synthesis of nitric oxide over an unsupported platinum-rhodium gauze.[19-20] An example for a supported catalyst is silver supported on alumina for the oxidation of

ethene to ethylene oxide which is subsequently used for the production of plastics like polyester or polyurethan.[21] The advantage of supported catalysts is the increased active surface area due to a higher dispersion of the metal and the cost reduction, especially in the case of noble metal catalysts.[22] Additionally, metal-support interactions can increase the catalytic activity.[23]

The synthesis of heterogeneous catalysts is often a complex process starting with the actual synthesis, which can be inter alia a precipitation, impregnation, or a sol-gel method. Often, a subsequent thermal treatment like a drying or a calcination step is needed. Additionally, in the case of industrially applied catalysts shaping processes (e.g., pelletizing) are often involved. In the case of late transition metals like noble metals or nickel/ copper catalysts a reductive (*in situ*) activation is often needed to form the active species.[5, 16, 24]

The universal reaction mechanism in heterogeneous catalysis involves different steps, starting with a mass transfer, a diffusion, and the adsorption of the substrates to the catalyst. The chemical reaction itself takes place on the surface of the catalyst. Subsequently, the converted substrates desorb from the catalyst surface and are released after diffusion and mass transfer.[3]

Hydrogenation reactions involve the reaction of hydrogen with another compound, often unsaturated organic compounds. In general, two similar reaction types are known: The addition of hydrogen to an organic compound under cleavage of a C-C or C-heteroatom bond is called hydrogenolysis. Thereby, a molecule is split into smaller fragments, or a functional group is removed. The actual hydrogenation reaction is the process of adding hydrogen to a compound, typically an unsaturated organic compound, to produce a more saturated product. Mostly, unsaturated C-C or C-O bonds are hydrogenated (Reaction scheme 1).[25-26]

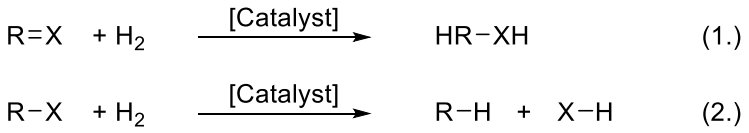

Reaction scheme 1: Simplified reaction of 1.) a hydrogenation and 2.) a hydrogenolyis. X = C, O, N.

Most of the hydrogenation reactions are catalyzed especially by late transition metals like palladium, platinum, or nickel.[27] The more expensive noble metals are often immobilized on a support like alumina or silica.[16] Hydrogenation reactions are often carried out under elevated pressure and/ or temperatures. They are exothermic in the range of ΔH = -100 kJmol^{-1}.[28]

The history of hydrogenation reactions dates to the late 19th century. In 1897, the French chemist Paul Sabatier discovered that hydrogen gas could be used to catalytically reduce organic compounds over nickel, such as carbon monoxide, to form methane.[29-31] Sabatier's work laid the foundation for the development of hydrogenation reactions, which quickly gained importance in the early 20th century. In the early 1900s, the German chemist Fritz Haber discovered that nitrogen can be directly hydrogenated to ammonia, a key component of

fertilizers and explosives.[12, 32] Haber's discovery led to the development of the Haber-Bosch process, which revolutionized the production of fertilizers and played a key role in the growth of agriculture around the world. During the 1920s and 1930s, hydrogenation became an important industrial process to produce a wide range of chemicals and materials, including fuels, plastics, and pharmaceuticals.[33]

Another important milestone in the history of hydrogenation catalysts is the development of the later so-called Adkins catalyst by Homer Burton Adkins in 1931. It is used for the selective hydrogenation of aldehydes to the desired alcohols. The Adkins catalyst is typically prepared by calcining a mixture of copper(II) oxide and chromium(III) oxide at high temperatures (above 700 °C), followed by reduction in hydrogen gas. The resulting catalyst is a finely dispersed copper-chromium species with a high surface area and specific activity.[34-35]

A generally valid mechanism for hydrogenation reactions was proposed by Horiuti and Polanyi in 1934. It explains how molecules are adsorbed onto the surface of a solid catalysts. According to the mechanism, the first step is the physisorption and subsequent the chemisorption of the unsaturated bond containing species. Hydrogen is dissociatively activated on the surface of the catalyst. A first, reversible addition of hydrogen to the unsaturated bond takes place. Subsequently, the second hydrogen atom is transferred, and the adsorbed substrate is hydrogenated and transferred into a more saturated product. After the reaction is complete, the product molecule desorbs from the surface of the catalyst and is released. This process is called desorption. The Horiuti-Polanyi mechanism is a key concept in the field of heterogeneous catalysis.[36]

Heterogeneous catalyzed hydrogenation reactions can be conducted both in the liquid and the gas-phase. In a gas-phase hydrogenation, the reactants are in a gaseous state while the catalyst is a solid state (e.g., as fixed bed). These reactions are typically carried out at increased temperature and pressure and are commonly used in the production of fuels and chemicals, such as ammonia and methanol. In a liquid-phase hydrogenation, the reactants are in a liquid-phase, typically in a solvent such as alcohol or water. Liquid-phase hydrogenation reactions are often carried out at lower temperatures and pressures and are commonly used in the production of fine chemicals, pharmaceuticals, and flavors. Liquid-phase hydrogenation is often preferred for reactions that require precise temperature and pressure control, while gas-phase hydrogenation is often preferred for reactions that require high throughput and rapid reaction rates.[37-38]

1.2 Production of copper and catalytic application

1.2.1 Mining and production of copper

Copper is one of the most widely produced metals in the world. It is commonly used in electrical wiring, plumbing, construction, and as a component in various alloys. Around 17 million tons of copper were produced 2020. The largest producers of copper are Chile, Peru, China, Congo, and the United States.[39]

Copper is obtained by mining and extracting copper ores, especially copper sulfides. Typical ores are chalcopyrite ($CuFeS_2$), bornite (Cu_5FeS_4) and covellite (CuS) which have a copper concentration below 1 % in average. These ores are then refined through a series of processes to obtain pure copper metal which include the sulphuric leaching, smelting and the application of the Cuprion process.[40]

To produce copper, copper matte (Cu_2S) is extracted from chalcopyrite ($CuFeS_2$). For this purpose, the starting material is roasted under addition of coke and iron oxides are slagged by siliceous aggregates (Reaction scheme 2, 1.). This iron silicate slag floats on the copper matte and can thus be easily poured off (2.). The copper matte is further processed into crude copper. Therefore, it is poured in molten form into a converter. In the first stage, the iron sulfide contained in the slag is roasted to iron oxide, which is bound by added quartz to form slag that can be poured off. In a second step, two-thirds of the remaining Cu_2S are oxidized to Cu_2O. The oxide then reacts with the remaining sulfide to form crude copper (3 + 4).[41-42]

Roasting:	$6\ CuFeS_2 + 10\ O_2$	⟶	$3\ Cu_2S + 2\ FeS + 2\ Fe_2O_3 + 7\ SO_2$	(1.)
Smelting:	$Fe_2O_3 + C + SiO_2$	⟶	$Fe_2SiO_4 + CO$	(2.)
Converting:	$2\ Cu_2S + 3\ O_2$	⟶	$2\ Cu_2O + 2\ SO_2$	(3.)
	$Cu_2S + 2\ Cu_2O$	⟶	$6\ Cu + SO_2$	(4.)

Reaction scheme 2: Mineralogical production of crude copper by 1.) roasting, 2.) smelting and 3.+ 4.) converting.

The obtained raw copper has a copper content of around 98%. The remaining 2% contain base metals such as iron and zinc as well as precious metals such as silver and gold. Fine refining of copper is done electrochemically in an anode furnace. During electrolysis, electrolytic copper with a grade above 99.9 % is produced on the cathode. Metals with a lower standard electrode potential than copper undergo oxidation and dissolve as cations, while the more inert noble metals sink as anode slimes.[43]

Copper has a wide range of applications in chemistry, including in electrochemistry, analytical chemistry, and coordination chemistry. Additionally, copper can act as a catalyst in a variety of reactions. This can be explained by the bifunctionality of copper which can act both as Lewis acid and a redox-active center, which allows to participate in a wide range of catalytic reactions. The redox pair Cu(II)/Cu(0) has a standard electrode potential of +0.34 V. This indicates that a reduction of copper oxide by hydrogen is electrochemically possible.[44-45]

1.2.2 Copper in catalytic applications as an alternative to noble metals

As stated, copper is widely used in catalytic applications ranging from oxidation over cross coupling to hydrogenation reactions. One of the most common applications of copper in catalysis is in the (selective) oxidation of alcohols, aldehydes, and other organic compounds to yield e.g., aldehydes, ketones or acids. While molecular oxygen is often used for bulk chemical processes, oxidizing agents like permanganate or dichromate are used for the oxidation of fine chemicals. A summary of the recent development in copper-catalyzed oxidation of organic compounds is given by Punniyamurthy and Rout.[46]

An industrial-scale oxidation reaction involving copper as (co-) catalyst is the Hoechst-Wacker process which converts ethylene into acetaldehyde. The process involves the use of a palladium-based catalyst, typically $PdCl_2$, in the presence of cuprous chloride (CuCl) and a water-soluble ligand such as triethylamine or pyridine. The reaction takes place in an aqueous solution at elevated temperature and pressure. In the first step of the reaction mechanism, ethylene coordinates to the palladium(II) site. Next, the coordinated ethylene is oxidized under reduction of palladium. The copper chloride serves as a co-catalyst, promoting the formation of the active palladium(II) species by reduction of copper(II) to copper(I). Copper is subsequently re-oxidized by molecular oxygen. The mechanism is summarized in Reaction scheme 3.[47-48]

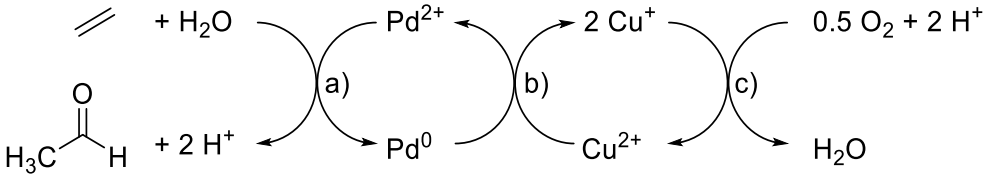

Reaction scheme 3: Oxidation of ethylen to acetaldehyde by the Hoechst-Wacker process: A) Oxidation of ethylene to acetaldehyde under reduction of Pd(II) to Pd(0). B) Reoxidation of Pd(0) to Pd(II) by reduction of Cu(II) to Cu(I). C) Oxidation of Cu(I) to Cu(II) by molecular oxygen.

In general, copper is often used as a catalyst in oxidation (and reduction) reactions due to its ability to cycle between different oxidation states, which allows it to participate in redox reactions. Copper can be easily oxidized from its zero valent state to a higher valent state such as copper(I) or copper(II), and then reduced back to its zero valent state.[49]

Another group of copper catalyzed reactions are the coupling reactions. These are used to introduce functional groups to an organic molecule. Especially the bond formation of carbon-carbon, carbon-nitrogen and carbon-phosphorus bonds is of huge interest.[50] A review by Rao and Fu summarized the recent developments in copper-catalyzed coupling reactions.[51] Often, the selectivity of such reactions can be tuned by the choice of the copper ligands or the solvent.[52]

The Ullmann coupling reaction is one of the first reported cross-coupling reactions used to form a carbon-carbon bond between two aromatic or heteroaromatic compounds. It was first described by Fritz Ullmann in 1901. The reaction typically involves the use of a copper catalyst, such as copper powder or a copper(I) halide.[53] One of the main advantages of the Ullmann

coupling reaction is its ability to form carbon-carbon bonds under mild conditions (Reaction scheme 4). The mechanism of the Ullmann coupling reaction involves the formation of a copper intermediate, which reacts with the aryl halide to form the biaryl product. The copper catalyst is thought to promote the reductive elimination of the halide, allowing for the formation of the carbon-carbon bond.[54] Further coupling reactions were reported by Goldberg in 1906 and Hurtley 1929.[55-56]

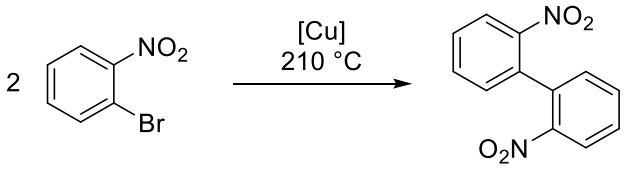

Reaction scheme 4: Ullmann cross-coupling reaction under formation of a biphenyl.[53]

Additionally, copper is commonly used as a catalyst for hydrogenation reactions due to its ability to activate molecular hydrogen. Hydrogenation reactions catalyzed by copper range from industrial-scale reactions like the methanol synthesis up-to the selective hydrogenation of organic compounds such as olefins, alkynes, and aromatic compounds.[57-58]

In the copper-catalyzed methanol synthesis process, carbon monoxide (or carbon dioxide) and hydrogen are mixed and passed over a copper-based catalyst at high temperature and pressure. The reaction typically occurs at a temperature of around 250-300 °C and a pressure of 50-100 bar.[59] The copper catalyst used in the process is typically a mixture of copper, zinc, and aluminum oxides (see also chapter 1.3). Under typical synthesis conditions, the reaction involves the hydrogenation of both carbon monoxide and carbon dioxide to methanol as well as the water gas-shift reaction (Reaction scheme 5).[60] The exact details of the reaction mechanism are still subject of ongoing research, a recent review is given by Guil-López *et al*.[61] Methanol is used as a raw material to produce inter alia formaldehyde (61 %), acetic acid (18 %), chloromethane (7 %) as well as fuels (synthesized by the methanol to gasoline process, MTG).[62]

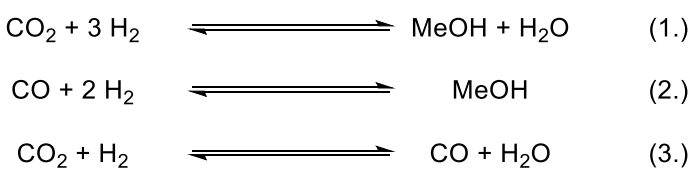

Reaction scheme 5: Reactions involved in the synthesis of methanol over copper-based catalysts. Synthesis from 1.) carbon dioxide and 2.) cabon monoxide. 3.) Water gas-shift reaction.

On the other hand, the selective hydrogenation of a broad range of carbonyl compounds, such as aldehydes, ketones, carboxylic acids and their derivatives is catalyzed by copper systems. An important milestone in the process of copper catalyzed selective hydrogenation reactions was a pioneering report by the American chemist H. Adkins in 1931. He described a copper-chromite catalyst which allows the hydrogenation of aldehydes and ketones. A quantitative reduction of nearly every carbonyl group to the desired alcohol was possible at reaction conditions of 100-150 bar hydrogen and 150-180 °C.[35] This catalyst allows

additionally the hydrogenation of esters but need slightly harsher reaction conditions (250 °C, 220 bar).[63] As the European Union (EU) implemented a regulation under REACH (Registration, Evaluation, Authorization and Restriction of Chemicals) in 2007 that effectively banned the use of chromium(VI) compounds in most applications, researchers focused on the investigation of copper-aluminum as well as copper-zinc catalysts for the selective C-O bond hydrogenation.[64-66]

Yang et al. reported a copper-zinc-aluminum oxide catalyst which allows the selective hydrogenation of furfural in a fixed-bed reactor setup (Reaction scheme 6, 1). A selectivity to furfuryl alcohol of above 98 % was reported at a conversion of 98 % at 120 °C and 72 % at 100 °C.[67] Pospelova et al. reported copper-zinc catalysts as environmentally friendly alternative to the Adkins catalyst used in the hydrogenolysis of esters (Reaction scheme 6, 2). They compared different synthesis routes for the synthesis of a copper-zinc catalyst with a copper loading of 8 wt-% used in the dimethyl adipate hydrogenolysis. Especially co-precipitated and deposition-precipitated copper-zinc catalysts result in small copper nanoparticles below 15 nm and a large copper surface area above 4 m^2g^{-1} (which is quite high for this copper loading). This results in a superior catalytic activity.[65] Another copper catalyzed selective C-O bond hydrogenation is reported by Wang et al. They investigated silica supported copper-zinc catalysts for the selective hydrogenation of dimethyl oxalate to ethylene glycol (Reaction scheme 6, 3). They claimed that highly active catalysts for the vapor-phase hydrogenation (conversion above 99.6 %, selectivity to ethylene glycol above 96 %) can be obtained by ammonia evaporation-impregnation. Additionally, superior long-term stability above 800 h was achieved by the copper-zinc interface which prevents sintering.[68]

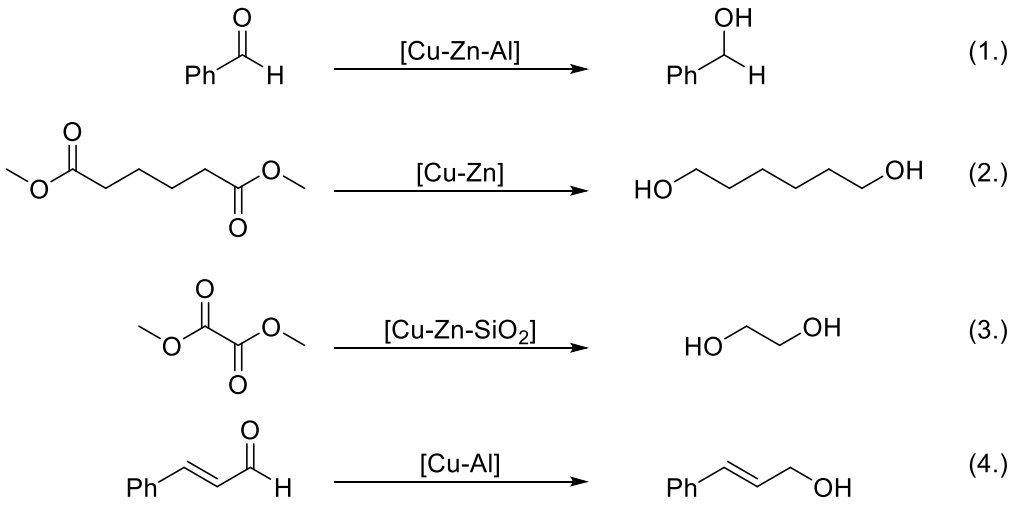

Reaction scheme 6: Copper catalyzed selective C-O bond hydrogenation. Hydrogenation of 1.) furfural by Yang *et al.*, 2.) dimethyl adipate by Pospelova *et al.*, 3.) dimethyl oxalate by Wang *et al.* and 4.) cinnamaldehyde by Gutierrez/ Valange *et al*. [65, 67-70]

Furthermore, copper-aluminum catalysts were investigated for the selective C-O bond hydrogenation in cinnamaldehyde by Gutierrez *et al.* (Reaction scheme 6, 4). They reported that in general copper catalysts are unselective toward the hydrogenation of α,β-unsaturated compounds to yield the desired saturated alcohols. Nevertheless, the selectivity towards the

unsaturated alcohol can be increased by a) using isopropanol as hydrogen donor compound in the transfer hydrogenation of cinnamaldehyde and b) switching to mesoporous silica as support.[70] Valange *et al.* reported copper-impregnated mesoporous alumina which is active in the liquid-phase cinnamaldehyde hydrogenation (Reaction scheme 6, 4). A selectivity of above 70 % in the C-O bond hydrogenation yielding the desired cinnamyl alcohol could be achieved by careful optimization of the synthesis parameters. The high selectivity is obtained by the presence of Cu_2O particles in strong interaction with the alumina support. In contrast to classically impregnated copper supported on γ-alumina catalysts, a difference in the electronic state is reported.[69] Dörfelt *et al.* investigated the reaction mechanism of manganese doped copper aluminate spinel catalysts in the hydrogenation of butyraldehyde. They claimed that the spinel lattice acts as support, as additional copper source and as proton reservoir for the hydrogenation reaction.[71]

The investigation of these catalysts focuses not only on academic but also on industrial research. Starting from 1991, Wegman *et al.* investigated copper aluminate spinel catalysts as Adkins-analogous catalysts for C-O bond hydrogenation reactions.[72] They investigated a copper-oxide on copper aluminate spinel system as highly active catalysts for the hydrogenation of aldehydes to the corresponding alcohols. Kadono *et al.* described similar catalysts as highly active, selective and long-term stable in the aldehyde hydrogenation.[73] Paulus et al. focused on copper-aluminum-manganese catalysts for the hydrogenation of carbonyl functions. The described catalysts are additionally active in the hydrogenation of fatty acids and esters.[74]

Summarizing, copper is used in a broad range of catalytic applications. This can be explained by the incredible diversity of the copper chemistry. Depending on the oxidation state, copper can catalyze reactions involving both one and two-electron mechanisms (radical and polar) effectively. Additionally, copper can coordinate to heteroatoms like nitrogen, oxygen and phosphorus and in general to π-bonds.

As briefly presented, copper catalysts are in general active in a broad range of hydrogenation reactions. Especially the selective hydrogenation of α,β-unsaturated aldehydes is of huge interest in industrial and academic research. In the synthesis and production of fine chemicals and pharmaceuticals, the selective hydrogenation of either the C-C or the C-O bond is often an important production step.[75-76] While the hydrogenation of the C-C bond yields the saturated aldehyde, the hydrogenation of the C-O bond yields the unsaturated alcohol. A complete hydrogenation of both C-C and C-O bond yields the saturated alcohol (which is often undesired). The general reaction pathway is given in Reaction scheme 7. A review about the selective hydrogenation of α,β-unsaturated aldehydes is given by Gallezot and Richard.[77]

While the beforehand presented reports deal with copper catalyzed hydrogenation, the selective hydrogenation is also possible over noble metals. Contrary to the copper catalyzed

selective hydrogenation to the unsaturated alcohol, noble metals like platinum or palladium favor in general the (thermodynamically favored) hydrogenation of the C-C bond. The selectivity in the C-C bond hydrogenation follows the sequence of osmium < iridium < platinum < ruthenium < rhodium < palladium (crotonaldehyde hydrogenation).[77-78] In general, palladium catalysts are very promising regarding the selective hydrogenation of the C-C bond.[79]

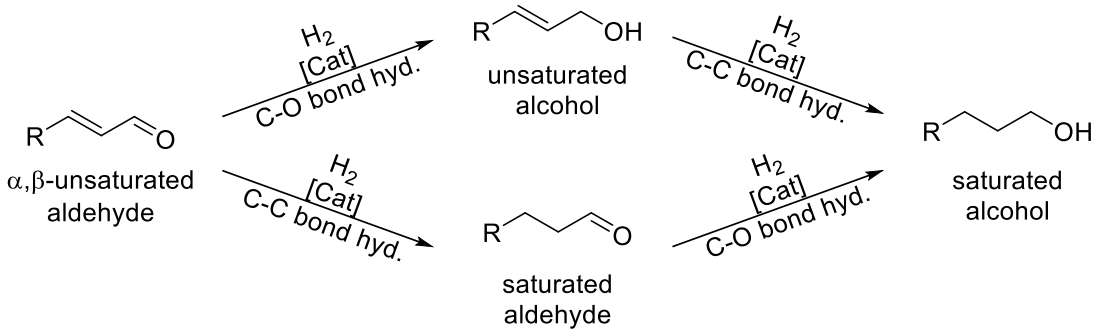

Reaction scheme 7: Pathway of the hydrogenation of α,β-unsaturated aldehydes.[77]

Jiang *et al*. focus on the influence of particle size of palladium catalysts applied in the selective hydrogenation of cinnamaldehyde to hydrocinnamaldehyde (the saturated aldehyde). They found out that smaller palladium particles favored the C-C bond hydrogenation. The difference in selectivity is explained by a change of the palladium surface. Larger palladium particles form a flat surface which favors the C-O centered adsorption of the cinnamaldehyde yielding the undesired unsaturated alcohol.[80]

Campo *et al.* investigated a variety of palladium and platinum catalysts used in the liquid-phase hydrogenation of crotonaldehyde. They found out that the selectivity of pure palladium catalysts towards the C-O bond hydrogenated crotyl alcohol is nil. Although the addition of an oxide species as promotor activates the C-O bond, it is nearly impossible to increase the selectivity towards the crotyl alcohol.[81]

As discussed, both copper and noble metals can be used in general as catalyst in hydrogenation reactions. These hydrogenation catalysts tend to activate the hydrogen-hydrogen bond under dissociative adsorption. Although the activation energy of the dissociative adsorption of hydrogen to the metal surface is similar for platinum (9.5 $kcalmol^{-1}$) and copper (9.0 $kcalmol^{-1}$), noble metals generally tend to activate the hydrogen bond even at room temperature.[82-83] Slightly elevated temperatures are necessary for copper catalysts, although some reports deal with the ability of special copper sites(711) to be active in the dissociative hydrogen adsorption even at room temperature.[84] Another interesting difference between copper and noble metal catalysts can be identified regarding the selective hydrogenation of α,β-unsaturated aldehydes. While copper catalysts tend to hydrogenate the C-O bond, noble metal catalysts tend to activate the C-C bond. Often, an interplay between copper(0) and (I) sites is reported as active site for the selective hydrogenation of C-O bonds over copper catalysts.[85] Contrary, the active site of noble metal catalysts is generally reported as the noble metal(0) site.[77]

1.3 Synthesis of copper catalysts

As shown before, copper catalysts are used in a broad range of applications due to its incredibly diverse chemistry. Similar to the huge range of applications, also a broad variety of synthesis routes are available for the synthesis of copper catalysts and nanoparticles. Not only chemical methods like precipitation or reductive methods are available, also physical methods like the laser deposition or mechanical methods (e.g., ball milling) can be applied. Additionally, the biosynthesis of copper catalysts and nanoparticles is possible, inter alia with the help of enzymes or proteins.[86-87]

For the synthesis of industrially applied catalysts, mainly chemical synthesis methods are used like a thermal treatment or an electrochemical or wet chemical method. Especially wet chemical methods like the impregnation or the precipitation are very common. The precipitation and co-precipitation of copper catalysts are among the most important synthesis route to obtain copper (nanoparticle) catalysts.[88]

The precipitation is a process which transforms a metal salt solution with the aid of a precipitation agent into an insolvable phase, the precipitate. Often, nitrates, chlorides or acetates are used as metal precursors. The (co-) precipitation of copper catalysts is often performed with alkaline precipitation agents like soda or sodium hydroxide (or mixtures of both). Additionally, a slightly alkaline pH value and (slightly) elevated temperatures are applied. A precipitation at acidic conditions can lead to the precipitation of undesired hydroxynitrates while strong alkaline conditions can lead to direct precipitation of copper oxide due to oxolation.[89]

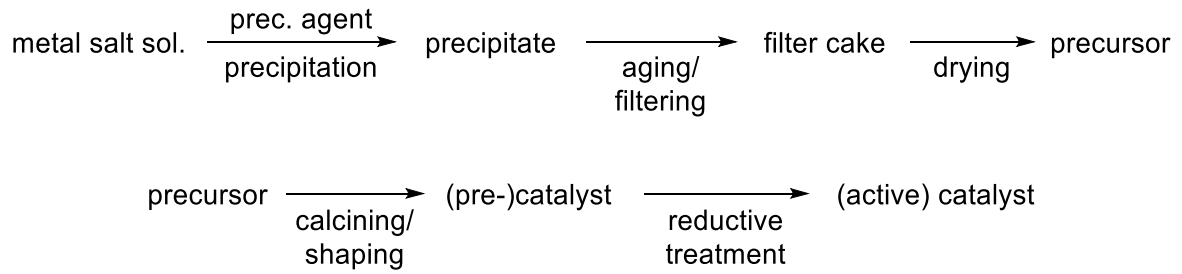

Figure 1: General scheme of the synthesis of copper catalysts via precipitation, aging, drying, calcination and reductive activation.

During the precipitation, the solvable metal salts are transferred into insolvable precipitates. In the case of an alkaline precipitation, the precursors are often hydroxides or hydroxycarbonates. An aging step which is often conducted after the precipitation leads to recrystallization effects or the phase transformation of precursor phases. After the precipitation and aging, the precursor is dried (e.g., by a spray dryer) and calcined. In general, an oxidic copper catalyst is obtained after the calcination. In case of hydrogenation reactions, the oxidic copper is normally transferred into its metal state by a reductive thermal treatment.[89-91] The complex process of the precipitation of copper catalysts is summarized in Figure 1.

A typical example for the precipitation of copper catalysts is the co-precipitation of copper-zinc(-aluminum) oxide catalysts used in the methanol synthesis. The metal nitrate precursors are mixed and precipitated with sodium hydroxide. After the precipitation, aging and drying, the hydroxycarbonate precursor is obtained. In the case of the methanol synthesis catalyst, this consists mainly of zinc-malachite ($(Cu,Zn)_2(OH)_2CO_3$) and aurichalcite ($(Cu,Zn)_5(OH)_6CO_3)_2$). This precursor phase is subsequently calcined to yield the desired oxidic structure. After a reductive thermal activation, the actual catalyst is obtained. The complete process is summarized in Reaction scheme 8.[59]

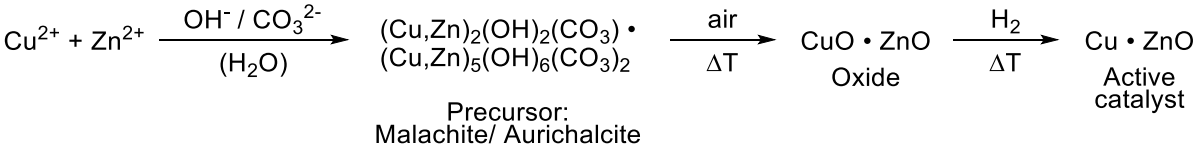

Reaction scheme 8: Synthesis of copper-zinc catalysts used for the methanol synthesis.

Many research reports deal with the investigation of optimal synthesis conditions for the (co-)precipitation of copper catalysts. As an example, studies focus on the question about the optimum precipitation pH during the synthesis of the typical copper-zinc oxide methanol catalyst. Another crucial factor is the copper-zinc ratio which has significant influence on the composition of the precursor phase and the physico-chemical properties of the actual catalyst. Furthermore, the thermal treatment (oxidative (calcination) and reductive (activation)) is an important factor in the synthesis of an active and stable copper catalyst. Many other factors can be mentioned like the influence of promotors, the type of stirring during the precipitation or the temperature and aging conditions.[92-96]

1.4 Synthesis and hydrogenation of aldehydes

1.4.1 Synthesis of aldehydes via hydroformylation

The technical process of the aldehyde synthesis is the hydroformylation, also known as oxo synthesis. Around 10 million tons of oxo products were synthesized in 2008. It is an industrially applied process to produce aldehydes from olefins and synthesis gas (Reaction scheme 9). The process is carried out under high pressure and temperature (300 bar, 150-170 °C) and with the aid of a transition metal catalyst, such as cobalt, rhodium or iridium. The resulting aldehydes are important building blocks for the production of a wide range of chemicals and materials, including detergents, plastics, and pharmaceuticals.[6, 97-98]

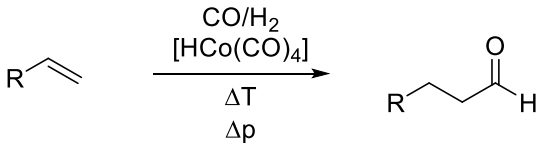

Reaction scheme 9: Synthesis of aldehydes via hydroformulation over a homogeneous cobalt catalyst.

The hydroformylation reaction mechanism involves the insertion of a carbon monoxide molecule into the olefin double bond, followed by the addition of hydrogen to form the aldehyde product. The actual mechanism is shown in Reaction scheme 10. The first step is the cleavage of a metal carbon monoxide bond under formation of a free coordination site (1). The olefin coordinates to the free site (2) and is inserted under formation of an alkyl tricarbonyl. Additionally, carbon monoxide is inserted under formation of an alkyl tetracarbonyl (3). A migratory insertion of carbon monoxide yields the acyl species (4). Under oxidative addition of hydrogen and reductive elimination of the aldehyde, the active 16 electron cobalt species is regenerated (5). This step is known to be the rate-determining step.[99-100]

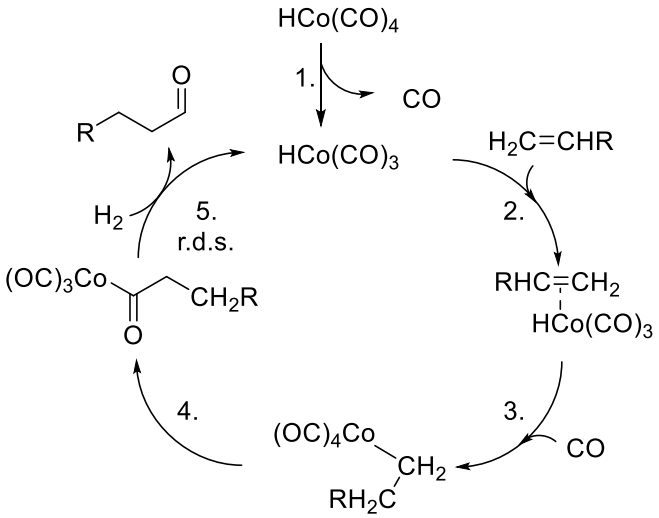

Reaction scheme 10: Reaction mechanism of the hydroformulation over a cobalt catalyst.

1.4.2 Hydrogenation of aldehydes

The main product of the industrial hydroformylation is *n*-butyraldehyde with over 70 % of the total production. Additionally, around 20 % of the aldehyde production are C5 to C13 aldehydes. The obtained aldehydes are often used as platform chemicals which are subsequently hydrogenated to the desired alcohol, the so-called oxo-alcohols. Especially in the case of *n*-butyraldehyde, an additional aldol condensation to 2-ethylhexenal and follow up hydrogenation to 2-ethylhexanol is often performed (Reaction scheme 11).[101-102]

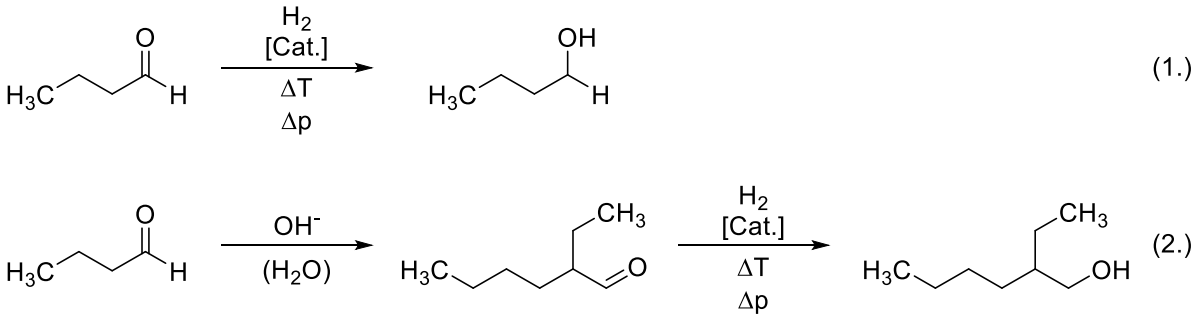

Reaction scheme 11: Reductive reaction pathway of butyraldehyde: 1.) hydrogenation to *n*-butanol and 2.) aldol condensation and hydrogeantion to 2-ethylhexanol.

n-Butanol is an important intermediate for the production of butyl esters such as butyl acrylate, and dibutyl phthalate. *n*-Butanol is additionally used in the production of pharmaceuticals, and polymers as well as as solvent and for esterifications. Both *n*-butanol and isobutanol can be used pure or blended into gasoline engine fuels. These alcohols have a higher energy density compared to ethanol.[102-103]

2-Ethylhexanol is mainly used as plasticizer for polyvinyl chloride. Therefore, it is converted with phthalic anhydride to form dioctyl phthalate. Furthermore, it is used as nonionic surfactant.[104] The hydrogenation of butyraldehyde to *n*-butanol is industrially performed both in the liquid and the gas-phase and usually catalyzed by late transition metals like nickel and copper as well as noble metals like platinum. The one pot synthesis of 2-ethylhexanol under simultaneous aldol condensation and hydrogenation is additionally reported.[101]

Cropley *et al.* investigated the optimal design of a plant-scale catalytic reactor for the hydrogenation of butyraldehyde. They developed a design which allows a high catalytic productivity and an efficient energy utilization.[105] Noller *et al.* examined alumina supported nickel-copper catalysts for the hydrogenation of butyraldehyde and crotonaldehyde. Additionally, they investigated the reaction network of the crotonaldehyde hydrogenation over these catalysts.[106] Englisch *et al.* focused on silica supported platinum catalysts for the liquid-phase hydrogenation of crotonaldehyde. They found out that catalysts with larger platinum particles show a lower deactivation rate while small particles tend to deactivate faster. This deactivation is caused by surface poisoning due to carbon monoxide adsorption. Carbon monoxide is formed mainly due to decarbonylation of crotonaldehyde. An oxidative treatment can restore the initial activity of the catalyst.[107] Subbotin *et al.* studied the reaction kinetics of the butyraldehyde hydrogenation over copper containing catalysts in the temperature range

between 100 and 200 °C. Therefore, isotope exchange reactions with deuterium were performed which showed that dissociatively adsorbed hydrogen is formed on copper(0) sites.[108] Wu *et al.* examined a silica supported ruthenium catalyst for the vapor-phase hydrogenation of butyraldehyde. They found that carbon monoxide is formed due to decarbonylation and negatively affects the hydrogenation turnovers resulting in a decreased activity by blocking of active ruthenium centers.[109]

As shown, the hydrogenation of butyraldehyde (and crotonaldehyde) can be performed over a variety of late transition metals, ranging from copper and nickel over to noble metals like platinum and ruthenium. Furthermore, the reaction can be performed both in the liquid and the gas-phase. Many studies deal with the development of the most active catalyst, the investigation of reaction mechanism as well as the kinetics and the understanding of the deactivation of the catalyst.

1.5 Scope of the present work

This thesis focuses on copper catalysts used for the hydrogenation of aldehydes, in particular butyraldehyde. These heterogeneous catalysts are synthesized by co-precipitation, thermal treatment and reductive activation. Mainly two groups of copper catalysts shall be investigated: Copper-zinc/ copper-aluminum oxides and copper aluminate spinels. The work is carried out within the framework of the Clariant Hydrotech cluster.

A multipurpose test plant (ILS-601) for the gas-phase hydrogenation of butyraldehyde is commissioned and used to determine the performance of the investigated catalysts. The first part of this thesis focuses on the structure-activity relationships of copper catalysts. The influence of a variety of synthesis conditions on structural properties as well as the catalytic activity is investigated. Especially the influence of the copper loading of copper-zinc oxide catalysts as well as the precipitation pH-value is in detail investigated. Different series of catalysts are synthesized by co-precipitation and subsequent thermal treatment. The precursors and the calcined oxides are in detail characterized and the findings are related to the catalytic activity of these catalysts used in the gas-phase hydrogenation of butyraldehyde. Especially the precursor phase composition is related to the structure and morphology of the calcined oxides as well as the catalytic properties of the activated catalysts. Additionally, copper-aluminum oxide and spinel catalysts are in detail characterized by various techniques including surface area determination and temperature-programmed methods and catalytically investigated. The influence of the calcination temperature of copper-zinc oxide catalysts on structural properties and catalytic activity is examined. Deeper knowledge of the complex precipitation and aging process during the synthesis of copper-zinc catalysts shall be gained by a systematic design of experiments approach. In general, structure-activity relationships of copper-zinc and copper-aluminum catalysts shall be acquired by systematic synthesis and characterization of these catalysts. Morphological properties are related to the catalytic performance of the catalysts.

The second part of this thesis focuses on the stability and the hydrogenation mechanism of copper-zinc and copper-aluminum catalysts. Therefore, the long-term stability of these catalysts used in the gas-phase hydrogenation is compared to the activity and selectivity of the same catalysts used in liquid-phase hydrogenation. A test setup is upgraded to allow the inert handling of used catalysts. A detailed characterization of the used catalysts applied in the gas-phase hydrogenation is performed under inert conditions. Morphological changes of these catalysts due to the butyraldehyde hydrogenation are recorded and related to their long-term stability. Especially *in situ* characterization techniques are included. A comparison between the gas- and the liquid-phase butyraldehyde hydrogenation is aspired to gain a deeper knowledge of the hydrogenation mechanism of butyraldehyde over copper-zinc and copper-aluminum catalysts. The activity and selectivity as well as the leaching behavior of these catalysts used in the liquid-phase hydrogenation shall be investigated.

2

Commissioning of a Multipurpose Test Plant

Within this chapter the commissioning of the *Integrated Lab Solutions*®-601 (ILS-601) as well as the development of the online gas chromatography (GC) analysis is described. In the first section the installation of the unit as well as the pipe and instrumentation diagram are discussed. Furthermore, the prerequisites for the continuous and steady feed dosing and vaporization are analyzed. In the third section preliminary tests to check for isothermal conditions as well as the exclusion of transport limitations are described. Also, the verification of the catalysis tests and their reproducibility is discussed. In the last section the setup of the online gas chromatography analysis is described.

2.1 Installation of the test plant

The ILS-601 is a four-fold multipurpose fixed bed hydrogenation unit (Figure 2, A). The feed which is hydrogenated is either carbon dioxide (CO_2) or organic liquid feed (e.g., aldehydes, fatty acid methyl esters, ketones) which is continuously vaporized in the reactor. The reactors itself are four individual 65 cm long (0.5 inch outer diameter) stainless steel tubes with an empty pipe in the middle (0.125 inch outer diameter) where a thermocouple is positioned. With this thermocouple, the temperature can be measured in direct contact to the catalyst bed. Additionally, the feed dosing pipe is placed into the reactor and ends at around 15 cm from top.

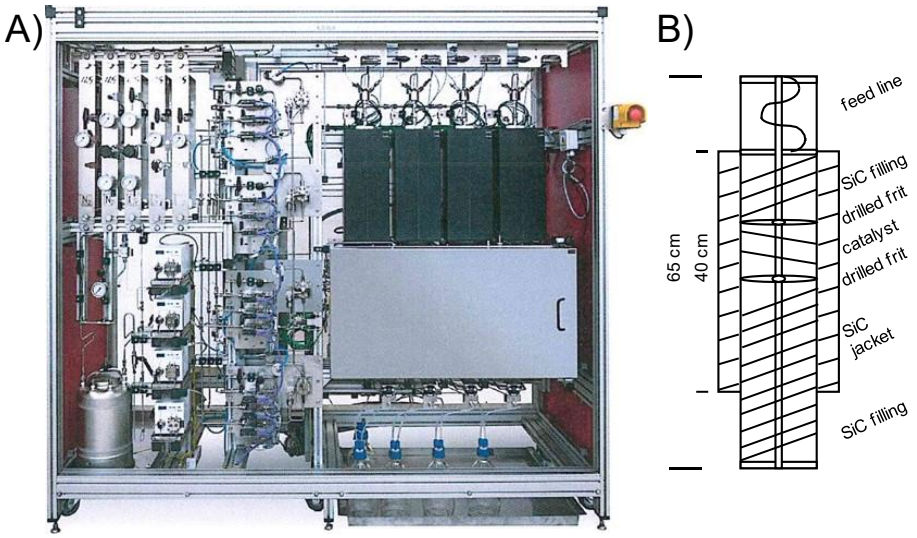

Figure 2:A) Picture of the ILS-601 test plant and B) schematic drawing of the reactor with catalyst filling.

At this position, the isothermal zone starts (Figure 4) and the liquid is released on a layer of glass wool. The liquid feed is mixed at this position with hydrogen where the vaporization immediately takes place due to the decrease of the partial pressure and the temperature (above 80 °C). The catalyst is loaded in the middle of the isothermal zone and the thermocouple pipe is fixed in the middle of the reactor by placing a frit with a drilled hole before and after the catalyst bed (Figure 2, B). Each reactor is placed in a tube furnace which can handle temperatures up to 500 °C. Each reactor is covered with a 40 cm silicon carbide jacket which is positioned in the middle of the reactor (15-55 cm). This cover is used to keep the temperature is this region constant (isothermal zone). The flow of the gaseous feed (N_2, H_2,

CO_2) is regulated by three mass flow controllers for each reactor while the liquid feed is dosed over HPLC-pumps (one for each reactor). The organic liquid feed is kept under inert atmosphere under slightly elevated N_2 pressure in a stainless-steel vessel (V_{max} = 10 l). Each HPLC pump is connected to this feed vessel so that the feed is the same for every reactor. The pressure is controlled individually for each reactor with four backpressure regulators. This backpressure regulators as well as the downstream side of the four reactors are placed in an oven to overcome feed condensation after reaction. This oven can oversee temperatures up to 200 °C. In this downstream oven, a multipurpose valve is positioned which connects the reactors both with the online analysis as well as the exhaust. While one reactor is connected to the online analysis, the other three reactors are connected with the exhaust. The position of the valve can be switched so that each reactor can be connected to the analysis line. The piping between the online analysis and the downstream oven is additionally heated by a heating tube which can handle also temperatures up to 200 °C. A simplified piping and instrumentation (PI) diagram is given in Figure 3. The online analysis is done by an Agilent® 7890 B GC equipped with an Agilent® CP-Sil 5 column, a thermo-conductivity-detector (TCD) as well as a valve box to switch between different columns (not necessary for the butyraldehyde hydrogenation). A detailed description of the analytics is provided later in this thesis (chapter 2.4).

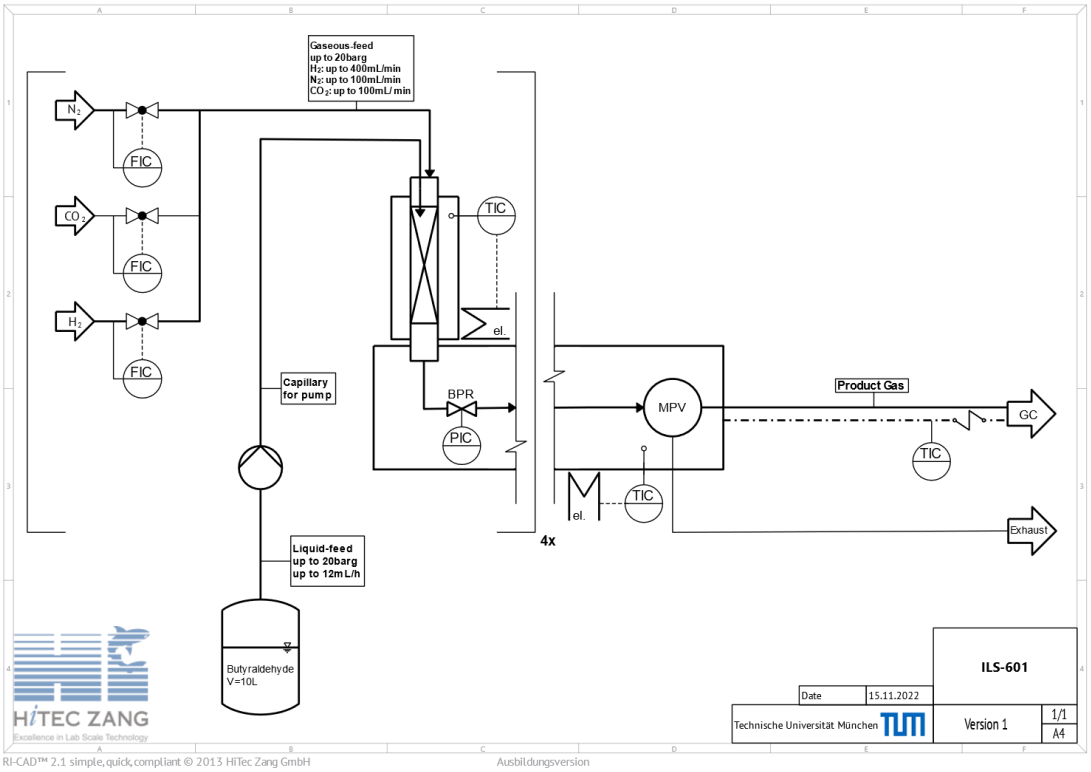

Figure 3: Simplified pipe and instrumentation (PI-) diagram of the 4-fould gas-phase reactor ILS-601 test plant.

All settings (gas and liquid flow, temperatures of the reactors, downstream oven as well as heating tube to the GC, pressure, position of the multipurpose valve) are controlled by a PC with the *ProControl* software. This software allows the individual control of each parameter as well as the controlling with complexes recipes to run catalysis experiments automatically. Also, all measured parameters (temperature, pressure, volumetric flow, etc.) are recorded and can exported afterwards. Additionally, the software can control the GC and start GC measurements. GC reports are exported by the GC software.

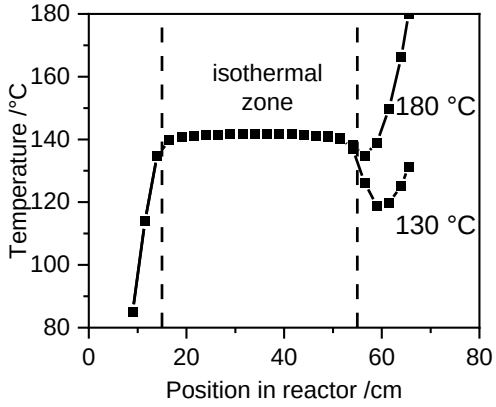

Figure 4: Temperature profile of the ILS reactor. Set temperature: 140 °, downstream oven: 130 / 180 °C.

A thermoprofile of the reactor was measured to verify the position of the isothermal zone of the reactor. Therefore, an inert filled (SiC) reactor was placed in the oven which was set to 140 °C. The thermocouple in the thermocouple tube was moved through the reactor and the temperature was recorded (Figure 4). It could be shown that the isothermal zone is around 40 cm long and in the middle of the reactor between 15-55 cm from top. This is in accordance with the position of the SiC jacket around the reactor. At both ends of the isothermal zone the temperature drops slightly (around 2 K). The temperature deviation in the isotherm zone is below 0.5 K. Before the SiC jacket, the temperature is lower than set and significantly decreasing. It has to be considered that the first part of the reactor is not placed in the furnace. At the lower side of the reactor, the temperature decreases slightly before the temperature of the downstream oven is received in the reactor itself. The last part of the reactor is positioned in the downstream oven.

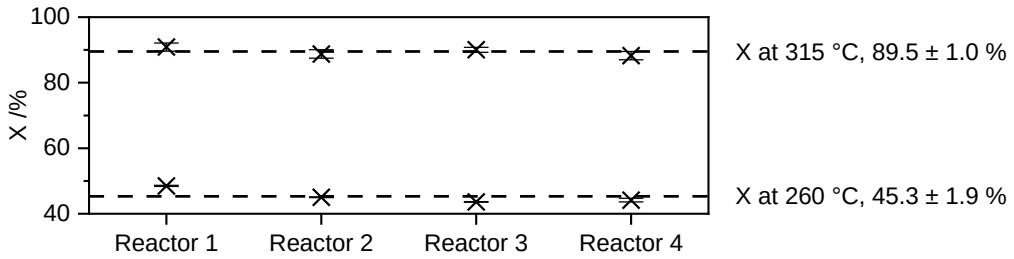

Figure 5: Comparison of the four reactors during CO_2 methanation as test reaction. Catalyst: 60 wt-% Ni/Al_2O_3. Activation: 3 K/min, 500 °C, 2 h; pure H_2, GHSV = 16 000 . Reaction: CO_2:H_2 = 1:4, GHSV = 50 000 h^{-1}.

It was considered to test the unit first with a pure gas-phase reaction without any liquid feed due to the complexity of feed dosing and vaporization. With this, problems regarding temperature or pressure control or the gas feeding by mass flow controllers could be revealed. The carbon dioxide (CO_2) methanation was considered as useful reaction (Reaction scheme 12) to verify the reproducibility of the unit and to get a feeling for the handling of the reactors and the unit. A standard 60 wt-% nickel-alumina catalyst was synthesized by co-precipitation and subsequently drying/ calcination. All reactors were filled equally with the same amount of catalyst placed at the same position. The catalysts were activated equally in all four reactors (500 °C, pure hydrogen, 2h). The activation and reaction conditions as well as the synthesis of the catalyst were taken according to T. Burger *et al.*[110]

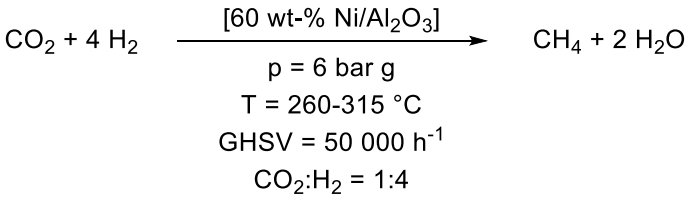

Reaction scheme 12: Methanation of CO_2 over a Ni/Al_2O_3 catalyst as model reaction.

The CO_2 conversion was determined at two different temperatures (260 respectively 315 °C) and the standard deviation of each temperature step was calculated (Figure 5). Additionally, the overall standard deviation over all four reactors is given. The conversion at 260 °C was measured with 45.3 % (± 1.9 %) and 89.5 % (± 1.0 %) at 315 °C (average over all four reactors). The standard deviation per temperature step and reactor is below 1 %. This conversion temperature dependence is in accordance with T. Burger *et al.*[111] The deviation of 1.9 respectively 1.0 % for the conversion over all four reactors shows that pure gas-phase reactions can be driven under nearly equivalent conditions over all four reactors and no reproducibility problems occur.

2.2 Liquid feed dosing and vaporization

Within this thesis, the gas-phase hydrogenation of butyraldehyde to *n*-butanol is investigated (Reaction scheme 13). Butyraldehyde is under standard conditions liquid. Therefore, the liquid feed must be feeded without fluctuations and vaporized continuously.

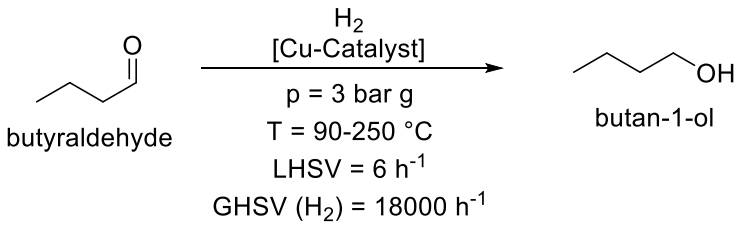

Reaction scheme 13: Hydrogenation of butyraldehyde to *n*-butanol over a copper catalyst.

At standard reaction conditions (3 bar g, n(H_2:feed = 10:1) → 300 mbar butyraldehyde vapor pressure) the temperature has to be above 40 °C to allow direct evaporation (Figure 6). If full conversion is reached and all butyraldehyde is hydrogenated to butanol, the temperature to allow complete evaporation and to prevent condensation must be at least 80 °C. Therefore, it was decided to drive the gas-phase hydrogenation at least at 90 °C to prevent problems with incomplete vaporized feed and condensation.

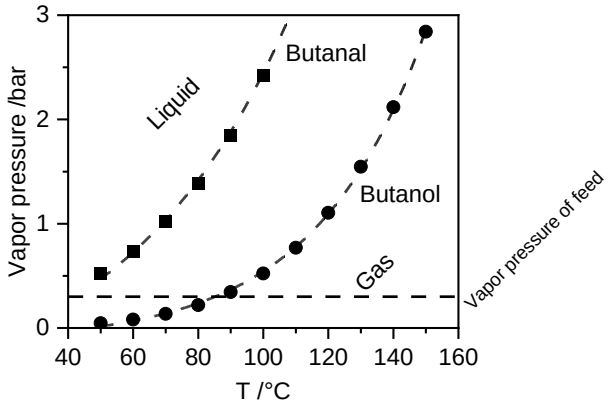

Figure 6: Vapor pressure of butyraldehyde and butanol as function of the temperature. At least 80 °C are necessary to prevent condensation at full conversion and standard reaction conditions.

The dependence of the butyraldehyde conversion regarding the liquid hour space velocity (LHSV) was determined due to initial problems with accurate and fluctuation free feed dosing. Therefore, an external and calibrated HPLC pump was used. It could be shown that the conversion depends strongly on the LHSV (Figure 7, A). At 140 °C, a conversion of around 50 % is reached at LHSV = 3 h^{-1} while the conversion drops to nearly 10 % at LHSV = 11 h^{-1}. This indicates that initial problems regarding reproducibility are mainly due to inaccurate feed dosing. Therefore, the type of HPLC pump controlling was investigated as possible reason for inaccurate feeding. It could be shown that controlling the HPLC pump directly with the ILS-software gives a strong feed flow fluctuation of around 30 %, while the feed flow is quite stable when the HPLC pump is controlled directly by the pump (Figure 7, B). Nevertheless, a short initial phase of around 30 min must be considered till the feed flow is accurate. The feed flow fluctuation after the initial phase is below 3 %. Therefore, it was decided to control the

pump not via the ILS-software but directly from the pump. A special *Knauer* software for accurate controlling of the pump would be also available.

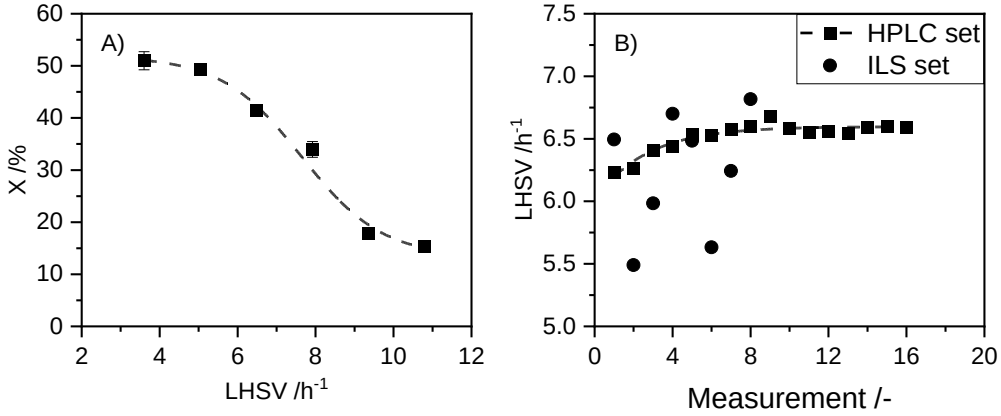

Figure 7: A) Butyraldehyde conversion as function of the LHSV. Catalyst: Benchmark Cu-Zn oxide. Activation: 2 K/min, 200 °C, 2 h; 20 % H_2, GHSV = 3000 h^{-1}. Reaction: 140 °C, GHSV = 18000 h^{-1}. B) LHSV in dependence of the pump controller. Set LHSV = 6.5 h^{-1}.

To examine the accuracy of the feed flow and to test if the vaporization takes place constantly, mass spectrometer measurements were done in addition to the standard GC experiments. Therefore, a mass spectrometer was connected via a T-pipe between the GC and the heated analysis pipe. The connection was additionally heated via a heating band to prevent condensation. For this experiment, an inert filled reactor was used.

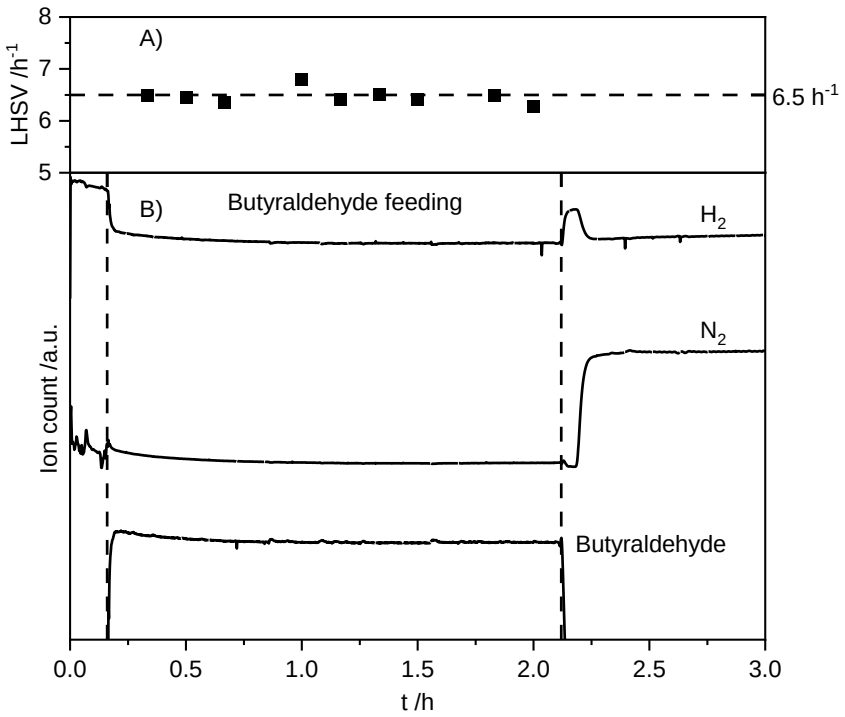

Figure 8: Continuous vaporization of butyraldehyde over inert filled reactor monitored via a) GC and b) MS. Set LHSV = 6.5 h^{-1}.

It could be shown that the butyraldehyde vaporization over the glass wool takes place continuously and without fluctuation (Figure 8). Nearly immediately after switching on the feed the butyraldehyde signal appears in the mass spectrometer and both the hydrogen and nitrogen signal are slightly decreasing. During feeding, no fluctuation of the butyraldehyde

signal appears and a constant signal is obtained. After around 2 h, the pump was switched off and the butyraldehyde signal vanishes while the signal for hydrogen and nitrogen are slightly increasing. Additionally, the amount of vaporized feed was quantified by GC measurements. The set flow rate of 6.5 h^{-1} (LHSV) was confirmed by the experiment. As seen before, the feed flow deviation was measured with around 3 %. It could be shown that the accurate feeding and vaporization of butyraldehyde is required to allow reproducible catalyst measurements with acceptable variations.

2.3 Exclusion of limitations by preliminary tests

As external and internal transport limitations as well as non-isothermal conditions can occur during heterogeneous catalysis and falsify test results, it is necessary to exclude these limitations. Therefore, to obtain ideal plug flow conditions and to prevent bypass effects, the particle size should be at least 10 times smaller compared to the inner diameter of the reactor and 50 times smaller than the height of the catalyst bed. Different preliminary tests were performed to exclude these limitations.[112-114]

As the butyraldehyde hydrogenation is exotherm (65 $kJmol^{-1}$), the reaction should be tested for isothermal conditions.[115-116] Therefore, all reaction parameters are kept constant while the catalyst bed dilution is varied, and the conversion is determined at a certain temperature. A standard copper-zinc oxide catalyst was used for this experiment (chapter 3.2). A catalyst bed dilution ratio of 1:3 (catalyst:dilution) up to 1:9 was tested (Table 1). As material for dilution, α-Al_2O_3 with a sieve fraction of 250 uM was chosen. Although the thermal conductivity is higher for silicon carbide (SiC) compared to Al_2O_3, the advantage of Al_2O_3 is that the sufficient blending between catalyst and dilution agent can be seen better due to the color change. It could be shown that a dilution of 1:3 is not enough to obtain isothermal conditions. The catalyst bed dilution is too low, and the resulting reaction heat is not fully removed. This would result in an overestimation of the conversion. While a conversion of 77 respectively 76 % was measured for the dilution 1:6 and 1:9, a conversion of 93 % was found for the dilution 1:3. The butanol selectivity was found to be 100 % for all reactors and no side products could be quantified.

Table 1: Test for isothermal conditions and external/ internal transport limitations.

Isothermal conditions	**T = 165 °C**	
α-Al_2O_3 dilution	**Conversion /%**	**Selectivity /%**
1:3	93	100
1:6	77	100
1:9	76	100
External transport limitations	**T = 150 °C**	
Superficial velocity/mh^{-1}	**Conversion /%**	**Selectivity /%**
210	45	100
255	44	100
290	44	100
Internal transport limitations	**T = 140 °C**	
Particle size/ uM	**Conversion /%**	**Selectivity /%**
20-100	14	99
100-300	14	97
300-500	13	98

The existent of internal and external transport limitations was checked additionally (Table 1). To test for external transport limitations, the superficial velocity is changes by adapting feed

flow and catalyst load while all other reaction parameters are kept constant. It could be shown that the conversion at a superficial velocity between 210-290 mh^{-1} (corresponds to 250-350 $mLmin^{-1}$ H_2) is between 44-45 % and no external transport limitations occur. The selectivity is 100 % for all experiments. External transport limitations could be identified by lower conversion rates.

In a last preliminary experiment, internal transport limitations were examined. Therefore, the particle size of the catalyst was varied while all other reaction parameters are kept constant. It could be shown that no transport limitations occur at a particle size range between 20 and 500 uM. Nevertheless, this test was done at quite low temperatures (140 °C) so that the conversion was already quite low. The selectivity was found to be between 97-99 %. The selectivity is slightly lower at low conversion rates (especially butyl butyrate is found at low temperatures). No trend regarding particle size fraction and selectivity was determined.

Standard reaction conditions were determined with these preliminary tests: Catalyst bed dilution of 1:6, particle size of 100-300 uM (best fraction for reactor filling) und a superficial velocity if 210 mh^{-1} (corresponds to 250 $mLmin^{-1}$ H_2). Afterwards, the reliability of these test conditions was tested. Therefore, all four reactors were loaded with the same amount of standard copper-zinc oxide catalyst and the reaction was driven parallel with the same reaction conditions over all four reactors. Two different sets of reaction conditions were tested. In a first experiment, the reproducibility of the standard reaction conditions was tested while in a second experiment the reaction conditions for the design of experiments approach (DoE, chapter 3.6) was tested (Figure 9). It could be shown that in both experiments the conversion temperature curve is nearly equivalent. The temperature conversion course has a sigmoidal behavior with an initial activity of around 10 % at 100 °C and reaches 80 % conversion at around 150 °C. 50 % conversion is reached at around 127 °C (T_{50}). To examine the fluctuation, the standard deviation of the T_{50} over all four reactors was calculated. It could be shown that a quite low deviation is obtained: T_{50} = 126.7 °C (± 0.9 K). It was considered that at least a 3 K difference in the T_{50} value is necessary to see reliable differences in the catalysts.

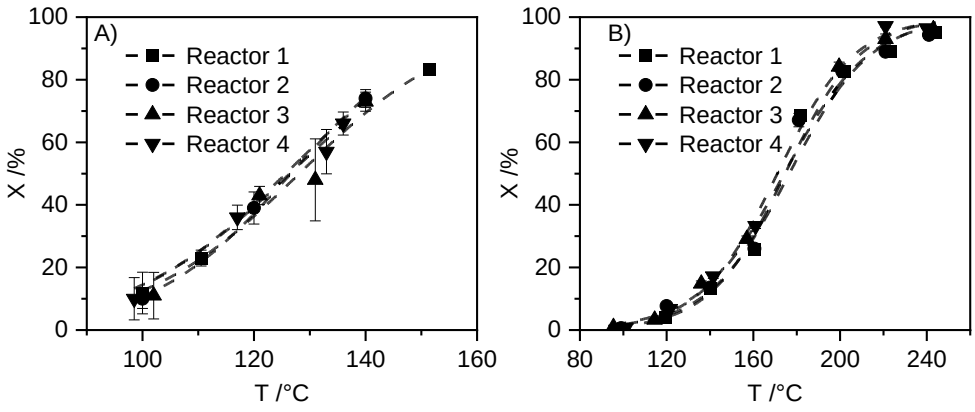

Figure 9: Comparison of the butyraldehyde conversion as function of time over all four reactors. Catalyst: Cu-Zn oxide. A) Standard activation and reaction conditions applied. B) design of experiments conditions applied: 90 - 240 °C, GHSV = 90 000 h^{-1}, LHSV = 30 h^{-1}.

Additionally, the reproducibility for the modified design of experiments reaction conditions were tested. The reaction conditions were slightly adapted to obtain a broader temperature conversion curve to see differences in the DoE catalysts more significant. Under these conditions, the initial activity lowers to around 2 % at 90 °C while (nearly) full conversion is reached at around 240 °C. A sigmoidal curve is obtained as well with a T_{50} of around 174 °C. The T_{50} deviation was measured with ± 2.0 K. It was considered to take differences in the T_{50} of above 5 K as significant.

2.4 Setup of the online gas chromatography analysis

The analysis and quantification of educt and product as well as the side products is done by an online GC method. Therefore, an Agilent® 7890 B was used which was equipped with a CP-Sil column and a thermal conductivity detector (TCD). During the preliminary tests, two main side products were found: Butyl butyrate which is formed in the *Tishchenko* reaction and 2-Ethylhexenal which is formed in an aldol condensation (Reaction scheme 14).[117-118] The quantification of both side produces as well as the educt and the product are done by referencing against nitrogen as internal (gas) standard.

The concentration of nitrogen in hydrogen was varied between 0-10 V-% and the respective peak area was measured (Figure 10). A linear trend was obtained.

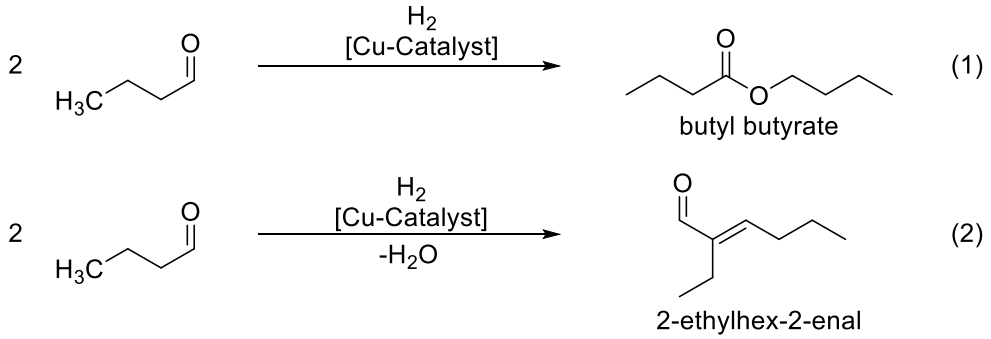

Reaction scheme 14: Possible side reactions during the butyraldehyde hydrogenation: Formation of 1.) butyl butyrate (Tishchenko) and 2.) 2-ethylhexenal (aldol condensation).

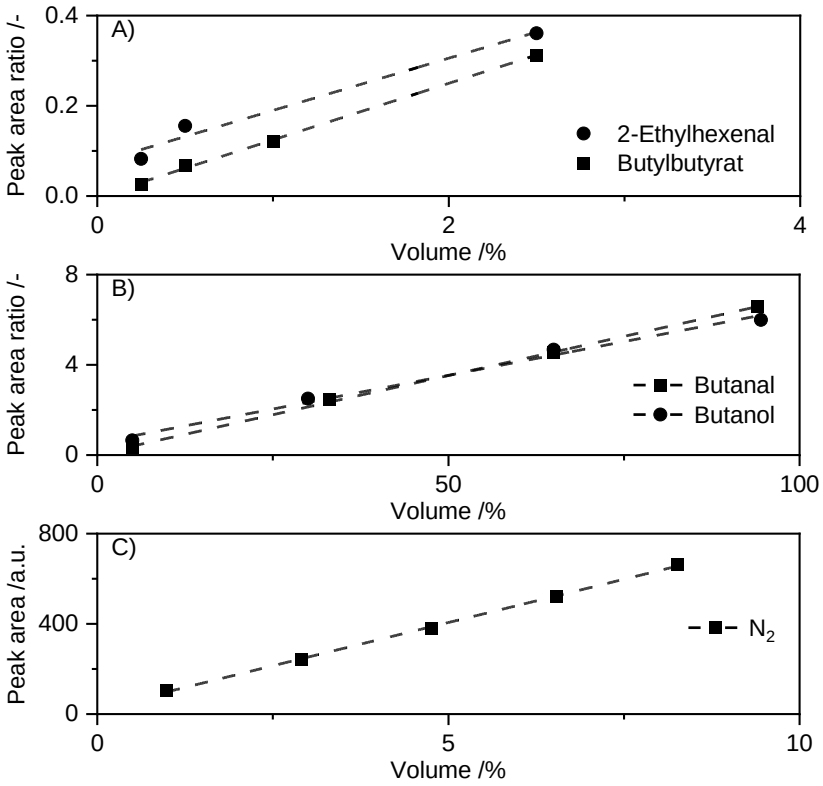

Figure 10: A) Peak area ratio (organic feed/N_2) of a) butyl butyrate and 2-ethylhexenal and B) butyraldehyde and butanol respectively C) peak area (N_2) as function of the V-% in the feed stream.

For the quantification of educt, product, and the side products the concentration in the gas stream was adapted according to the reaction conditions. The concentration of educt and

product was varied between 0-100 V-% (corresponds to 0-100 % X) while the concentration of the two side products was varied between 0-2.5 V-% (corresponding to 95-100 % S, both side products are C8 species in comparison to the C4 species butyraldehyde and butanol). For both educt and product, a linear trend was found with a similar slope and intercept (Figure 10). This fits to the similar thermal conductivity (a TCD is used as detector in the GC). For the side products, a linear trend is found as well. While the slope is nearly the same, 2-Ethylhexenal has a slightly higher intercept. Nevertheless, it must be considered that these species are calibrated between 0-2.5 V-% of organic feed. The total gas stream consists of roughly 90 V-% hydrogen and 10 V-% organic feed. This indicates that the quantification of the side products is done nearly at the detection limit of the TCD. At these low concentrations, the resulting variation is slightly higher compared to the calibration of educt and product. Nevertheless, both for educt and product as well as for the side products a linear detector signal as a function of the concentration was obtained with high coefficients of determination (Table 2).

Table 2: Linear equation (slope, intercept, and coefficient of determination (RSQ)) for the feed calibration.

	Slope	**Intercept**	**RSQ**
N_2	76.72	22.40	1.00
Butanal	0.07	0.05	1.00
Butanol	0.06	0.55	0.99
Butyl butyrate	0.13	0.00	1.00
2-Ethylhexenal	0.12	0.07	0.98

To summarize, a successful commissioning of the test unit ILS-601 was reached. In the first experiment, the reliability of the test unit was examined by a pure gas-phase reaction. It could be shown that the CO_2 methanation can be performed without problems and that all parts apart from the liquid feed dosing and vaporization of the unit work well. Subsequently, the dosing and vaporization of the feed were examined in detail. Accurate feed dosing was obtained by a change in the control of the HPLC pump. Mass spectrometry experiments coupled with GC experiments confirmed that the liquid feed is dosed accurately and that the vaporization takes place continuously. Feasible and reliable catalysis test conditions were obtained by preliminary tests. Transport limitations were excluded and isothermal conditions are guaranteed. Additionally, the educt and product as well as the two main side products were identified and can be quantified in a useful concentration range. The reliability of the whole unit during the butyraldehyde hydrogenation was reviewed and it was shown that catalysis tests can be performed reproducibly. The standard deviation was determined with 1 respectively 2 K depending on the reaction conditions.

3

Synthesis, Characterization and Catalytic Activity of Copper Catalysts

3.1 Introduction

Copper catalysts are used in a broad range of catalytic applications ranging from photocatalysis, electrocatalysis up to large scale gas-phase reactions.[66, 119-122] Especially in hydrogenation reactions copper is often used as preferred catalyst material.[123-124] Due to the favored hydrogenation of C-O bonds compared to C-C bonds, copper catalysts are often used for the hydrogenation of organic compounds like aldehydes, esters, ketones or acids.[125-128] Copper catalysts are also used for industrial scale gas-phase reactions, like the oxidation of carbon monoxide (CO), the reduction of nitrogen oxides (NO_x) the reverse water-gas shift reaction (RWGS) of the synthesis of methanol (CH_3OH).[129-133]

A huge variety of synthesis routes are available for pure and supported copper and copper nanoparticle catalysts ranging from electrochemical, photochemical, microwave and especially wet chemical methods.[87, 134-137] Important wet chemical methods are the impregnation, sol-gel methods and the precipitation.[89, 128, 138-139] The latter one is often used for the synthesis of metal oxide supported copper catalysts used in industrial scale gas-phase hydrogenation reactions, e.g., the methanol synthesis.[131] In this case, often precipitated copper-zinc(-aluminum) oxide catalysts are used. These catalysts are synthesized in a complex process starting with the co-precipitation of water-soluble copper, zinc and aluminum salts (e.g., nitrates) with an alkaline precipitation agent (e.g., sodium hydroxide or soda). Different precursor phases are obtained after precipitation and aging. After drying and a thermal treatment, an oxidic species is obtained which has to be (*in situ*) activated to aim the active catalyst which has preferable a high copper surface area.[140-141]

The obtained precursor phases are mainly hydroxycarbonates and hydroxynitrates which are formed during the precipitation and aging in their mother liquor. For commercially used methanol synthesis catalysts, in particular hydrozincite (HZ, $Zn_5(CO_3)_2(OH)_6$), aurichalcite (AU, $(Cu,Zn)_5(CO_3)_2(OH)_6$) and (zinc)-malachite ((Zn-)MA, $(Cu,Zn)_2(CO_3)(OH)_2$) are the predominant precursor phases. Additional phases like aluminum containing copper-hydrotalcite ($Cu_6Al_2(CO_3)(OH)_{16} \cdot 4\ H_2O$), georgeite ($Cu_5(CO_3)_3(OH)_4 \cdot 6\ H_2O$) and rosasite ($(Cu,Zn)_2(CO_3)(OH)_2$) are found, too. During the aging, a complex phase transformation of the precursor phases takes place.[142]

Although a thermal treatment and an activation step is conducted subsequently to the precipitation, the phase composition and the properties of the different precursor phases show a strong influence on the physical properties and the catalytic activity of the obtained copper-zinc catalyst. Behrens *et al.* attributes this to a “chemical-memory” in the multi-step synthesis process of copper-zinc catalysts.[141]

A variety of synthesis and precipitation conditions influence the properties and the phase composition of these precursors (which subsequently effects the active catalyst). The precipitation pH effects mainly the phase composition of the precursor. An optimum of around 8 is found for methanol catalysts as Baltes *et al.* claim. Li *et al.* found out that slightly acid

conditions (pH ≤ 6) lead to the formation of undesired hydroxynitrates which yields in less active catalysts. On the other hand, a precipitation pH above 10 allows the direct formation of copper oxide by oxolation. This leads to a decreased activity of the catalysts as Behrendt *et al.* state.[92-93, 140]

The copper-zinc ratio is another important factor and directly influences the precursor phase composition. While zinc rich catalysts precipitate predominantly in the aurichalcite precursor phase, (zinc-) malachite is the main precursor phase in copper rich catalyst. Behrens *et al.* claim that highly active catalysts are obtained if a maximum of zinc incorporation in the malachite structure is achieved. Porta *et al.* found that depending on the copper-zinc ratio a phase pure zinc-malachite structure (up to 15 % zinc) or a mixture of aurichalcite and zinc-malachite is formed.[94, 141]

Another important aspect is the use of additional metals and/ or metal oxides as promotors. Aluminum is often used as structural promotor. While Gusi *et al.* showed that aluminum influences the reduction behavior of copper-zinc catalysts, Wang *et al.* showed that the addition of aluminum as promotor to copper based catalyst leads to beneficial surface properties like smaller copper crystallites and a larger copper surface area resulting in a higher catalytic activity.[95, 143]

In addition to the influence of precipitation parameters, the thermal treatment subsequently to the precipitation is an important step in the complex synthesis procedure of copper catalysts. Tarasov *et al.* investigated in detail the decomposition of different copper-zinc hydroxycarbonates and showed that at least four decomposition steps under evolution of carbon dioxide and water take place and a high-temperature carbonate is formed as metastable intermediate. Interestingly, a direct activation of these oxycarbonates is possible and inconsistent reports regarding their catalytic activity are found.[144] While Baltes *et al.* reports an increase in activity compared to completely calcined catalysts, Schumann *et al.* report detrimental effects on the catalytic activity if phase pure HT-carbonates are used as catalyst precursor for the methanol synthesis.[92, 96, 145]

While a lot of work is done in the field of methanol synthesis over copper-zinc catalysts, only a limited number of reports deals with copper-zinc catalysts used in the hydrogenation of aldehydes or esters. While Rodrigues *et al.* discussed the influence of zinc on copper-silica catalysts used for the continuous gas-phase hydrogenation of crotonaldehyde, Pospelova *et al.* investigated the influence of synthesis methods of copper-zinc catalysts used for the slurry hydrogenolysis of esters. Yang *et al.* investigated the influence of aluminum on copper-zinc catalysts used for the gas-phase fixed bed furfural hydrogenation.[128, 146-147]

Another drawback is that most of the literature investigates the influence of one individual synthesis parameter of the catalyst on the properties and the catalytic activity while all other factors are kept constant. This can lead to the misinterpretation or overlooking of interaction effects which could take place during the synthesis of copper-zinc catalysts. As an example,

Li *et al.* showed that synthesis parameters like the aging temperature or the precipitation pH result often in similar effects on the precursor composition and the precipitation kinetics.[93]

To overcome these drawbacks, a detailed investigation of copper-zinc(-aluminum) catalysts used for the gas-phase hydrogenation of butyraldehyde is presented. A benchmark copper-zinc oxide catalyst is synthesized by classic co-precipitation, in detail characterized and used as reference system for comparison with a broad range of different copper-zinc(-aluminum) catalysts. The influence of a variety of synthesis and precipitation parameters like the copper to zinc ratio, the precipitation pH or the influence of aluminum on the precursor phase composition, the properties of precursor, calcined and activated species and the catalytic activity is presented. Therefore, different series of copper catalysts were synthesized by co-precipitation, aged in their mother liquor and dried to yield the hydroxycarbonates. These hydroxycarbonates as well as the oxide species obtained after a thermal treatment were characterized by elemental analysis (CHNS and ICP-OES), powder X-Ray diffraction (p-XRD), temperature programmed reactions, and the determination of the BET and the copper surface area. Selected catalysts were additionally characterized under different reaction atmospheres (inert, reductive, oxidative) by *in situ* p-XRD and thermal analysis methods as a function of temperature and/ or time. The catalytic activity of these catalysts was determined in a fixed bed setup during the gas-phase hydrogenation of butyraldehyde. In addition, a design of experiments approach is used to gain better understanding of the catalysts and the influence of different precipitation parameters. Furthermore, the possibility of the direct reductive activation of hydroxycarbonate/ oxycarbonate copper-zinc precursor phases is presented and beneficial effects are shown. Structurer-activity relationships of copper catalysts in the gas-phase hydrogenation of butyraldehyde are presented.

3.2 Synthesis, characterization and catalytic activity of a copper-zinc oxide catalyst

Within this chapter, the synthesis setup for copper catalysts as well as the standard copper-zinc benchmark catalyst is presented. The synthesis procedure, a detailed characterization of the catalyst as well as the catalytic properties are discussed. This benchmark catalyst is used for the comparison with a variety of copper catalysts, where a detailed study of the influence of synthesis conditions like the copper to zinc ratio, the precipitation pH value as well as the influence of aluminum is discussed. Furthermore, a direct activation approach of the catalyst precursors is presented as well as a systematic study of the influence of precipitation conditions by mean of a statistic design of experiments approach.

All copper catalysts discussed in this thesis were synthesized by (co-) precipitation in a double-walled glass setup stirred by a *KPG* stirrer (Figure 11). The synthesis setup consists of a double walled glass autoclave which can be pressurized by CO_2 (or any other gas) up to 0.5 bar g and heated with heating water over a thermostat (up to 95 °C). The precipitation is controlled by a *Metrohm* titrator which measures the pH-value during the synthesis by a pH-electrode and keeps the pH-constant by adding proper amount of the precipitation agent. The metal solution (e.g., copper-zinc nitrate solution) is added with a constant flow by a peristaltic pump. After precipitation and aging, the precipitate is filtered and washed with bi-distilled water until the conductivity of the washing water is below a certain value. The obtained precursor is subsequently dried and calcined. The activation is done *in situ* in the catalysis test setup before catalytic measurements.

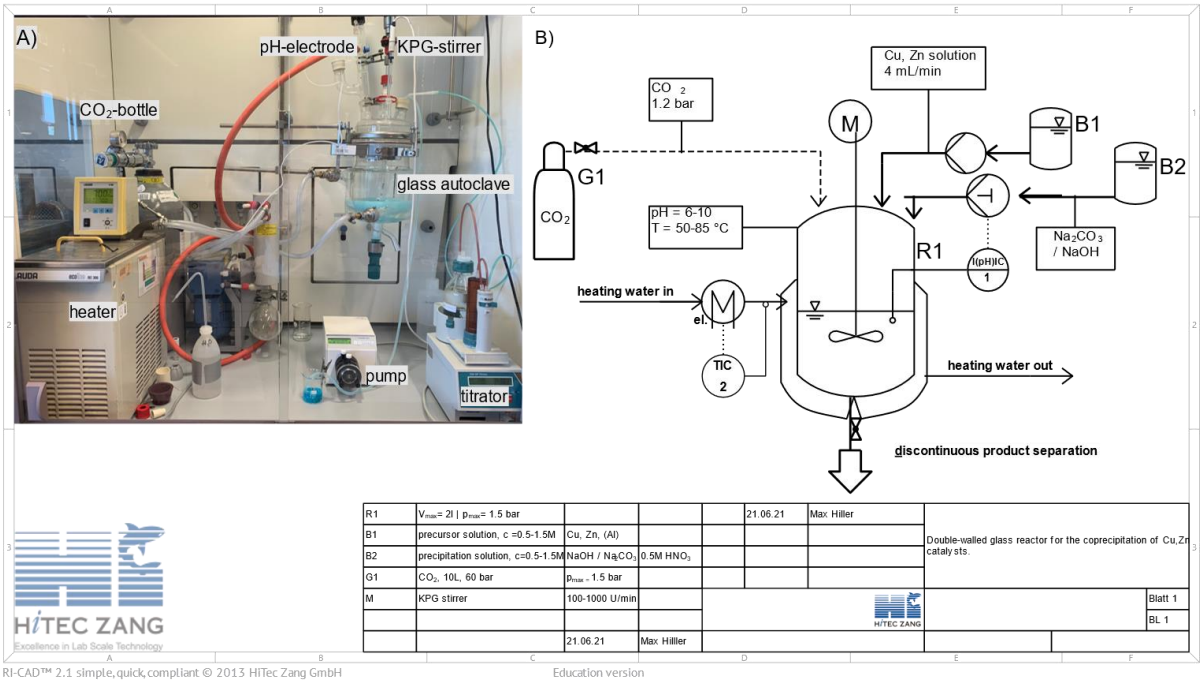

Figure 11: Precipitation setup for the synthesis of copper catalysts: A) Picutre of the double-wall glass synthesis autoclave and B) PI-diagram of the setup.

The standard synthesis route starts with a copper-zinc solution which is precipitated by soda, sodium hydroxide or mixtures of both. After precipitation, aging and washing, a copper-zinc hydroxycarbonate (precursor) is obtained which is subsequently dried and calcined to the corresponding oxide (Reaction scheme 15).

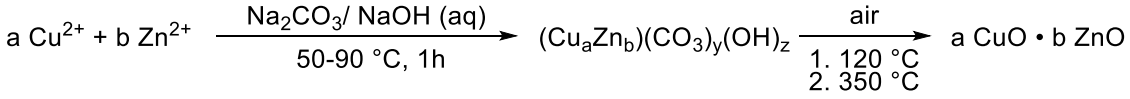

Reaction scheme 15: Standard synthesis of copper-zinc catalysts with soda/ sodium hydroxide yields. The precursor phase is obtained after precipitation, calcination yields the oxide.

The benchmark catalyst is synthesized starting from a copper-zinc nitrate solution with a copper to zinc ratio of 1:2 and soda as precipitation agent. After precipitation, aging, washing and drying a light blue powder is obtained. Elemental analysis was performed by both ICP-OES and CHNS. The molar copper to zinc ratio was found to be 1:2 while the total metal loading of the precursor is 65.3 wt-%. Furthermore, carbon (4.2 wt-%) and hydrogen (1.1 wt-%) are found yielding a molar ratio of hydrogen to carbon 3:1 (Table 3). Powder XRD analysis of the precursor shows main reflexes according to aurichalcite and hydrozincite.[148-149] Furthermore, reflexes according to (Zn-) malachite can be found.[150] A quantitative Rietveld refinement yields in phase composition of 33.1 % Hydrozincite, 56.6 % Aurichalcite and 10.3 % (Zn-) malachite (Figure 12, A). Raman spectroscopy confirmed the existence of both carbonate and hydroxide groups (Figure 13, A). The carbonate group is indicated at 1072 cm^{-1} ($v1(CO_3)^{2-}$) as well as 1506, 1485 and 1337 cm^{-1} ($v3(CO_3)^{2-}$)). Additionally, the intense band at 1060 cm^{-1} is attributed to the OH deformation mode.[151] The measured spectrum is in accordance with the reference spectrum for aurichalcite.

Table 3: Elemental analysis (ICP-OES and CHNS) of the precipitated and calcined copper-zinc reference catalyst.

Sample	Cu	Zn	M	n(Zn:Cu)	C	H	n(H:C)
	wt-%	wt-%	wt-%	-	wt-%	wt-%	-
Cu-Zn precipitated	21.2	44.0	65.3	2.0	4.2	1.1	3.1
Cu-Zn calcined	27.3	57.4	84.7	2.0	0.3	0.0	n.d.

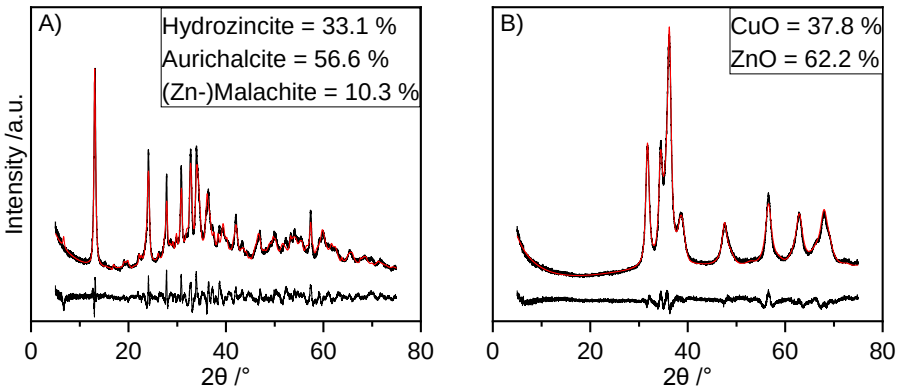

Figure 12: Rietveld refinement of the copper-zinc reference: A) precipitated and B) calcined. Measured (black line) and refinement (red line). Difference between refinement and measured in black, bottom line. Reference patterns from the COD data base (HZ: 96-900-7482, AU: 96-900-7689, MA: 96-900-7491, CuO: 96-101-1149, ZnO: 96-900-4179).[148-150, 152-153]

Summarizing these results, the precursor phase can be described mainly as a 1:2 mixture of the zinc pure hydrozincite phase ($Zn_5(CO_3)_2(OH)_6$) as well as the copper and zinc-containing aurichalcite phase ($(Cu,Zn)_5(CO_3)_2(OH)_6$). The molar metal ratio of copper:zinc 1:2 is in accordance both with the desired copper to zinc ratio as well as with the predominant zinc rich aurichalcite phase. In addition, the total metal loading is in rough accordance with both aurichalcite and hydrozincite phase (65.3 wt-% found, around 60 wt-% expected). The slightly higher metal loading could be explained by a partial decomposition process which takes place already during the drying at 120 °C. The CHNS results fit both hydrozincite and aurichalcite phase very well (expected for both phases: carbon 4.4 %, hydrogen 1.1 %). The hydrogen to carbon ratio in both phases is 3:1 as found in the CHNS analysis. The quantitative XRD refinement confirmed the existence of the two main phases hydrozincite as well as aurichalcite with a ratio of around 1:2. Furthermore, Raman spectroscopy indicates both hydroxy as well as carbonate groups and the reference pattern for aurichalcite matches the measured spectrum quite well.

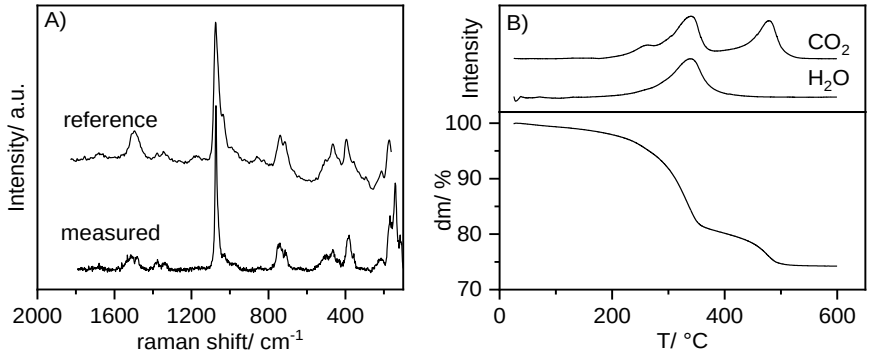

Figure 13: A) Raman spectrum (reference: aurichalcite) and B) thermogravimetric analysis of the precipitated copper-zinc reference catalyst.

The calcination process of the precursor to the oxide was monitored via thermogravimetric analysis coupled with mass spectroscopy (TGA-MS). Both mass loss and the MS signals for H_2O (m/z = 18) and CO_2 (m/z = 44) were recorded (Figure 13, B). The two decomposition steps can be found in the calcination to the oxide. In the first step, a mass loss of around 18 % under release of both water and carbon dioxide is found at 180-300 °C while the second step between 300-450 °C shows a mass loss of around 7 % under release of only carbon dioxide. The intermediate can be described as high temperature carbonate, an oxycarbonate species.[145, 154] Summarizing, the decomposition from the precursor to the oxide takes place in two steps where a meta-stable high temperature carbonate modification is found as intermediate (Reaction scheme 16). A detailed discussion of the high temperature carbonate is given later (chapter 3.5).

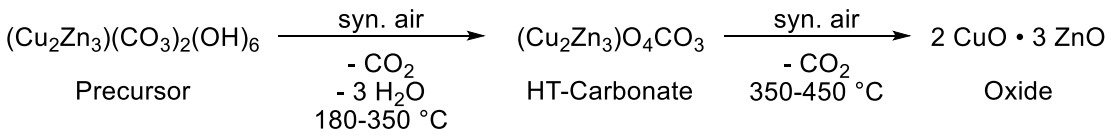

Reaction scheme 16: Decomposition of the precipitated copper-zinc reference catalyst.

The total metal loading of the complete calcined oxide was found to be 84.7 wt-% while the copper to zinc ratio was not affected and remains at 1:2 (Table 3). The carbon amount was found to be 0.3 % while hydrogen could not be detected in the CHNS analysis. Reflexes according to copper oxide as well as zinc oxide could be found in the XRD pattern (Figure 12, B).[153, 155] Additional phases could not be found. The phase composition (by quantitative Rietveld refinement) was determined to be 37.8 to 62.2 % copper oxide to zinc oxide. The total surface area (BET-surface area) was found to be 48 m^2g^{-1} while the particle size of copper oxide and zinc oxide were determined by Scherrer equation (Table 5).[156] The copper oxide particles are slightly smaller compared to the zinc oxide particles (4.4 respectively 7.4 nm). Summarizing, a nearly phase pure copper-zinc oxide with a copper to zinc ratio of around 1:2 is obtained after calcination. Minor carbon residuals of 0.3 % indicate that traces of high-temperature (HT) carbonate species could be left in the catalyst after calcination at 350 °C. The copper-zinc oxide precatalyst is activated in the catalysis test setup to form the active species. Therefore, copper oxide is reduced to copper(0) under hydrogen. In industrial scale applications, the catalyst activation is performed at very mild conditions (minimal heating ramps, low hydrogen concentration in the gas stream, low total volumetric gas stream (GHSV)) to prevent hotspots and to yield a high copper surface area. The activation takes normally often one or even more days.[157] To obtain appropriate activation conditions, a reduction condition screening was performed with the benchmark copper-zinc catalyst. The heating ramp was varied between 2 to 5 $Kmin^{-1}$ and the hydrogen concentration in the gas stream was varied between 5 to 50 V-%. Due to limitations of the mass flow controllers of the catalysis test setup, with decreasing hydrogen concentration, the GHSV was increased from 1.000 to 10.000 h^{-1}. The catalysts were heated to 200 °C under flowing hydrogen and kept at this temperature for one hour. The reduction was monitored with TPR-MS and XRD pattern of the reduced catalyst were taken under inter conditions. The phase composition (copper(0), copper oxide and zinc oxide) and the particle size of copper(0) and zinc oxide (Scherrer equation) were calculated.

It could be shown that the reduction at a heating ramp of 5 $Kmin^{-1}$ and a high and middle hydrogen concentration (50 respectively 20 V-%) yields in a quite sharp reduction peak in the temperature range of around 175-200 °C (option 1 and 2). The reduction of copper oxide to copper(0) takes place in around 10 to 15 minutes (Figure 14). In the case of the 5 V-% hydrogen reduction, the reduction starts in the isothermal region at 200 °C. The reduction peak is much broader and the reduction takes longer (over 30 minutes, option 3). For the reduction with 2 $Kmin^{-1}$ and 20 V-% hydrogen, the reduction peak is also very broad and starts in the isothermal region at 200 °C (option 4). This reduction takes also around 30 minutes.

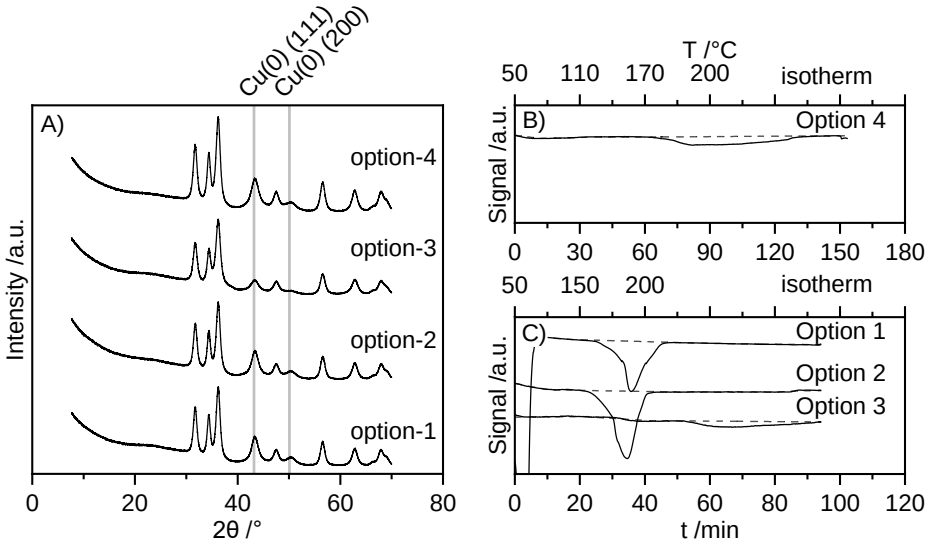

Figure 14: Different reduction options of the copper-zinc reference catalyst. A) Capillary XRD of the four options and B) + C) TPR (2 respectively 5 $Kmin^{-1}$ heating ramp). Reference patterns from the COD data base (Cu: 96-151-2505).[158]

It could be shown that in the case of option 1,2 and 4 a complete reduction of copper(II) to copper(0) was obtained (around 30-35 % copper and 65-70 % zinc oxide) while the reduction is not complete in the case of option 3 (Table 4). In this case, only 3 % copper(0) are found while still large amounts of copper(II) oxide are present (19 %). This indicates a very low reduction degree of only around 15 %. While the copper(0) crystallite size was determined to be 3.7 respectively 4.1 nm for option 1 and 2, the crystallite size found for option 3 and 4 is significant smaller for option 3 and 4 (3.1 respectively 3.2 nm), indicating that a reduction over a longer time is milder and yields in smaller copper crystallites. The zinc oxide crystallite size is not affected from the copper reduction and stays nearly constant with 7.1-7.4 nm.

Table 4 Reduction condition screening of the copper-zinc reference catalysts. a) determined by Rietveld refinement; b) Crystallite size determined by Scherrer equation.

Option	**V (H_2)**	**GHSV**	**T. ramp**	**Cu[a]**	**CuO[a]**	**ZnO[a]**	**Cu cry. size[b]**	**ZnO cry. size[b]**
	%	h^{-1}	$Kmin^{-1}$	%	%	%	nm	nm
1	50	1 000	5	36	0	64	3.7	7.1
2	20	3 000	5	32.7	0	67.3	4.1	7.3
3	5	10 000	5	2.6	19	78.4	3.1	7.3
4	20	3 000	2	31	0	69	3.2	7.4

In conclusion, it could be shown that the reduction at 2 $Kmin^{-1}$ (20 V-% hydrogen) is beneficial regarding both a small copper crystallite size as well as a full reduction of copper (option 4). If the hydrogen concentration is too low and the GHSV to high (5 V-% hydrogen, 10.000 h^{-1} total GHSV) the reduction is incomplete and a reduction degree of only 15 % is reached. A heating ramp of 5 $Kmin^{-1}$ and a middle and high hydrogen concentration leads to a complete reduction but larger crystallites compared to the reduction at 2 $Kmin^{-1}$ heating ramp. It could be shown that option 4 (2 $Kmin^{-1}$ and 20 V-% hydrogen) has significant advantages compared to the other activation options and was chosen as standard (*in situ*) activation procedure (Reaction scheme 17).

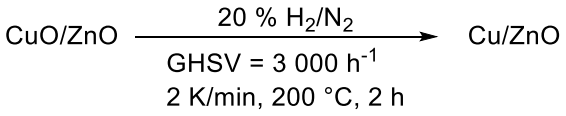

Reaction scheme 17: Standard activation of the copper-zinc reference catalysts.

The copper surface area was determined by standard nitrous oxide titration after reduction at the above discussed conditions.[159] A surface area of 10 m^2g^{-1} respectively a copper dispersion of 5.9 % were determined (Table 5). This is in accordance to literature for standard copper-zinc catalyst synthesized by co-precipitation with a medium copper loading.[160] Additionally, the reduction degree was determined by a TPR-TCD measurement (Table 5). A reduction degree of 99 % was obtained indicating a complete reduction of copper.

Table 5: Physical properties of the copper-zinc reference catalyst before and after reduction. A) Determined by TPR-TCD; b) Determined by N_2 isotherm before reduction; c) determined by N_2O copper surface area titration after reduction and d) determined by Scherrer equation before and after the reduction.

Reduction degree [a]	**BET-SA** [b]	**Cu-SA** [c]	**Cu-Dispersion** [c]	**Cry. Size Cu** [d]	**Cry. Size CuO** [d]	**Cry. Size ZnO** [d]
%	m^2g^{-1}	m^2g^{-1}	%	nm	nm	nm
99	48	10	5.9	3.2	4.4	7.4

The hydrogenation of butyraldehyde (Reaction scheme 13) was used as model reaction to determine the catalytic activity of the benchmark copper-zinc catalyst. The reaction was performed in a temperature region between 90-140 °C. A sigmoidal curve is obtained where an initial activity of a few percent is obtained at 90 °C (Figure 15). The T_{50} was determined to be 113 °C while full conversion is reached at around 140 °C. A sigmoidal function was used to fit the measured temperature-conversion points. The selectivity to *n*-butanol was determined to be above 99.7 % at full conversion, only traces of butyl butyrate could be found.

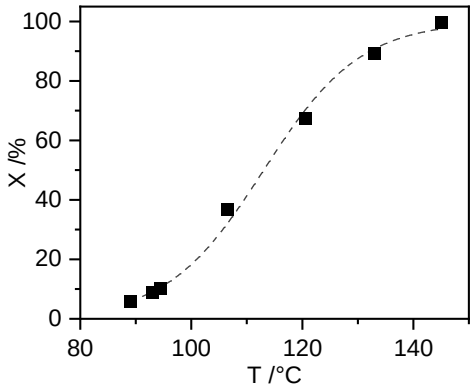

Figure 15: Catalytic activity (conversion as function of the temperature) of the copper-zinc reference catalyst.

Summarizing, a benchmark copper-zinc oxide catalyst was synthesized by coprecipitation, fully characterized and the catalytic activity was determined. Additionally, feasible activation conditions were identified. This system is used as a reference system for the further thesis.
The precipitation of copper and zinc in a ratio of 1:2 and soda as a precipitation agent leads to a precursor consisting mainly of zinc pure hydrozincite and the copper and zinc-containing aurichalcite phase. The calcination to the oxide undergoes two decomposition steps, where a

metastable high-temperature carbonate is found as an intermediate. The fully calcined catalyst consists of copper(II) and zinc(II) oxide with a ratio of around 40 to 60 as expected. Under feasible activation conditions (20 V-% hydrogen, 2 $Kmin^{-1}$, 200 °C), a mild reduction is obtained yielding in small copper(0) crystallites (3.2 nm), a full reduction of copper and a high copper surface area (10 m^2g^{-1}). A sigmoidal temperature conversion behavior was obtained in the hydrogenation of butyraldehyde with a T_{50} of 113 °C. This benchmark copper-zinc oxide catalyst is used as a reference system.

3.3 Influence of precipitation parameters on physical properties and catalytic activity

The influence of a variety of precipitation conditions of copper catalysts on their physical properties as well as the catalytic behavior is investigated. The investigated copper-zinc catalysts were synthesized by (co-) precipitation and the influence of the copper to zinc ratio and the pH value during the precipitation is investigated. After precipitation, the precursor phase is obtained which is characterized by p-XRD as well as elemental analysis (ICP-OES and/ or CHNS). The precursor phase is calcined to yield the desired oxide, which is analyzed regarding surface properties (total BET surface area, active copper surface area) as well as the reduction behavior by temperature programmed reduction. Additionally, elemental analysis as well as p-XRD is measured. The obtained catalysts were *in situ* activated and the catalytic activity as well as selectivity was determined in the hydrogenation of butyraldehyde to *n*-butanol. Structure-activity relationships shall be drawn.

3.3.1 Influence of the copper loading

Different loaded copper-zinc catalysts were synthesized by (co-) precipitation. The copper loading was varied between 10 to 80 wt-% copper regarding the total metal content. The remaining precipitation conditions (precipitation agent and concentration, pH during the precipitation, aging conditions) were kept constant for all catalyst. At the applied precipitation conditions (soda as precipitation agent, pH = 8), copper-zinc hydroxycarbonates are obtained as precursor phase.[160-162] Depending on the copper-zinc ratio, a variety of different precursor phases will be obtained (Reaction scheme 18). Hydrozincite ($Zn_5(CO3)_2(OH)_6$) is expected as predominate phase for zinc pure catalysts, while with increasing copper loading aurichalcite ($(Cu,Zn)_5(CO3)_2(OH)_6$) and zinc-malachite ($(Cu,Zn)_2(CO_3)_2(OH)_2$) will be present. Aurichalcite is the predominate phase for zinc rich catalyst (30-90 % zinc) while zinc-malachite is expected for copper rich catalysts (70-100 % copper). For pure copper catalysts the zinc-free malachite phase ($Cu_2(CO_3)_2(OH)_2$) is expected. Nevertheless, for both copper and zinc-containing catalysts a mixture of different phases is expected.

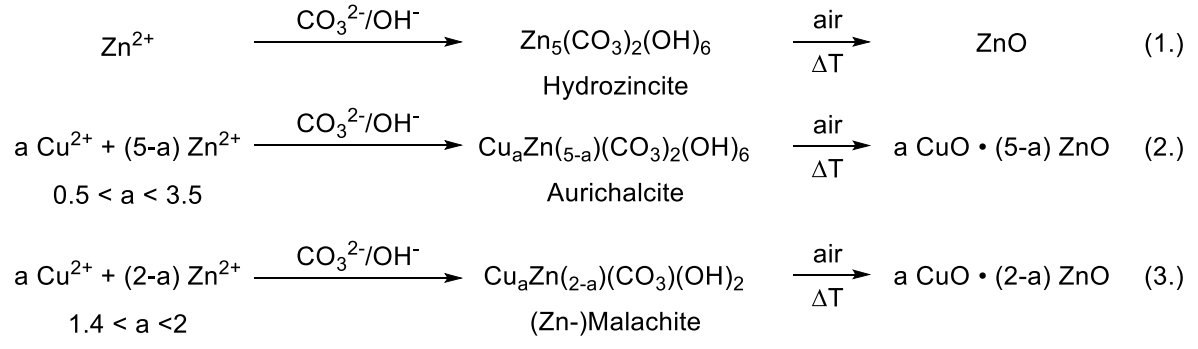

Reaction scheme 18: Influence of the copper-zinc ratio on the precursor phase of copper-zinc catalysts.

The copper and zinc loading of the catalysts was determined by ICP-OES (Table 6). It could be shown that the aspired copper-zinc ratio starting from 10 to 90 wt-% up to 80 to 20 wt-% copper to zinc was obtained. Only minor deviation of less than one percent could be found. The total metal loading was measured to be between 63.5-68.2 wt-%, no clear trend could be indicated. For both precursor phases, aurichalcite and zinc-malachite, a total metal loading of around 60 wt-% is expected. The slightly higher metal loading found can be explained by a partial decomposition which takes place already during the drying process at 120 °C. A minor mass loss can already be found at temperatures up to 120 °C in the thermogravimetric analysis for the benchmark copper-zinc catalyst (Figure 13, B).

XRD pattern were taken for selected catalysts. While zinc rich catalysts show mainly reflexes according to hydrozincite (HZ) and aurichalcite (AU), copper rich catalysts show mainly reflexes according to malachite (MA, Figure 16, A).[148-150] The phase composition of the obtained precursors was determined for selected catalysts by quantitative Rietveld refinement (Table 6). The 10:90 copper-zinc catalyst consists of 90 % hydrozincite and around 10 % aurichalcite. Zinc-malachite is not found as precursor phase. For the 30:70 copper-zinc catalyst, aurichalcite is found to be the predominant phase with nearly 60 %. Additionally, around 30 % hydrozincite and 10 % zinc-malachite are found. With increasing copper loading, the amount of hydrozincite decreases drastically. For both 60:40 and 80:20 copper-zinc catalysts no hydrozincite can be found anymore. On the other hand, the amount of zinc-malachite increases from 10% for the 30:70 copper-zinc catalyst over 63 % to nearly 80 % for the 60:40 and 80:20 copper-zinc catalyst). Summarizing, with increasing copper loading the proportion of the hydrozincite phase decreases (this phase is only found up to around 30 % copper) while the zinc-malachite phase increases (for the 80:20 copper-zinc catalyst nearly 80 % zinc-malachite phase is obtained). The aurichalcite phase is predominant for low to medium loaded copper catalysts and has its maximum at around 30 % copper (Figure 16, B).

Table 6: Physical properties of precipitated copper-zinc catalysts with varied Cu-loading. A) Metal loading determined by ICP-OES; b) Phase composition determined by Rietfeld refinement; c) Mass loss during calcination.

Cu-loading	**Cu [a]**	**Zn [a]**	**Cu/(Cu+Zn) [a]**	**HZ [b]**	**AU [b]**	**(Zn)-MA [b]**	**Mass loss calcination [c]**
%	%	%	%	%	%	%	%
10	6.3	59.9	9.6	89.8	10.2	0	24.4
20	13.3	53.1	20.0	n.d.	n.d.	n.d.	23.7
30	18.9	44.6	29.7	30.7	59.9	9.4	20.5
40	26.7	40.0	40.0	n.d.	n.d.	n.d.	19.2
50	32.2	32.8	49.6	n.d.	n.d.	n.d.	19.0
60	38.4	26.4	59.2	0	37.1	62.9	20.3
70	47.4	20.4	69.9	n.d.	n.d.	n.d.	23.7
80	54.4	13.8	79.7	0	23.3	76.7	25.1

The obtained precursor phases were calcined to yield the desired copper-zinc oxide catalysts. The mass loss during the calcination was determined to be between 19-25 % (Table 6). A

mass loss of around 25 % would be expected for the calcination of the precursor phases to the oxide. It could be shown that the medium loaded copper-zinc catalysts show with around 19 % a slightly lower mass loss than expected. It can be expected that these catalysts decompose slightly more in the drying process compared to catalysts with a quite high or low copper amount.

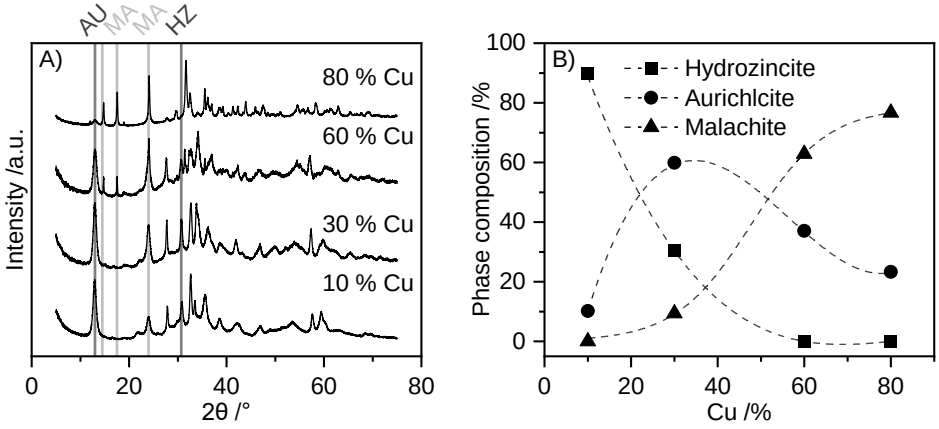

Figure 16: A) pXRD pattern of the precipitated copper-zinc catalysts and B) phase composition in dependence of the copper loading. Reference patterns from the COD data base (HZ: 96-900-7482, AU: 96-900-7689, MA: 96-900-7491).[148-150]

Compared to the phase pure hydrozincite and malachite phase, the decomposition starts at slightly lower temperatures for the mainly aurichalcite containing copper catalysts (Figure 13, B).[163-164] On the other hand, no clear trend could be found for the total metal loading (Table 6). A minor deviation in the temperature during the drying could also explain the slightly lower mass loss during the calcination found for the medium loaded copper catalysts. Another hypothesis could be that a higher copper-zinc interaction which can be assumed for aurichalcite rich catalysts (due to a better chemical mixture between copper and zinc compared to mainly zinc or copper containing hydrozincite/ malachite) supports a partial decomposition already at very mild temperatures.[165]

Table 7: Physical properties of calcined copper-zinc catalysts with varied copper loading. A) Metal loading determined by ICP OES; b) Phase composition determined by Rietfeld refinement; c) determined by TPR; d) determined by N_2O copper surface area titration.

Cu-loading	**Cu** [a]	**Zn** [a]	**Cu/(Cu+Zn)** [a]	**CuO** [b]	**ZnO** [b]	**Red. degree** [c]	**Mean red. T.** [c]	**Cu-SA** [d]	**Cu-Disp.** [d]
%	%	%	%	%	%	%	°C	%	%
10	8.4	78.1	9.7	11.7	88.3	91	166	3	4.8
20	17.3	68.7	20.1	n.d.	n.d.	90	170	7	6.4
30	24.6	56.7	30.3	37.4	62.6	97	181	13	8.4
40	32.9	48.5	40.4	n.d.	n.d.	n.d.	n.d.	n.d.	n.d.
50	40.0	39.4	50.4	n.d.	n.d.	n.d.	166	18	7.0
60	48.8	32.3	60.2	63.3	36.7	97	158	15	4.9
70	53.1	22.7	70.1	n.d.	n.d.	n.d.	n.d.	n.d.	n.d.
80	59.4	14.9	79.9	81.4	18.6	96	179	13	2.9

The copper-zinc ratio in the calcined catalysts follows the trends found for the precursor phase catalysts and was found to be nearly as expected (Table 7). The total metal content for fully

calcined copper-zinc oxide catalysts would be expected to be around 80 wt-%. It could be shown that a roughly linear trend is obtained (Figure 17). The total metal loading for nearly phase pure zinc catalysts was measured to be 86.5 % while this value decreases to 74.3 % for the 80:20 copper-catalysts. It can be expected that 350 °C calcination temperature is slightly too low to allow full calcination to the oxide phase for the high loaded copper catalysts. This is in rough agreement with thermogravimetric analysis of phase pure hydrozincite and malachite phase, where the malachite phase needs slightly higher temperatures for full decomposition compared to the hydrozincite and aurichalcite phase.[163-164]

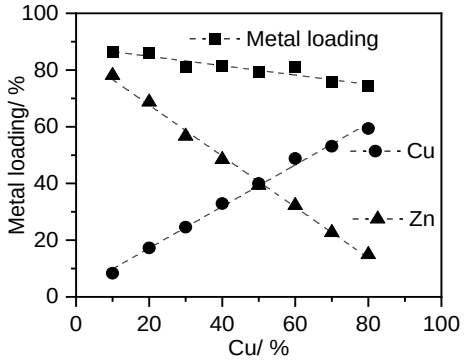

Figure 17: Metal loading of the calcined copper-zinc catalysts in dependence of the copper-loading.

The analysis of the p-XRD pattern revealed that only reflexes according to copper(II) oxide as well as zinc(II) oxide are present (Figure 18, A).[153, 155] A quantitative Rietveld refinement shows a linear increase of the copper oxide phase with increasing copper loading while the zinc oxide phase is decreasing (Figure 18, B). The composition between copper and zinc oxide fits quite well to the elemental analysis results, only the 30:70 copper-zinc catalyst shows with 37 % copper(II) oxide a slightly higher value than expected. Although the quality of the refinement for the oxide catalysts was quite high, small uncertainties have to be considered. It can be assumed that the copper-zinc oxide phase ratio is also around 30:70 %.

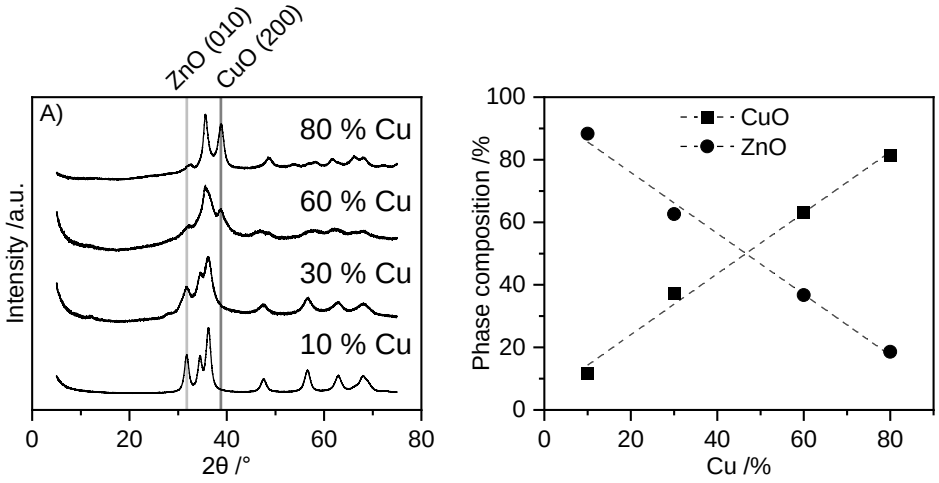

Figure 18: A) pXRD of calcined copper-zinc catalysts and B) phase composition in dependence of the copper loading. Reference patterns from the COD data base (CuO: 96-101-1149, ZnO: 96-900-4179).[153, 155]

Thermogravimetric data reveal that the decomposition of mainly zinc-containing precursor phases (hydrozincite, aurichalcite) takes place at slightly lower temperatures compared to

copper rich precursor phases ((zinc-) malachite) indicating that probably both copper and zinc are decomposed to the corresponding oxide. Therefore, a slightly deviation from the Rietveld refinement seems reasonable.

Temperature programmed reduction of the obtained catalysts was measured after the calcination (Figure 19, A). A single reduction peak is obtained for all catalysts, only the highest loaded 80 % copper catalyst shows a very broad shoulder at higher temperatures. The reduction takes place at around 150-200 °C for all catalysts. A parabolic shaped curve is obtained when the mean reduction temperature is plotted against the copper loading (Figure 19, B). The mean reduction temperature was highest for the 30 % copper catalyst with 181 °C, both increasing and decreasing copper loading leads to a lower mean reduction temperature. Only the highest loaded 80 % copper catalyst shows with 179 °C also a quite high reduction temperature. It can be assumed that the reduction temperature is influenced by the interaction of copper and zinc, where a high copper-zinc interaction leads to a higher reduction temperature. This indicates that especially the from the mainly aurichalcite containing precursors synthesized catalysts show a high copper-zinc interaction which is harder to reduced compared to copper oxide obtained from the zinc-malachite precursor. The copper pure malachite phase is also harder to reduce compared to both copper and zinc-containing zinc-malachite phase.[166] The reduction degree was found to be nearly 100 %, only the lower loaded 10-20 % copper catalysts have with 90-91 % a slightly lower reduction degree. It can be assumed that a minor amount of copper is incorporated into the hydrozincite lattice which cannot be reduced anymore.[160] The remaining catalysts show a full reduction within the tolerance of the TPR method.[161, 167]

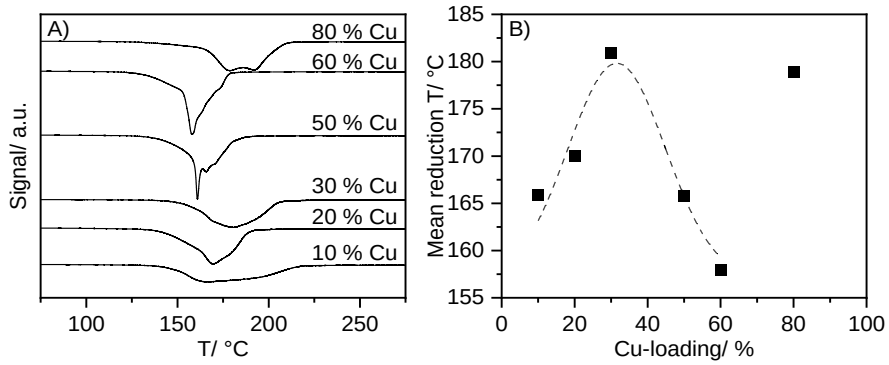

Figure 19: A) Reduction profile of the copper-zinc catalysts and B) mean reduction tempearture in dependence of the copper loading.

The copper surface area was determined to be between 3 to 18 m^2g^{-1} with its maximum found for the 50 % copper loaded catalyst. Related catalysts show similar results.[161] Both increasing and decreasing copper loading reduces the copper surface area. A parabolic course is obtained which is also found for the copper dispersion. For the copper dispersion, the trend is slightly shifted to lower loaded copper catalyst. The minimum dispersion of 2.9 % is found for the 80 % copper catalyst while the highest dispersion of 8.4 % is found for the 30 % copper catalyst. Decreasing the copper loading further also decreases the copper dispersion. This

supports the hypothesis further that catalysts synthesized from the aurichalcite precursor have a slightly higher copper-zinc interaction and show beneficial surface properties.

The hydrogenation of butyraldehyde was used to determine the catalytic activity and selectivity of the synthesized catalysts (Table 8). For all catalysts a sigmoidal temperature conversion behavior is obtained (Figure 20, A). Initial conversion is found for all catalyst at temperatures between 80-100 °C, while at around 180 °C all catalysts show full conversion. The selectivity was determined to be above 99.5 % for all catalysts at full conversion, so the selectivity is not affected by the copper loading or the phase composition of the precursor. The T_{50} (temperature where 50 % conversion is reached) was determined by a sigmoidal curve fit and was used to describe the activity of the catalysts in dependence on the copper loading. It could be shown that the 30 and 50 % copper catalyst show the lowest T_{50} (highest activity) while increasing or decreasing the copper loading leads to less active catalysts. The T_{50} – copper loading dependences follows roughly a parabolic trend (black curve, Figure 20, C). The same trend is obtained for the copper dispersion in dependence on the copper loading (red curve, Figure 20, B). The highest copper dispersion is also obtained for the catalysts which have a medium copper loading.

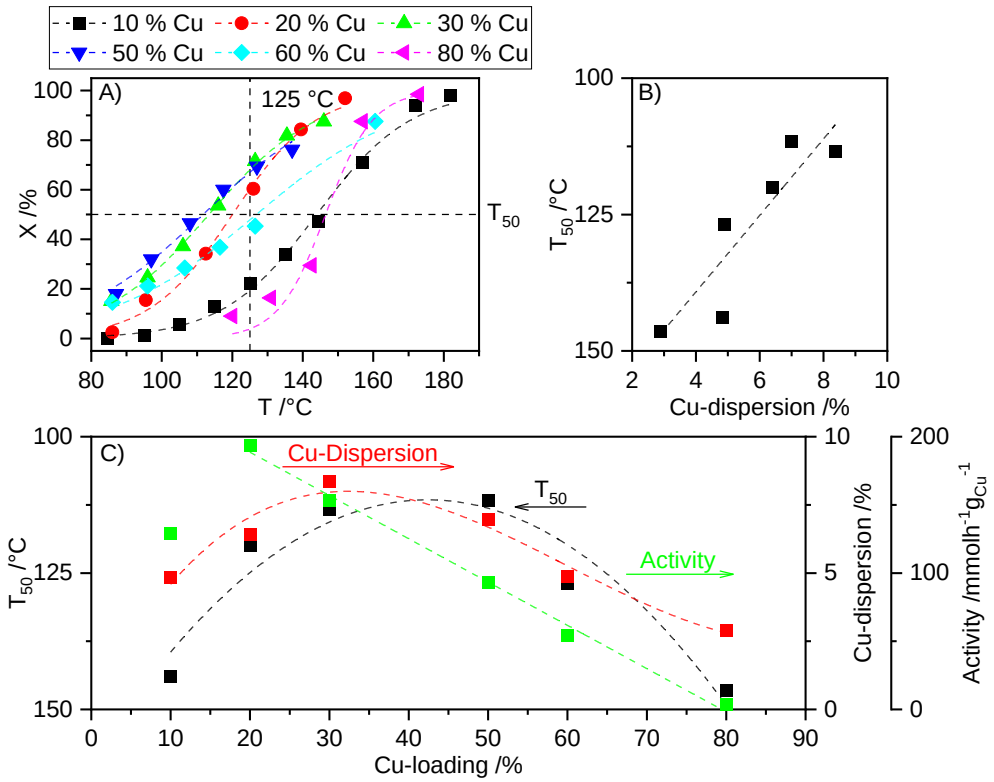

Figure 20: A) Conversion-temperature dependence of copper-zinc catalysts; B) catalytic actvity (T_{50}) as function of the copper dispersion and C) T_{50} (black, left y-axis), copper dispersion (red, right y-axis) and activity (green, right 2nd y-axis) in dependence of the copper loading.

A similar parabolic trend is obtained for both the T_{50} and the copper dispersion in dependence on the copper loading. This indicates a clear dependence of the catalytic activity and the copper dispersion. This can be also seen if the T_{50} is displayed as a function of the copper dispersion, where a linear trend is obtained (Figure 20, B). An increasing copper dispersion

leads to a higher number of active centers which increase the catalytic activity. On the other hand, it has to be mentioned that the trend cannon be described perfectly by a linear trend, so it seems that there are also other parameters which influence the catalytic activity.

Another trend can be identified when the catalytic activity in dependence on the copper amount of the catalyst (in mmol $h^{-1}g^{-1}_{Cu}$) is displayed as a function of the copper loading (green curve, Figure 20, C). Therefore, the conversion at 125 °C was extrapolated from the sigmoidal curve fit and the activity in dependence on the copper amount of the catalysts at this temperature was calculated. Here, a linear decreasing trend is obtained starting from the 20 % copper catalyst. This catalyst has an activity of around 200 mmol butyraldehyde conversion per hour and gram copper while with increasing copper loading the activity decreases to around 3 mmol butyraldehyde conversion per hour and gram copper. The only catalyst which does not fit in this trend is the 10 % copper catalyst which has a slightly lower activity compared to the 20 % copper catalysts. It can be assumed that this catalyst is slightly less active due to its huge amount of copper free hydrozincite in the precursor phase which leads to lower copper-zinc interactions compared to higher loaded copper catalysts. Additionally, as seen from the TPR results, it can be assumed that a part of the copper is incorporated in the hydrozincite phase. Regarding the copper amount, lower loaded copper catalysts show a higher activity at 125 °C.

Table 8: Catalytic activity and copper dispersion of copper-zinc catalysts.

Cu-loading	**Cu**	**T_{50}**	**Cu-Dispersion**	**X at 125 °C**	**Activity**
%	%	°C	%	%	$mmolh^{-1}g_{Cu}^{-1}$
10	8.4	143.9	4.8	19.4	129.1
20	17.3	120.0	6.4	60.3	193.9
30	24.6	113.4	8.4	68.0	153.5
50	40.0	111.7	7.0	67.1	93.2
60	48.8	126.8	4.9	47.9	54.4
80	59.4	146.5	2.9	3.9	3.6

In conclusion, it could be shown that all copper-zinc catalysts show activity in the butyraldehyde conversion in the temperature range between 100 to 200 °C. Catalysts with a higher copper dispersion are in general more active. These catalysts are especially gained from precursors which contain mainly aurichalcite as the predominant precursor phase. These catalysts seem to have stronger copper-zinc interactions compared to catalysts gained from zinc-malachite-rich precursor phases. This fits additionally to the trend that the catalytic activity as a function of the copper loading is highest for low-loaded copper catalysts. These are mainly gained from aurichalcite-containing precursors. In the field of methanol synthesis (where similar copper-zinc oxide catalysts are used), a “chemical memory effect” is attributed to the catalysts. This memory effect transfers properties from the precursor over the calcined oxide to the active catalyst.[168] For the butyraldehyde hydrogenation, it can be concluded that catalysts gained from aurichalcite-rich precursor phases are beneficial regarding physical properties (e.g., a broader reduction profile, higher copper-zinc interaction), as well as the catalytic activity.

3.3.2 Influence of the precipitation pH-value

The influence of the pH value during the precipitation of copper-zinc catalysts on surface properties as well as the catalytic activity in the hydrogenation of butyraldehyde was investigated. A series of copper-zinc oxide catalysts were synthesized by (co-) precipitation starting from the metal nitrates and soda as precipitation agent. The copper to zinc ratio was fixed to 1 to 2 (preliminary results revealed the highest activity for these catalysts in the hydrogenation of butyraldehyde, chapter 3.3.1). While the pH value was varied during the precipitation, all other precipitation parameters (aging conditions, concentration, stirring) were kept constant (Reaction scheme 18.2). After precipitation, the obtained precursors were characterized by p-XRD, BET surface area determination as well as elemental analysis. Subsequently, the precursors were calcined to yield the desired copper-zinc oxide and characterized as well with the above-mentioned techniques. The activity of the catalysts was determined in the butyraldehyde hydrogenation.

Table 9: Physical properties of the precipitated catalysts. a) Amount of soda used for the precipitation. b) determined by ICP-OES, c) determined by CHNS residual gas analysis, d) determined by Scherrer equation (reflex at 13 °2θ), e) determined by N_2-isotherm and BET/ BJH method.

Prec. pH	**V (Na_2CO_3)[a]**	**Cu[b]**	**Zn[b]**	**n (Zn:Cu)[b]**	**C[c]**	**H[c]**	**N[c]**	**Cry. Size Aurichalcite[d]**	**BET-SA[e]**	**Pore Vol[e].**
-	mL	%	%	-	%	%	%	nm	m^2g^{-1}	cm^3g^{-1}
6	28.5	21.8	42.0	1.9	4.1	1.3	0.1	14.4	44	0.14
7	37.0	21.0	40.9	1.9	n.d.	n.d.	n.d.	13.2	57	0.25
8	39.1	18.1	43.7	2.3	4.2	1.1	b.d.l.	12.3	54	0.31
9	52.4	20.7	42.9	2.0	n.d.	n.d.	n.d.	9.2	67	0.42

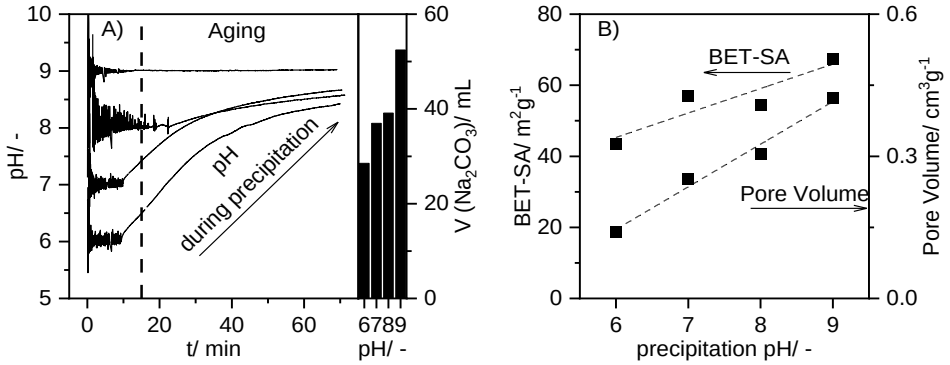

Figure 21: A) Precipitation pH as function of the precipitation and aging time and consumed soda and B) infleunce of the pH value on BET surface area and the pore volume.

The pH value during the precipitation was fixed by adding the proper amount of sodium carbonate while the copper-zinc solution was added with constant flow. During the aging, the pH was monitored but not fixed to a certain value. It could be shown that during the aging an increase up to pH of around 8 is obtained (Figure 21, A). Additionally, the amount of soda increases roughly linear with increasing precipitation pH. A higher amount of soda is needed to keep the solution at pH 9. The slight increase of the pH value during the aging is assumed to result from a complex precursor phase transition during the aging where a variety of phases (e.g., malachite, aurichalcite, gerhardtite, rosasite and hydrozincite) are involved.[169] Both the

BET surface area as well as the pore volume of the precipitates are increasing with increasing precipitation pH value. While the BET surface area increases from around 40 to nearly 70 m^2g^{-1}, the pope volume increases from around 0.14 to around 0.42 cm^3g^{-1}. Both trends can be described roughly linear (Figure 21, B).

P-XRD revealed that the synthesized precursors consist mainly of the aurichalcite as well as the hydrozincite phase.[148-149] A minor reflex according to the gerhardtite phase (25.9 ° 2θ) could be found for the pH 6 precursor.[170] A quantitative Rietveld refinement was not performed due to the similarity of the XRD patterns (Figure 22, A). The particle size of the aurichalcite phase was determined by the Scherrer equation. A slight decrease in the aurichalcite particle size is obtained (Figure 22, B). While the pH 6 precursor has an aurichalcite particle size of 14.4 nm, this decreases to 9.2 nm for the pH 9 precursor (Table 9).

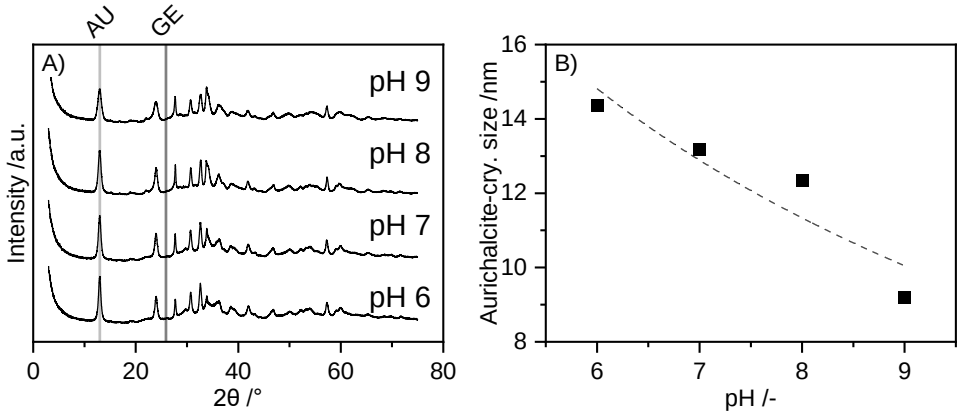

Figure 22: A) p-XRD patter of the precipitates and B) influence of the precipitation pH value on the crystallite size of aurichalcite. Reference patterns from the COD/ ICCD data base (AU: 96-900-7689, GE: 00-014-0687).[149, 170]

The decrease in the particle size in in accordance with the increased BET surface area. The elemental analysis confirmed the desired zinc to copper ratio to be 2:1, only the pH 8 catalyst shows with 2.3:1 a slight deviation. It can be assumed that the mixture of copper and zinc precursor solution was not prepared accurately. CHNS analysis was performed for the pH 6 and the pH 8 catalyst precursor (Table 9). Both values for carbon (4.1 respectively 4.2 wt-%) and hydrogen (1.3 respectively 1.1 wt-%) fit quite well to the expected value (C: 4.4, H: 1.1 wt-%) for the hydrozincite and aurichalcite precursor phase. Interestingly, for the pH 6 precursor catalyst a minor amount of nitrogen of 0.1 % was found while for the pH 8 catalyst no nitrogen could be detected. This fits to findings obtained from p-XRD where a minor amount of gerhardtite phase could be identified for the pH 6 catalyst. Gerhardtite is found to crystallize at slightly acidic conditions (Reaction scheme 19).[171-172] Assuming the 0.1 wt-% nitrogen, the pH 6 precursor catalyst consists of a few percent gerhardtite phase.

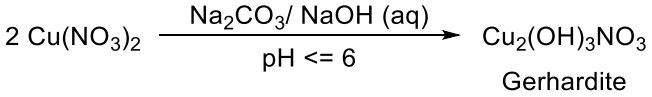

Reaction scheme 19: Precipitation of copper in an acidic aquous solution.

Summarizing, the pH value during the precipitation of copper-zinc oxide precursors influences the phase composition as well as the physical properties of the obtained precursors slightly. A

minor amount of gerhardtite phase is found for the pH 6 precursor while a higher pH leads to precursors consisting only of aurichalcite and hydrozincite. The BET surface area is slightly increasing with higher pH value while the aurichalcite particle size is decreasing. It can be assumed that a higher pH value during precipitation leads to a faster precipitation due to a higher amount of hydroxide and carbonate ions in the precipitation solution. As a result, poorly soluble copper-zinc hydroxycarbonates are formed faster and the risk of sintering and the formation of large crystallites during the precipitation is minimized. Beneficial surface properties are obtained for catalysts precipitated at slightly higher precipitation pH (e.g., the higher BET surface area).

Table 10: Physical properties of the calcined catalysts. a) determined by ICP-OES. b) Determined by Rietfeld refinetent,c) determined by temperature programmed reduction, d) determined by copper surface area titration with nitrous oxide and e) determined by Scherrer equation (reflex at 38.8 °2θ).

Prec. pH	**Cu[a]**	**Zn[a]**	**n (Zn:Cu)[a]**	**CuO[b]**	**ZnO[b]**	**Red. degree[c]**	**Mean red. Temp.[c]**	**Cu-SA[d]**	**Cu-Disp.[d]**	**Cry. Size CuO[e]**
-	%	%	-	%	%	%	°C	m^2g^{-1}	%	nm
6	29.2	54.8	1.8	36	64	91	157	9	4.8	5.4
7	29.4	55.5	1.8	36	64	91	163	8	4.3	4.6
8	24.4	57.6	2.3	36	64	97	163	10	5.9	4.4
9	26.3	56.0	2.1	35	65	91	164	8	4.5	4.5

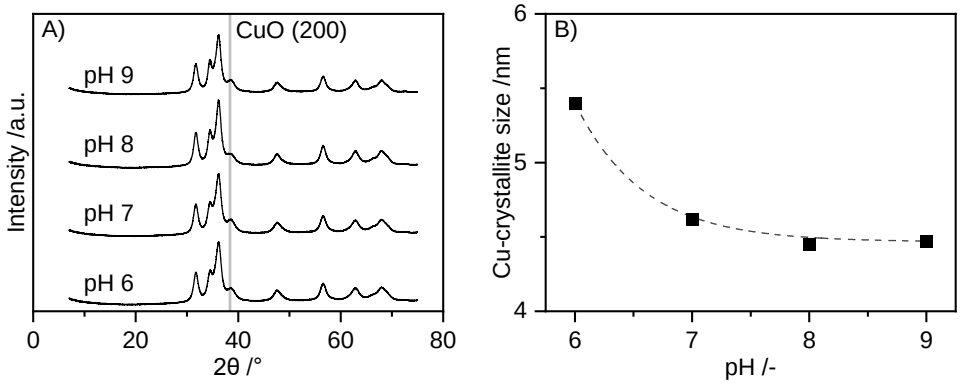

Figure 23: A) p-XRD patter of the calcined catalysts and b) influence of the precipitation pH value on the crystallite size of copper(II) oxide. Reference patterns from the COD data base (CuO: 96-101-1149)[155].

The precipitated catalysts were calcined at 350 °C to obtain the desired oxide. The calcination process was monitored via thermogravimetric analysis and was found to be nearly the same for all catalysts (Figure 25, A). A noteworthy distinction of the TGA pattern cannot be presented, indicating that the decomposition of different copper-zinc hydroxycarbonates proceeds similar. Two decomposition steps could be identified while the first decomposition step takes place between 200 to 300 °C and the second decomposition step in the temperature range of 300 to 450 °C. In the first decomposition step a metastable high temperature carbonate is formed while the second decomposition step yields in the pure oxide. A detailed description of the decomposition is be given earlier (chapter 3.2; Figure 13, B; Reaction scheme 16). Elemental analysis confirmed the desired zinc to copper ratio of 2:1, only the pH 8 catalysts has a slight deviation (as found also for the precursor phase). The zinc to copper ratio is not affected from

the calcination process as expected (Table 10). Only reflexes according to copper(II) oxide and zinc(II) oxide are found in the P-XRD pattern (Figure 23, A).[153, 155] A quantitative Rietveld refinement shows a zinc to copper oxide ratio of around 2 to 1 as the elemental analysis indicates. The copper oxide particle size was calculated by Scherrer equation and was found to be around 5.4 nm for the pH 6 catalysts while increasing the precipitation pH leads to a slightly smaller particle size of around 4.5 nm (Figure 23, B). It can be assumed that the presence of gerhardtite phase in the precursor leads so slightly larger copper oxide crystallites after calcination due to a higher copper density in the unit cell of gerhardtite compared to the unit cell of aurichalcite.[149, 171] On the other hand, no clear trend is obtained for the copper surface area and the copper dispersion. While the copper surface area was measured to be between 8 to 10 m^2g^{-1}, the copper dispersion was found to be between 4.3 to 5.9 %. A significant interpretation cannot be given due to the tolerance of error of this method (2 m^2g^{-1} for the copper surface area, 1 % for the copper dispersion). Interestingly, although a clear trend could be given for the copper oxide crystallite size (larger for the pH 6 catalyst), this is not the case for the copper surface area. This indicates that the composition of precursor phases influences the copper oxide phase but has no or only minor effects on the activated catalyst.

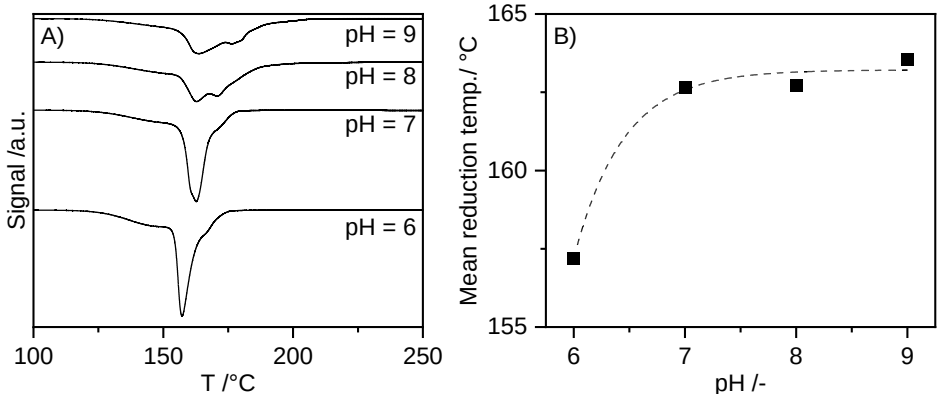

Figure 24: A) Temperature programmed reduction profiles of the calcined catalysts and B) influence of the pH-value during precipitation on the mean reduction temperature.

To study the reductivity in detail, temperature programmed reduction of the catalysts were performed (Figure 24, A). While the degree of reduction is not affected by the pH value during the precipitation and all catalyst show a complete reduction (reduction degree ranging from 91 to 97 %, slight inaccuracy within this measurement set), the shape of the reduction peak changes slightly. Catalysts precipitated under slight acidic and neutral conditions (pH 6 and 7) show a sharper reduction curve compared to the catalysts synthesized at higher pH value. Especially the mean reduction temperature is influenced by the precipitation pH value (Figure 24, B). While the pH 6 catalyst has a mean reduction temperature of 157 C, the catalysts synthesized at pH 7 to 9 have with 163 to 164 °C a slightly higher reduction temperature. In general, a sharper reduction profile and a lower reduction temperature obtained for copper catalysts indicates a more uniform particle size distribution. Additionally, larger copper particles can be reduced at slightly lower temperatures.[173-174] This in accordance to results obtained from the evaluation of the copper oxide particle size.

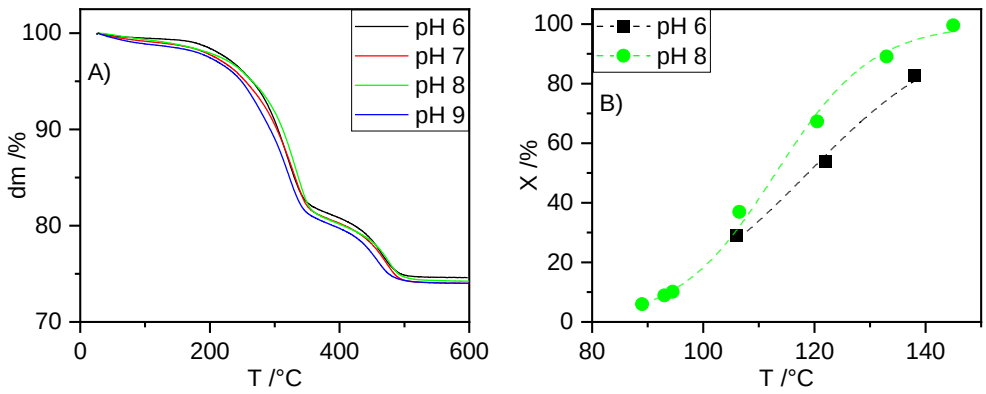

Figure 25: A) Themrogravimetric analysis of the precipitated catalysts and B) influence of the precipitation pH-value on the catalytic activity in the hydrogenaition of butyraldehyde.

The hydrogenation of butyraldehyde was used to describe the catalytic activity of the synthesized catalysts (Figure 25, B). Both catalysts show activity in the temperature range between 80 to 150 °C. The activity of the pH 8 catalyst is slightly higher compared to the activity of the pH 6 catalyst. The *n*-butanol selectivity is not affected and was determined above 99 % for both catalysts. Only traces of butyl butyrate could be detected. The slightly higher activity for the pH 8 catalyst agrees with the beneficial surface properties found for catalysts which are synthesized from gerhardtite free precursor phases.

Summarizing, the pH value during the precipitation of copper-zinc catalysts influences the surface properties and the catalytic activity. Although the main precursor phases were identified to be equal for all synthesis pH values, a too-low pH value leads to the synthesis of gerhardtite as an additional precursor phase. This leads to a larger aurichalcite crystallite size and especially larger copper oxide crystallites after calcination. This can be additionally seen by a sharper reduction profile and a lower reduction temperature obtained for the pH 6 catalyst compared to catalysts synthesized at higher pH values. The beneficial surface properties for catalysts synthesized at higher pH value lead additionally to slightly more active catalysts. This agrees with Gudkov *et al.* who report that copper catalysts obtained from hydroxy nitrates are not active at all in the hydrogenation of butyraldehyde.[175] In general, the synthesis conditions should be chosen so that gerhardtite as an additional precursor phase will be avoided. Although the calcination process seems to be nearly equal and leads to catalysts consisting only of copper and zinc oxide, physical properties and catalytic activity is still affected. A memory effect exists that transfers properties from the precursor through the whole synthesis process (precipitation, calcination, activation) in the active catalyst.

3.4 Aluminum containing copper catalysts

3.4.1 Synthesis, thermal treatment and characterization

Aluminum containing copper (zinc) catalysts were synthesized by co-precipitation. Two types of catalysts were synthesized: The first type are copper-zinc-aluminum catalysts similar to the ones described earlier (chapter 3.2) where around 10 % aluminum was added to the copper-zinc solution (copper to zinc ratio set to 1:2; chapter 3.3.1). This type of catalysts is similar to industrial methanol catalysts with a slightly shifter copper to zinc ratio.[121, 176-177] The second type of catalysts are pure copper-aluminum catalysts with a fixed molar copper to aluminum ratio of 1:2. These catalysts are used in the methanol synthesis but also in the emission control, especially for the reduction of nitrogen oxides and the oxidation of carbon monoxide.[178] The catalysts were synthesized by precipitation from the according metal salts and calcined in the temperature range between 350 to 450 °C to yield the desired oxide and 800 °C to allow the crystallization of a spinel phase. For the copper aluminate spinel catalysts an additional leaching step in ammonium carbonate solution was performed to get rid of potentially formed copper(II) oxide and to synthesize a phase pure spinel catalyst (Reaction scheme 20).

$$a\,Cu^{2+} + b\,Zn^{2+} + c\,Al^{3+} \xrightarrow[50\text{-}90\ °C,\ 1h]{Na_2CO_3/\ NaOH\ (aq)} (Cu_aZn_bAl_c)(CO_3)_x(OH)_y \qquad (1.)$$

$$(Cu_aZn_bAl_c)(CO_3)_x(OH)_y \xrightarrow[350\ °C]{syn.\ air} a\,CuO \bullet b\,ZnO \bullet 0.5c\,Al_2O_3 \qquad (2.)$$

$$Cu^{2+} + 2\,Al^{3+} \xrightarrow[50\text{-}90\ °C,\ 1h]{Na_2CO_3/\ NaOH\ (aq)} Cu(CO_3)_x(OH)_y \bullet 2\,Al(OH)_3 \qquad (3.)$$

$$Cu(CO_3)_x(OH)_y \bullet 2\,Al(OH)_3 \xrightarrow[450\ °C,\ 4h]{air} CuO \bullet Al_2O_3 \qquad (4.)$$

$$Cu(CO_3)_x(OH)_y \bullet 2\,Al(OH)_3 \xrightarrow[800\ °C,\ 4h]{air} (CuO) \bullet CuAl_2O_4 \xrightarrow[Ultrasonic,\ 1h]{Leaching\ (NH_4)_2CO_3} CuAl_2O_4 \qquad (5.)$$

Reaction scheme 20: Synthesis and calcination of copper-(zinc)-aluminum catalysts.

P-XRD pattern were taken from the calcined catalysts (Figure 26). While the oxide modification of the copper-zinc and copper-aluminum catalysts (350-450 °C calcination temperature) are roughly amorphous and no clear reflexes can be identified, clear crystalline pattern are obtained for the 800 °C calcined catalysts. In a rough estimation, the main reflexes according to copper(II) oxide can be found for the copper-zinc-aluminum catalyst calcined at 350°C.[155] Additionally, the main reflexes according to zinc(II) oxide can be found imprecisely.[153] A very broad shoulder at 38.7 °2θ indicates the existence of copper(II) oxide in the copper-aluminum catalysts which was calcined at 450 °C. A quantitative refinement is not possible for such amorphous structures. Even adding a low amount of aluminum (10 % in the case of the copper-zinc-aluminum catalyst) leads to very amorphous phases in comparison to the aluminum free copper-zinc catalyst (chapter 3.2). In comparison to the oxide structures, the 800 °C calcined

catalysts show clear crystalline phases according to copper(II) oxide and copper aluminate spinel ($CuAl_2O_4$).[155, 179] Additionally, reflexes according to zinc(II) oxide can be found for the copper-zinc-aluminum catalyst.[153] While the copper-zinc-aluminum catalyst shows mainly phases according to copper(II) and zinc(II) oxide, the main phase in the copper-aluminum catalysts can be identified as the spinel phase ($CuAl_2O_4$).[153, 155, 179] The leached version shows nearly no reflexes according to copper(II) oxide, minor reflexes can be found for the non-leached copper-aluminum catalyst.

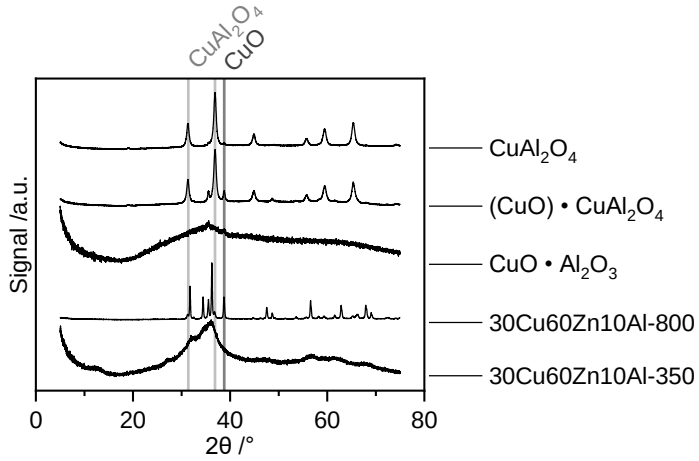

Figure 26: p-XRD pattern of the copper-zinc-aluminum catalysts. Reference patterns from the COD data base (CuO: 96-101-1149, $CuAl_2O_4$: 96-900-5717).[155, 179]

Rietveld refinement reveals a phase composition for the copper-zinc-aluminum catalyst consisting of 30 % copper(II) oxide, 54 % zinc(II) oxide and 16 % copper aluminate spinel (Table 11). The low amount of spinel phase fits to the minor amount of aluminum added, nevertheless, the total amount of copper containing phases is slightly higher than expected for the copper:zinc:aluminum ratio of 30:60:10. On the other hand, it has to be mentioned that both copper and zinc can crystallize with aluminum in a spinel phase with the same space group (and nearly the same lattice parameters) and so the distinction between $CuAl_2O_4$ and $ZnAl_2O_4$ is quite hard.[179-180] A crystallization of the zinc aluminate spinel phase is also possible. Only copper(II) oxide and copper aluminate spinel can be found in the refinement of the copper-aluminum catalyst (due to the absence of zinc the zinc aluminate spinel can be excluded). For the non-leached version 11 % copper(II) oxide are found while this can be reduced to 4% for the leached version.

Table 11: XRD Refinement data and copper surface area of the copper-zinc-aluminum catalysts.

Sample	**pretreatment**	**CuO**	**$CuAl_2O_4$**	**ZnO**	**Cu-SA**	**Cu-Dispersion**
	-	%	%	%	m^2g^{-1}	%
Cu-Zn-Al	350 °C Calc.	n.d.	n.d.	n.d.	12	3.6
Cu-Zn-Al	800 °C Calc.	30	16	54	b.d.l.	b.d.l.
Cu-Al	Precipitation	n.d	n.d	n.d	n.d.	n.d.
Cu-Al	450 °C Calc.	n.d	n.d	n.d	4	2.1
Cu-Al	800 °C Calc.	11	89	0	4	1.8
Cu-Al	800 °C Calc. + Leaching	4	96	0	4	1.9

For both 350 and 800 °C calcined copper-zinc-aluminum catalysts a zinc to copper ratio of around 2:1 was found (Table 12). Nevertheless, the amount of aluminum regarding the oxide (10 wt-% planned) was with 5 % in the oxide modification and only 2 wt-% in the spinel modification lower than expected. Both catalysts were obtained from the same precursor material and calcined at different temperatures, so the amount of aluminum should be roughly the same regarding aluminum oxide. It can be assumed that the dissolving of the catalysts (for the ICP measurements), especially for the high temperature calcined spinel version was not sufficient and harsher conditions are needed to dissolve aluminum from the spinel lattice. The aluminum to copper ratio for the zinc-free catalysts was found to be 1.8 to 1 for the precipitate the oxide and the non-leached spinel and 2.5 to 1 for the calcined and leached version. The ratio of 1.8 to 1 fits roughly to the desired ratio of 2 to 1 (a stochiometric spinel should be synthesized). The higher ratio for the leached spinel indicates that a part of the copper is removed (probably mainly from the copper oxide lattice). CHNS analysis was performed for the copper-aluminum catalysts. The carbon amount was determined to be 2.7 % for the copper-aluminum precipitation and 2.5 % for hydrogen. This would roughly fit to the precipitation of copper as malachite ($Cu_2(OH)_2(CO_3)$) while aluminum is precipitated as hydroxide ($Al(OH)_3$).

Table 12: Elemental analysis of the copper-zinc-aluminum catalysts by ICP-OES and CHNS.

Sample	**pretreatment**	**Cu**	**Zn**	**Al**	**wt-% Cu:Zn:Al**	**n (Zn:Cu)**	**n (Al:Cu)**	**C**	**H**
	°C	%	%	%	-	-	-	%	%
Cu-Zn-Al	350 °C Calc.	20.4	44.3	3.7	30:65:5	2.1	0.4	n.d.	n.d.
Cu-Zn-Al	800 °C Calc.	23.9	47.3	1.2	33:65:2	1.9	0.1	n.d.	n.d.
Cu-Al	Precipitation	24.3	b.d.l.	18.4	57:0:43	-	1.8	2.7	2.5
Cu-Al	450 °C Calc.	31.7	b.d.l.	24.2	57:0:43	-	1.8	2	0.5
Cu-Al	800 °C Calc.	33.9	b.d.l.	25.9	57:0:43	-	1.8	0.2	0.1
Cu-Al	800 °C Calc + Leaching	27.1	b.d.l.	28.5	49:0:51	-	2.5	1.3	0.9

Mixed copper-aluminum hydroxycarbonate phases are not known to be formed during the precipitation of copper and aluminum. In the case of precipitation as malachite and aluminum hydroxide, 2.3 % carbon and 2.6 % hydrogen would be expected. Minor deviations can come from a partial insertion of aluminum in copper containing hydroxycarbonates or a partial precipitation of aluminum as hydroxycarbonate.[181] 2 % carbon and 0.5 % are found for the copper-aluminum oxide catalyst which was calcined at 450 °C. A full decomposition to the oxide ($CuO \bullet Al_2O_3$) would be indicated by the absence of both carbon and hydrogen. Especially the quite high value for carbon indicates the existence of a metastable high temperature carbonate species. Nearly no carbon (0.2 %) and hydrogen (0.1 %) were detected for the non-leached spinel version which indicates the complete decomposition of any hydroxy carbonate residuals. The removal of copper(II) oxide by a leaching step in ammonium carbonate leads to a slight increase in carbon (1.3 %) and hydrogen (0.9 %). It can be assumed

that the washing step after the leaching was not complete sufficient to get rid of all ammonium carbonate. It can be assumed that further washing or a recalcination would decrease the carbon and hydrogen amount to a minimum.

Thermal treatment and calcination

To analyze the calcination process of the copper-aluminum catalyst in detail thermogravimetric analysis as well as *in situ* XRD of the calcination process were conducted (Figure 27, A). A total mass loss of around 35 % is obtained under heating to 850 °C. Two decomposition steps are obtained in the calcination of the copper-aluminum precursor. In a first decomposition step between around 150 and 300 °C, around 25 % mass lost are found under release of carbon dioxide and water. A second decomposition step if found to take place between 600 and 700 °C under release of carbon dioxide and a mass loss of around 5 %.

The *in situ* XRD reveals that a crystallization takes place between 550 and 650 °C (Figure 27, B). Complete amorphous patterns are obtained for the precursor and up to 550 °C. The pattern measured at 650 °C reveals the existence of copper(II) oxide, further temperature increase (up to 850 °C) leads to the crystallization of the spinel phase ($CuAl_2O_4$).

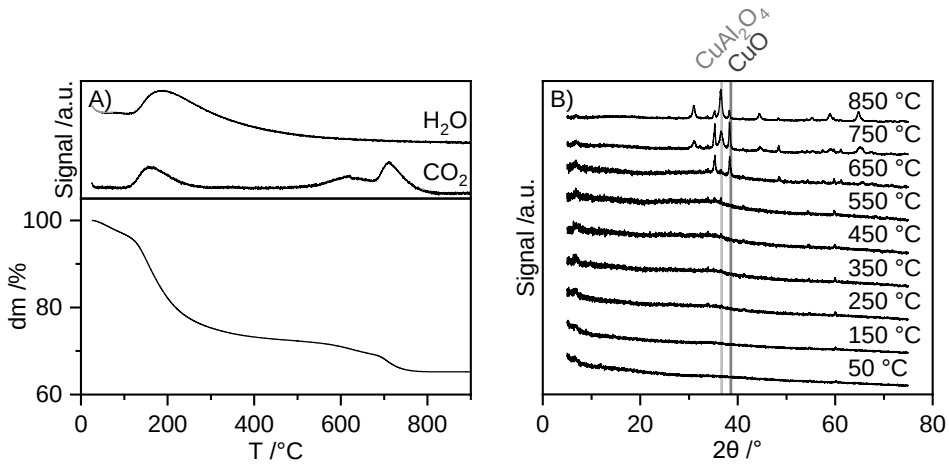

Figure 27: Calcination process of the copepr aluminum precursor monitore via A) Thermogravimetric analysis and B) *in situ* XRD. Reference patterns from the COD data base (CuO: 96-101-1149, $CuAl_2O_4$: 96-900-5717).[155, 179]

The combination of the TGA-MS and the *in situ* XRD data leads to the formation of a stepwise decomposition equation (Reaction scheme 21). In the first decomposition step between 150 to 300 °C a metastable high temperature copper carbonate supported on alumina is formed (mass loss of around 20 %, release of water and carbon dioxide, no crystalline phase in the XRD). Further temperature increase leads to the decomposition of the copper carbonate and copper(II) oxide supported on alumina is formed (mass loss of around 10 %, release of carbon dioxide, copper oxide can be found as predominant phase in the XRD pattern).[155] Temperature increase above 700 °C leads to the crystallization of copper aluminate spinel (no mass loss or release of carbon dioxide or water in the TGA but $CuAl_2O_4$ can be found as predominant phase in the XRD pattern).[179]

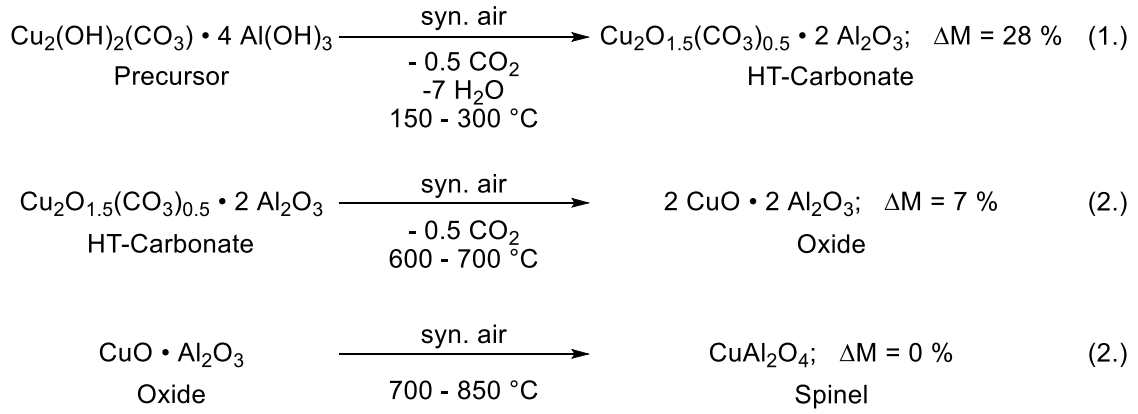

Reaction scheme 21: Decomposition of copper-aluminum precursor under formation of 1.) copper-aluminum HT-carbonate, 2.) copper-aluminum oxide and 3.) copper aluminate spinel.

Reductive behavior of copper-aluminum catalysts

The reduction behavior of the catalysts was investigated by temperature programmed reduction (Figure 28). Two separate reduction peaks are obtained for both copper aluminate spinel catalysts while the copper-zinc-aluminum and the copper-aluminum oxide catalyst show only one reduction peak. The two separate peaks of the copper aluminate spinel catalyst can be explained as the reduction of copper(II) oxide which takes place at temperatures between around 150 to 200 °C and the reduction of copper in the spinel lattice at temperatures between 300 and 400 °C. The second reduction peak is not affected by the leaching step while the first reduction peak is slightly larger and shaper for the non-leached copper aluminate spinel. This can be explained by a) the removal of copper(II) oxide during the leaching which leads to a smaller peak area of the first reduction peak for the leached spinel and b) less crystalline residuals of copper(II) oxide after the leaching step which leads to a broader first reduction peak. One broad reduction peak between 200 and 250 °C is obtained for the copper-aluminum oxide catalyst. In comparison to the reduction of pure copper-zinc catalysts with a similar copper loading (see also chapter 3.2) this reduction peak is a) slightly broader and b) shifted around 50 K to higher temperatures. This can be explained by strong metal support interactions (SMSI) between copper and alumina.[182] Both copper-zinc-aluminum catalysts show one reduction peak between 175 and 225 °C. While this peak is quite sharp for the oxide catalyst (like pure copper-zinc oxide catalysts, but slightly shifted to higher temperatures due to SMSI), the spinel version of this catalyst has a much broader reduction peak. This reduction peak can be also described as two meshing reduction peaks. In this case, the first one would be reduction of copper(II) oxide while the second one would be the reduction of the partially formed spinel phase. It can be assumed that due to the low amount of formed spinel this phase is mainly formed on the surface which leads to a lower reduction temperature compared to the reduction of bulk spinel.[183]

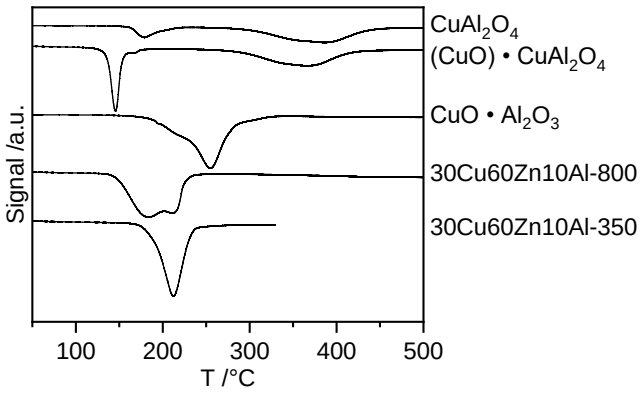

Figure 28: Reduction profiles of the copper-zinc-aluminum catalysts.

The copper surface area determination revealed that nearly no differences exist for the copper-aluminum catalysts (Table 11). After reduction at 350 °C, a surface area of 4 m^2g^{-1} and a copper dispersion of around 2 % is obtained for the copper-aluminum oxide as well as the non-leached and the leached copper aluminate spinel. This indicates that after activation a similar copper phase is obtained for all three copper-aluminum catalysts yielding in a similar copper dispersion. The lower dispersion compared to pure copper-zinc oxide catalysts could be explained by a potential blocking of active copper sites due to SMSI between alumina and copper. Additionally, it has to be considered that the reduction temperature was raised from 200 °C for pure copper-zinc catalysts to 350 °C to allow a complete reduction of copper in both the oxide and the spinel lattice. It can be assumed that an optimized reduction protocol which allows a reduction of both copper modifications but prevents copper sintering can lead to slightly higher dispersion for the copper-aluminum catalysts. For the copper-zinc-aluminum oxide catalyst, a surface area of 12 m^2g^{-1} and a dispersion of 4 % was obtained. This is similar to the aluminum free copper-zinc oxide catalyst with similar copper loading (chapter 3.2, Table 5). Nevertheless, the dispersion is slightly lower compared to the pure copper-zinc catalyst which can be explained by slightly higher reduction temperatures needed to yield in a complete reduced copper catalyst. A higher reduction temperature increases the risk of a partial sintering of the copper phase. Additionally, the SMSI between copper and aluminum oxide could block some of the active centers. The copper surface area as well as the copper dispersion were found to be below the detection limit for the spinel version of the copper-zinc-aluminum catalyst. This can be explained due to sintering of copper(II) oxide during the calcination at 800 °C. While a pure copper aluminate spinel phase calcined at 800 °C leads to a detectable copper surface area after activation, this is not the case for a mainly oxidic copper-zinc (aluminum) catalyst calcined at this temperature. This indicates that strong sintering effects take place in the copper(II) oxide phase during the calcination at elevated temperatures.

The reduction of the leached copper aluminate spinel was additionally investigated by reductive thermogravimetric analysis and *in situ* XRD (Figure 29). During TGA analysis, the leached copper aluminate spinel was heated in diluted hydrogen. The mass loss and release

of water was recorded. Additionally, the heat flow was monitored to gain qualitative information regarding the reaction enthalpy (exotherm or endotherm reaction). Two distinct mass loss steps are found in the thermogravimetric analysis which is in accordance to previously discussed TPR (Figure 28). A first reduction step takes place between 200 and 250 °C under release of water and a clear exothermic reaction enthalpy signal. Around 2 % mass loss is found. A second reduction step was recorded between 350 and 450 °C under release of water and a second exothermic signal. The mass loss was found to be around 6 %. As known from the p-XRD analysis, the leached spinel shows not only copper in the spinel but also in the oxide lattice due to copper(II) oxide residuals. It can be assumed that the first reduction peak is attributed to the reduction of copper(II) oxide while the second reduction step indicates the reduction of the spinel. As a mass loss if found in this reduction step as well as the formation of water, it can be assumed that the spinel lattice is dissolved and a recrystallization of copper on γ-alumina takes place.

Additionally, the reduction of the copper aluminate spinel was monitored via *in situ* XRD (Figure 29**,** B). Until heating up to 150 °C no phase change takes place and reflexes according to copper aluminate spinel as well as copper(II) oxide can be found. At around 200 °C the copper(II) oxide phase vanishes while copper(0) if formed. Further increase above 350 °C leads to a strong increase in the reflex intensity of the copper(0) reflexes as well as a slight shift to lower 2θ values for the spinel reflexes. The latter once indicates the crystallization of a γ-alumina phase.[184]

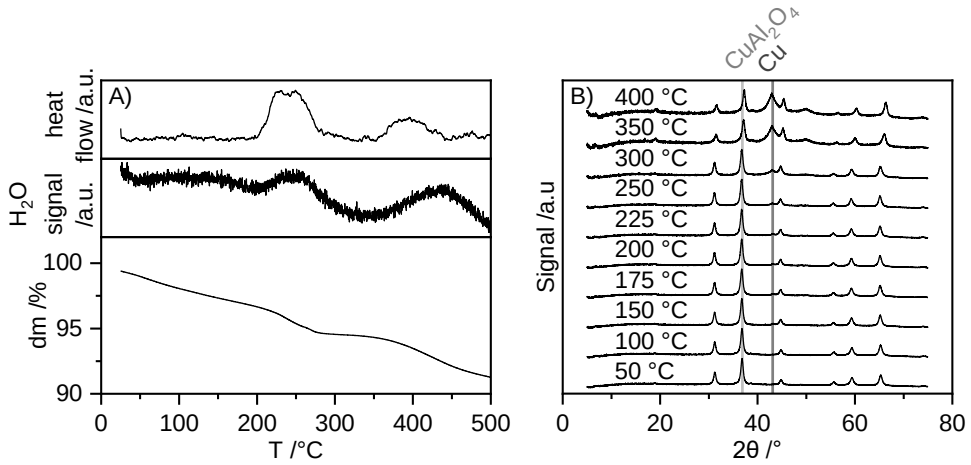

Figure 29: Reduction under H_2 of the copper-aluminum precursor monitored via A) TGA and B) *in situ* XRD. Reference patterns from the COD data base (Cu: 96-151-2505, $CuAl_2O_4$: 96-900-5717). [158, 179]

The results obtained from the reductive TGA and the *in situ* XRD provide clear insights in the reduction mechanism of the copper aluminate spinel catalyst. In a first reduction step at around 200 °C, the copper(II) oxide residuals are reduced and a small amount of copper(0) is formed.[155, 158] Further increase in temperature leads to the reduction of copper(II) in the spinel lattice as well as the complete dissolving of the spinel lattice under crystallization of γ-Al_2O_3. The release of water is found in both reduction steps as well as the release of reaction energy. Both reduction steps are found to be exothermic, from enthalpy data the reaction enthalpy is

calculated to be -85 kJmol^{-1} for the reduction of copper(II) oxide and -92 kJmol^{-1} for the reduction of copper(II) in the spinel lattice under recrystallization of γ-alumina.[185] Additionally, the calculated mass loss from the phase composition found by Rietveld refinement is calculated to be 2 % for the oxide reduction and 8 % for the spinel reduction and is in rough estimation with the values obtained from the thermogravimetric analysis. This reduction mechanism is in accordance with literature. Plyasova *et al.* observed the presence of different copper sites in copper aluminate spinels. By high temperature X-ray analysis, they showed that copper in tetrahedral sites can be reduced below 300 °C while the reduction of copper in octahedral sites needs temperatures above 300 °C. Above 400 °C, a partial dissolving of the oxygen framework takes place. This dissolving of the oxygen framework leads to a copper-aluminum oxide species.[186] Reaction scheme 22 summarizes the mechanism of the copper aluminate spinel reduction.

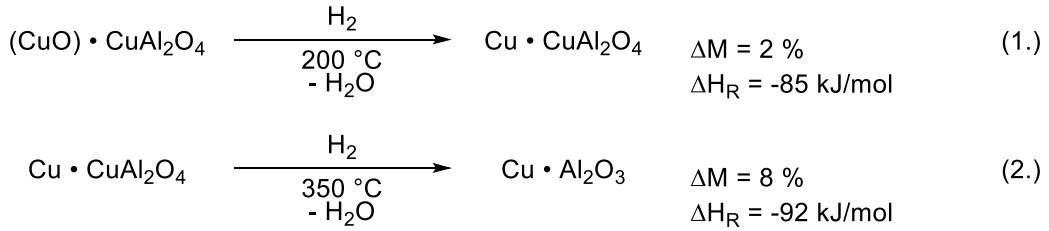

Reaction scheme 22: Reduction of the leached copper aluminate spinel.

3.4.2 Catalytic activity of copper-aluminum catalysts

The catalytic activity of the aluminum containing catalysts was tested in the hydrogenation of butyraldehyde to *n*-butanol and compared to the benchmark copper-zinc oxide catalyst (Figure 30, A). All tested catalysts show activity in the temperature range between 90-240 °C. The temperature conversion course can be described by a sigmoidal fit. Three different groups of catalysts can be described. The highest activity is found for the pure copper-zinc catalyst and both copper aluminate spinel catalysts (leached and non-leached). These catalysts show initial activity at around 90 °C while full conversion is reached at around 130 °C. The T_{50} was determined to be between 115 and 119 °C. Medium activity is obtained for the oxide versions of the copper-aluminum and the copper-zinc-aluminum catalysts. Initial activity is found at around 100 °C while full conversion is reached at around 140 °C. The T_{50} is with 132 and 135 °C higher compared to the pure copper-zinc oxide and both copper aluminate spinel catalysts. The spinel version of the copper-zinc-aluminum catalyst has the lowest activity. Initial conversion is found at 130 °C while full conversion is reached at around 240 °C. This catalyst has with 191 °C the highest T_{50}.

As discussed previously, the leached copper aluminate spinel shows two reduction steps. It could be shown that reduction at 200 °C to obtain only the reduction of copper(II) oxide residuals leads to a less active catalyst compared to the catalyst reduced at 350 °C (both copper in the oxide and the spinel lattice are reduced). Initial activity for the 200 °C reduced

leached copper aluminate spinel is found at around 120 °C, full conversion is reached at 200 °C (Figure 30, B). The T_{50} was determined to be over 50 K higher compared to the completely reduced spinel (T_{50} = 169 °C). This is a further prove that two different copper(II) sites exist in this catalyst which contribute to the active catalyst after reduction. If only copper from the oxide lattice is reduced, a lower number of active sites is obtained and the catalytic activity is lowered.

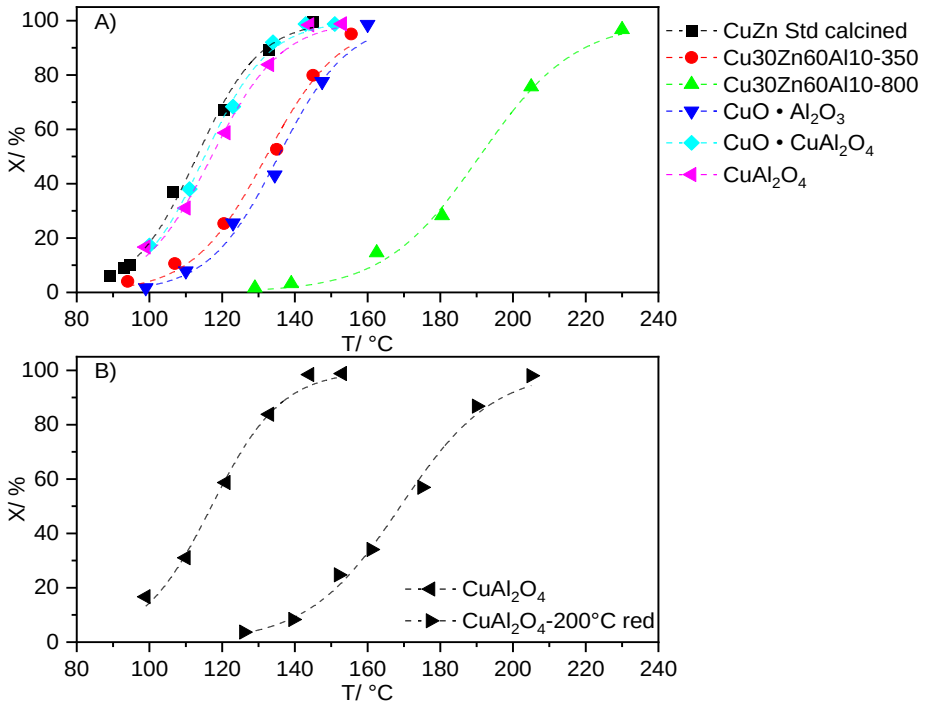

Figure 30: A) Catalytic activity (temperature-conversion plot) of the copper-zinc-aluminum catalysts and B) influence of the reduction temperature on the catalytic activity of the leached copper aluminate spinel.

Summarizing, two different groups of copper-(zinc)-aluminum catalysts were synthesized, characterized and tested in the butyraldehyde hydrogenation. It could be shown that even adding small amounts of aluminum leads to quite amorphous structures if the catalysts are calcined between 350 and 450 °C. Calcination at 800 °C leads to the formation of crystalline spinel phases. In the case of the copper-zinc-aluminum catalyst, only a small amount of spinel is found whereas, for the copper-aluminum catalysts, copper aluminate spinel is obtained as the predominant phase. Nevertheless, even in the case of a stochiometric copper-to-aluminum ratio of 1:2 copper oxide is present. This can be reduced to a minimum with a leaching step, but a complete phase pure copper aluminate spinel could not be obtained. The calcination process of the spinel could be revealed to be a complex decomposition process starting from a mixture of malachite and aluminum hydroxide which decomposes over a metastable high-temperature carbonate species and ends in a copper aluminate spinel with minor copper oxide residuals. Two different copper sites were found to be present for all spinel catalysts. These different copper sites are both involved in the reduction behavior as well as the catalytic activity. Copper in the oxide lattice is reduced at lower temperatures compared to the copper in the

spinel lattice. As seen also for the copper-zinc-aluminum oxide catalyst, the addition of aluminum leads to SMSI which increases the reduction temperature. Interestingly, it seems that a reduction of both copper sites in the copper aluminate spinel catalysts leads to similar copper surface properties compared to the copper-aluminum oxide catalyst. On the other hand, the catalytic activity for both copper aluminate spinel catalysts is slightly higher compared to the copper-aluminum oxide catalyst. Maybe, the presence of high-temperature carbonate (as found for the copper-aluminum oxide catalyst) decreases the number of active sites involved in the catalysis but does not interact with the measurement of the copper surface area. The existence of the two different copper sites in the copper aluminate spinel was additionally proven by detailed *in situ* studies of the reduction. It could be shown that a first reduction step reduces only copper in the oxide lattice while higher temperatures are needed to reduce copper in the spinel lattice. In the case of a high-temperature reduction above 350 °C, not only both copper sites are reduced but also a partial dissolving of the oxygen framework takes place.

In this case, a copper-aluminum oxide catalyst is formed which seems to have similar copper surface properties as the directly synthesized copper-aluminum oxide catalyst. Additionally, the long-term stability of copper oxide and copper spinel reduced at 350 °C is similar. A more detailed comparison of the long-term stability and the deactivation mechanism of copper spinel and copper oxide catalysts is given later (chapter 4.3). The partial reduction of the copper aluminate spinel catalysts at 200 °C (only copper in the oxide lattice is reduced) leads to less active catalysts compared to the complete reduction of both copper sites. A highly active catalyst can only be obtained if both copper sites are activated.

In general, the addition of aluminum to copper(-zinc) catalysts can have beneficial properties. Especially the zinc-free copper aluminate spinel catalysts seem to be an interesting group of catalysts for the hydrogenation of butyraldehyde and should be investigated further (see also chapter 4.3).

3.5 Direct reductive activation of copper-zinc oxide precursor catalysts

As discussed in previous chapters, bulk copper-zinc oxide hydrogenation catalysts are generally prepared by calcination of co-precipitated precursors followed by reduction. This subsection reports the direct reduction in hydrogen of co-precipitated oxy/hydroxy-carbonate precursors omitting calcination. Dried and incompletely calcined precursors are compared with calcined catalysts. The precursors were synthesized by co-precipitation followed by different thermal treatment resulting in different catalyst species. The hydroxycarbonate precursor is obtained after precipitation and drying. Incomplete calcination leads to the oxycarbonate species while full calcination yields the oxide species. The resulting catalysts were structurally characterized, and the activation pathways (reduction in hydrogen) and intermediates were investigated by *in situ* XRD and thermal analysis methods as a function of temperature and time. The activated catalysts were further tested in the hydrogenation model reaction of butyraldehyde to n-butanol.

3.5.1 Synthesis and characterization of the copper-zinc precursors and catalysts

The catalysts were synthesized by classic co-precipitation at a controlled pH value of 8 (Reaction scheme 16). After precipitation and drying, a blue powder was obtained and analyzed by p-XRD. The main XRD reflexes belong to aurichalcite ($(Cu,Zn)_5(OH)_6(CO_3)_2$) and hydrozincite ($(Zn)_5(OH)_6(CO_3)_2$) (Figure 31, B).[148-149] A quantification by Rietveld analysis yields an aurichalcite to hydrozincite ratio of around 2 to 1 (Figure 12, A). Additionally, a minor amount of (Zn-)malachite can be found.[150] The total metal content of 62.4 % (determined by ICP-OES) agrees quite well with the calculated value for phase pure aurichalcite (61.2 %). The copper to zinc ratio of 1.9 to 3.1 fits the desired ratio of 2:3 (Table 13). The HT-carbonate and the oxide species were obtained by partial or full calcination. This calcination process was monitored via *in situ* XRD. The decomposition of the precursor takes place between around 250 and 275 °C (Figure 31, B). The HT-carbonate which was calcined at 280 °C shows reflexes belonging to zinc oxide while reflexes according to copper oxide could not be found. The metal content of the HT-carbonate fits with 73.2 % quite well to the theoretical value of the HT-carbonate species ($Cu_2Zn_3O_4CO_3$, 72.2%).[96] As expected, the copper to zinc ratio did not change. The mass loss of 14.2 % obtained during the calcination is slightly below the expected value of 17.9 % indicating minor residues of undecomposed precursor phase (hydroxycarbonates). The full calcination at 350 °C resulted in a copper-zinc oxide catalyst. The oxide reflexes of both copper and zinc oxide are present.[153, 155] No additional reflexes could be found. A quantification by Rietveld analysis yields 62 % zinc(II) oxide and 38 % copper(II) oxide (Figure 12, B). The total metal content determined by ICP-OES is with 76.0 % slightly below the theoretical value of 80.0 % while the copper to zinc ratio stays at 1.9:3.1 and

fits exactly to the results obtained by the Rietveld refinement. The weight loss during calcination fits with 25 % quite well to the expected value of 26 %.

Table 13: Influence of the calcination temperature on the physical properties of the copper-zinc catalysts. A) ICP-OES, b) N_2-isotherm, c) nitrous oxide copper surface area titration, d) Scherrer equation, e) temperature programmed reduction and f) catalytic activity in the hydrogenation of butyraldehyde.

Sample	Calc. T	metal cont.[a]	n Cu:Zn	BET-SA[b]	Cu-SA[c]	Cu-Disp.[c]	Cu^0 crys. size[d]	T_{max} TPR[e]	Red. degree	T_{50}[f]
	°C	wt-%	-	m^2g^{-1}	m^2g^{-1}	%	nm	°C	%	°C
Aurichalcite	120	62.4	1.9:3.1	68	12	8.3	3.4	215	105	108
HT-Carbonate	280	73.2	1.9:3.1	60	14	8.4	3.6	175	106	110
Oxide	350	76.0	1.9:3.1	48	10	5.8	5.8	160	100	115

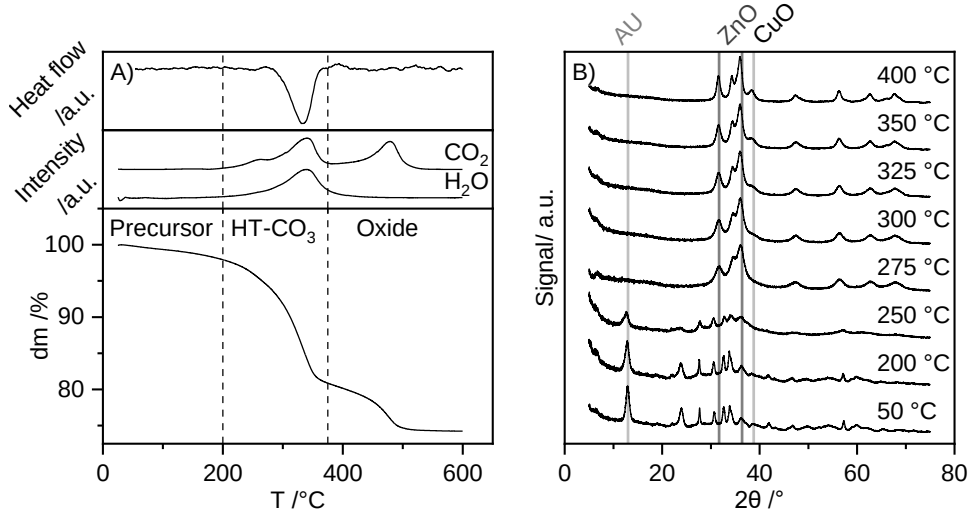

Figure 31: Decomposition of the copper-zinc precursor monitored via A) TGA and B) *in situ* XRD. Reference patterns from the COD data base (AU: 96-900-7689, CuO: 96-101-1149, ZnO: 96-900-4179).[149, 153, 155]

The decomposition of the dried precursor was additionally monitored by thermogravimetric analysis coupled with mass spectroscopy (Figure 31, A). Additionally, the heat flow during the decomposition was recorded to gain qualitative information regarding the reaction enthalpy. Two peaks can be found during the decomposition process. In the first decomposition stage, a mass loss of 18 % was observed between 180 and 350 °C under release of CO_2 and H_2O. This decomposition step shows a clear negative heat flow signal indicating that this decomposition step undergoes an endotherm reaction. In the second decomposition stage, 7 % mass loss was detected between 350 and 450 °C releasing CO_2. No additional water is released, indicating an oxycarbonate phase after the first decomposition step. No change in the heat flow is obtained in this decomposition step indicating that the release of carbon dioxide is neutral regarding the reaction enthalpy. Literature reports that the complete decomposition of the copper free hydrozincite precursor to zinc(II) oxide is an endothermic decomposition with a reaction enthalpy of 320 $kJmol^{-1}$ (Reaction scheme 23).[187] It can be assumed that the decomposition of copper containing aurichalcite phase yields a similar reaction enthalpy. Referring to the obtained data, it can be assumed that this change in reaction enthalpy is mainly found in the first decomposition step. Due to the experimental setup of the TGA

instrument, a reliable quantification of the heat flow signal (and so the calculation of the standard reaction enthalpy) is not possible.

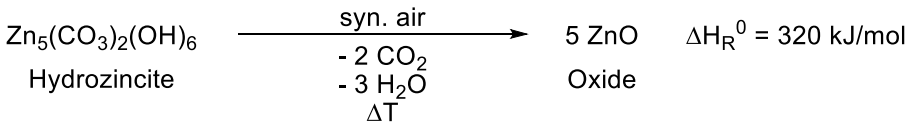

Reaction scheme 23: Decomposition of the copper free hydrozincite phase.

The intermediate species is known from literature as high temperature (HT-) carbonate with the formula $(Cu,Zn)_5O_4CO_3$.[168] Although higher temperatures are needed to form the HT-carbonate in the temperature-programmed thermogravimetric analysis, it can be assumed that 280 °C are sufficient high enough in the isothermal calcination to yield the pure oxycarbonate. Both the resulting metal content and weight loss during the calcination process agree well with the chemical formula of the HT-carbonate. Further increase in calcination temperature leads to the complete decomposition of the oxycarbonate to form copper and zinc oxide (calcined catalyst, Reaction scheme 24).

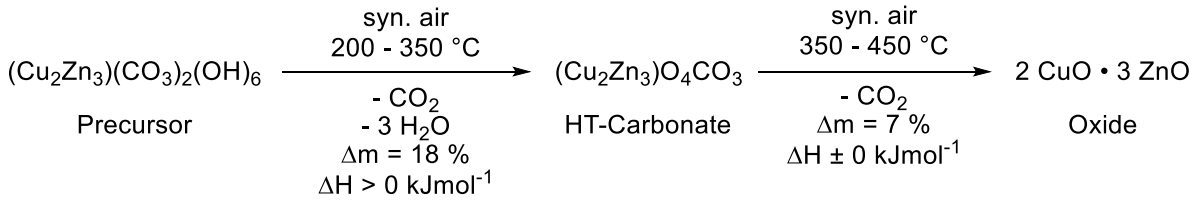

Reaction scheme 24: Decomposition of the copper-zinc precursor over HT-carbonate and oxide.

In summary, both phase pure HT-carbonate and copper-zinc oxide catalysts could be obtained by defined thermal treatment of the precursor phase, consisting mainly of aurichalcite and the zinc pure hydrozincite. Those findings were supported by elemental analysis (ICP-OES) compared to the resulting mass loss during calcination. Additionally, TGA-MS experiments illustrate stepwise decomposition from precursor over HT-carbonate to the final oxide catalyst.

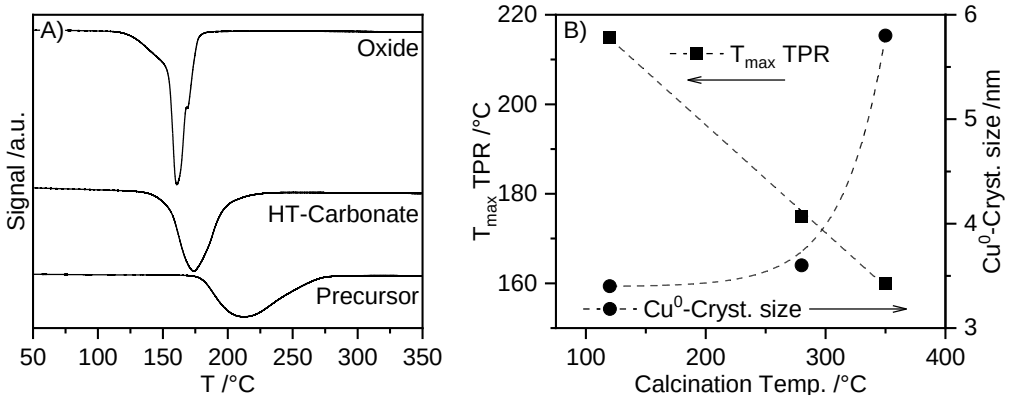

Figure 32: Influence of the calcination temperature on A) the reduction profiles and B) the mean reduction temperature and the copper(0) crystallite size.

The three pre-catalysts (precursor, HT-carbonate and oxide) were characterized by temperature-programmed reduction (TPR), the total (BET) surface as well as the active metal (copper-) surface area after activation. The TPR peaks of the dried precursor and the HT-carbonate are broader in comparison to the oxide peak. The peak maxima decrease with

increasing thermal treatment: from 215 °C for the precursor to 175 °C for the HT-carbonate and 160 °C for the oxide (Figure 32). The broader reduction peaks for both precursor and HT-carbonate could indicate a milder reduction progress. The reduction degree is above 100 % for both precursor and HT-carbonate (which can be explained by interference of the thermal conductivity detector (TCD) signal with released carbon dioxide during the decomposition of precursor). The reduction degree of the fully calcined oxide pre-catalyst is 100 % indicating complete reduction of copper(II) oxide to copper(0).

The total surface area (BET) and active copper surface area (determined by nitrous oxide chemisorption) are higher for the dried precursor and the HT-carbonate compared to the calcined oxide catalyst (Table 13). The total surface area decreases with increasing calcination temperature. A surface area of 68 m^2g^{-1} was found for the dried precursor while 60 m^2g^{-1} was found for the HT-carbonate. The fully calcined oxide has the lowest surface area with 48 m^2g^{-1}. After reduction in hydrogen at 250 °C, the active copper(0) surface area is highest for the HT-carbonate (14 m^2g^{-1}) followed by the precursor (12 m^2g^{-1}) and the reduced oxide (10 m^2g^{-1}). Although the copper surface area is higher for the HT-carbonate, the copper dispersion is nearly the same for the precursor and the HT-carbonate (8.3 and 8.4 %). The copper dispersion of the oxide is significantly lower (5.8 %). The BET surface area decreases around 10 % while the copper dispersion stays nearly the same during the first partial calcination step (precursor to HT-carbonate). The complete calcination from precursor to the oxide results in a 30 % decrease of BET surface area and copper dispersion. This indicates a partial relation between BET surface area and copper dispersion. A decrease of BET surface area at elevated calcination temperatures is known to take place for copper-zinc oxide catalysts.[188]

Summarizing the results reported so far, the following can be concluded: the variation of the thermal treatment resulted in three different catalyst variations. The precursor obtained after co-precipitation and drying consists of aurichalcite and hydrozincite, while the HT-carbonate formed after partial calcination represents a zinc oxide containing carbonate species (Figure 31, B). Crystalline copper-zinc oxide was obtained after full calcination at 350 °C (Figure 31, A). The direct activation of both the dried precursor and the HT-carbonate is possible and can be advantageous (Figure 32). Although slightly higher reduction temperatures are needed to reduce the precursor and the HT-carbonate, a higher copper dispersion as well as a higher total surface area is achieved in comparison to the fully calcined and subsequently reduced oxide catalyst (Table 13). In general, larger copper crystallites are obtained by reduction at higher temperature (Figure 32, B).[189] Potential explanations for the reverse observation in the present study are: a) the copper-zinc interaction is stronger in the dried precursor and HT-carbonate and b) the reduction progress of these catalysts occurs over a broader temperature range. It can be expected that potential hotspots during decomposition and reduction are prevented, decreasing the risk of sintering.

3.5.2 *In situ* investigation of the activation procedure

To get further information regarding the reduction process (formed intermediates, mechanism of reduction), both p-XRD and reductive TGA-MS measurements were performed *in situ*. First, the reduction processes of the three pre-catalysts were investigated by thermal gravimetric analysis coupled to a quadrupole mass spectrometer in flowing hydrogen (Figure 33).

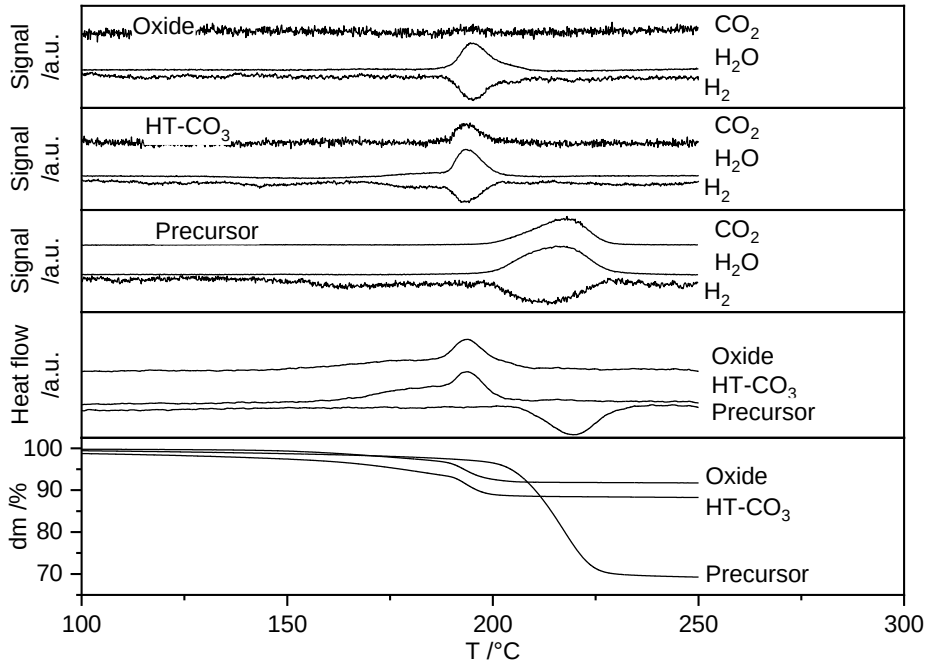

Figure 33: Reductive TGA-MS of the precursor, the HT-carbonate and the oxide. Delta M (bottom), Heat flow/ enthalpy diagram (second from the bottom) and m/z of H_2, H_2O and CO_2 (top to the mittlde).

For the reduction of the dried precursor a mass loss of 32 % is found under release of water and carbon dioxide. No intermediate species can be detected during the reduction at 195 °C. The reduction was identified to be endothermic. The HT-carbonate shows a mass loss of 17 % at 170 °C under release of water and carbon dioxide while a mass loss of 8 % at 160 °C under release of water is found for the fully calcined catalyst (oxide). The reduction of HT-carbonate and oxide were identified to be exothermic. The mass loss of the precursor, HT-carbonate and oxide was found to take place in one step. Additionally, the release of carbon dioxide (precursor and HT-carbonate) and water (all species) is a one step process. The release of water can be attributed to a) the decomposition of hydroxides and b) the reduction of copper oxide to copper(0). This clearly indicates that a) the reduction of copper(II) oxide to copper(0) and b) the decomposition of residual precursor species (hydroxide/ carbonate groups) take place simultaneously. This is further supported by the obtained reaction enthalpy data. While the pure reduction of copper(II) oxide to copper(0) is literature known to be slightly exothermic this could be also seen for the HT-carbonate.[190] On the other hand, the reduction of the precursor is endothermic, indicating that a) both decomposition and reduction take place simultaneously and b) that the decomposition is more endothermic than the reduction exothermic. The mass loss found by TGA measurements fits to model calculations (Reaction scheme 25) and the temperature range fits well to the results obtained from the TPR measurements.

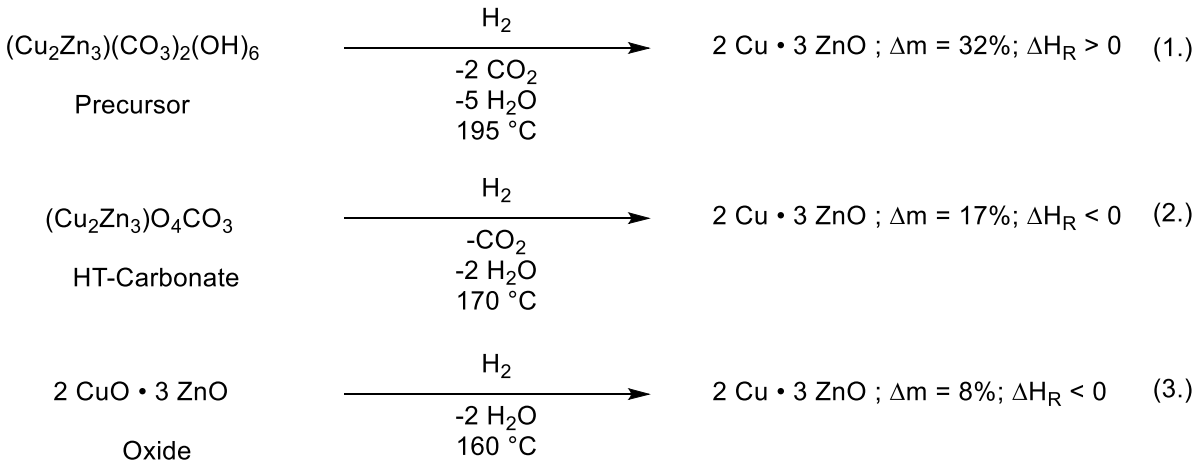

Reaction scheme 25: Direct reduction of 1.) the precursor, 2.) HT-carbonate and 3.) oxide.

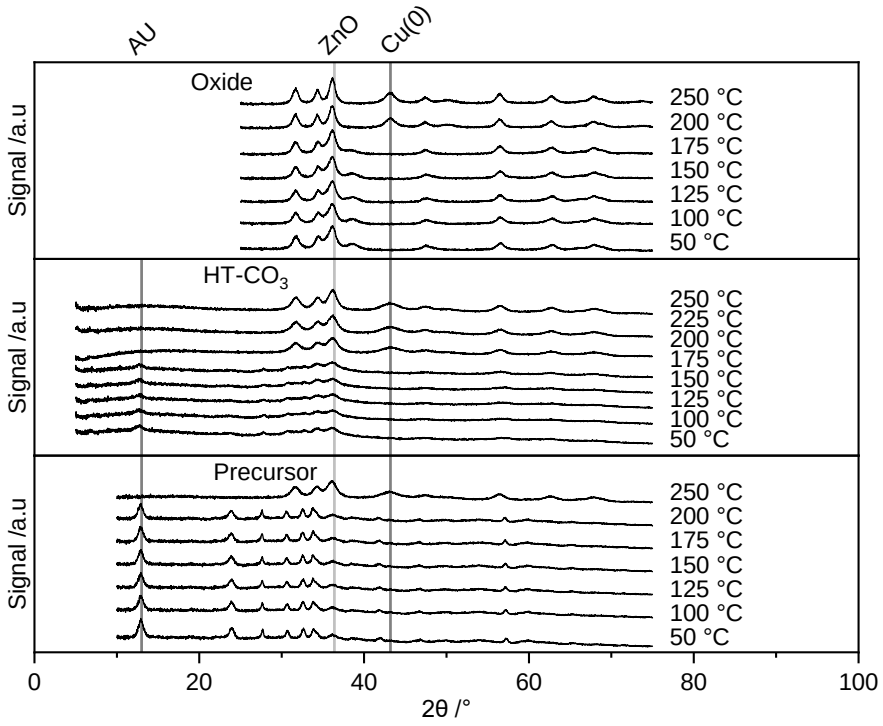

Figure 34: Reductive *in situ* XRD of the precursor, the HT-carbonate and the oxide. Main reflexes according to Aurichalcite, ZnO and Cu(0) are marked. Reference patterns from the COD data base (AU: 96-900-7689, ZnO: 96-900-4179, Cu(0): 96-151-2505)[149, 153, 158].

To get further insights into the activation, the reduction of precursor, HT-carbonate and oxide was also monitored by *in situ* X-ray powder diffraction under reductive atmosphere (Figure 34). For the dried precursor, reflexes belonging to aurichalcite and hydrozincite are present at room temperature.[148-149] No notable phase transformation is found up to 200 °C. At 250 °C, a phase transformation directly to zinc oxide and metallic copper is observed.[153, 158] For the HT-carbonate mainly reflexes belonging to zinc oxide and minor reflexes of remaining precursor phase can be found at room temperature. This indicates minor residues of the hydroxycarbonate phase. No notable phase transformation is observed up to 175 °C. At 200 °C only reflexes belonging to metallic copper and zinc oxide are detected. The copper-crystallite size does not change significantly between 200 to 250 °C. For the fully calcined

oxide catalyst, the phase transformation from copper oxide to metallic copper takes place between 175 to 200 °C.[155] At room temperature and up to 175 °C, reflexes belonging to both copper and zinc oxide are detected. Above 175 °C only metallic copper is found. The copper(0) reflex at 43.3 °2θ is narrower compared to both reduced precursor and HT-carbonate. The copper crystallite size was determined by Scherrer equation to be 3.4 respectively 3.6 nm for the reduced precursor/ HT-carbonate compared to 5.8 nm for the reduced oxide (Figure 32, B). The copper particle size of the directly reduced precursor and HT-carbonate is roughly 40 % smaller compared to the completely calcined and subsequently reduced oxide. This agrees with the decrease in dispersion of the oxide species compared to the precursor and HT-carbonate.

These complementary *in situ* studies confirmed that reductive activation starting from different pre-catalysts yields the completely reduced copper-zinc oxide catalyst in all cases (Reaction scheme 25). The decomposition of hydroxide and carbonate (precursors) and the reduction of copper take place at the same time (Figure 33**,** Figure 34). No (crystalline) intermediates e.g., an oxidic state were found. An increased calcination temperature of the pre-catalyst results in slightly lower reduction temperature but also larger copper crystallites and lower copper dispersions.

3.5.3 Catalysis

The three samples were tested in the gas-phase hydrogenation of butyraldehyde to *n*-butanol after *in situ* activation (Reaction scheme 13). The activities of the reduced precursor and the reduced HT-carbonate are higher compared to the activated oxide after calcination (Figure 35, A). For the precursor and the HT-carbonate conversion of 97 respectively 93 % are obtained, while the completely calcined and reduced catalyst shows a conversion of 81 % at 130 °C. The selectivity to *n*-butanol is for all samples above 99.5 %, only minor side products like 2-ethyl-2-hexenal and butyl butyrate are found. The selectivity was 99.8 % both for the oxide and HT-carbonate compared to 99.7 % for the precursor (measured at full conversion). In general, the selectivity is not affected by the calcination temperature. The activity (given as T_{50}) increases from 108 °C (precursor) over 110 °C (HT-carbonate) to 115 °C for the oxide (Figure 35, B). Full conversion is reached at 145 °C for the activated precursor, 150 °C for the activated HT-carbonate and 165 °C for the oxide. The modified thermal treatment (no or incomplete calcination) of the catalyst precursor does not only lead to higher copper dispersion but also to enhanced catalytic performance.

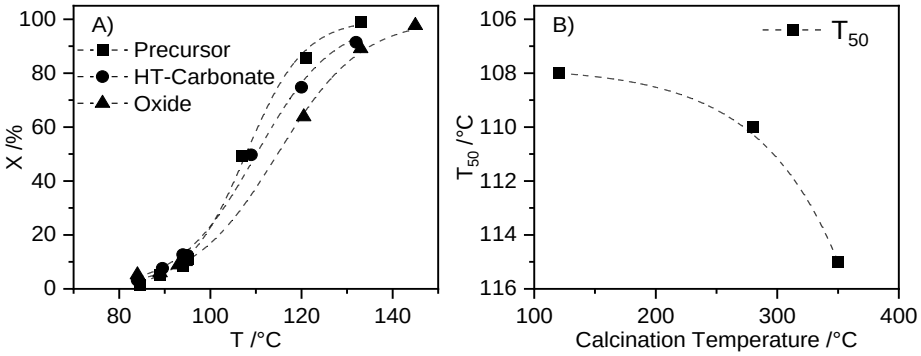

Figure 35: A) Catalytic activity of the precursor, the HT-carbonate and the oxide gives as temperature-conversion curve and B) T_{50} as function of the calcination temperature.

The control of the thermal treatment of co-precipitated copper-zinc precursors allows for the targeted synthesis of any of the three described catalyst phases: Bulk copper-zinc oxide hydrogenation catalysts can be prepared by reductive activation after full calcination to the copper-zinc oxides. Additionally, the direct reduction of both precursor and partially calcined HT-carbonate in hydrogen yields an active hydrogenation catalyst. The direct activation of the dried or incompletely calcined precursors leads to a higher copper dispersion and increased catalytic activity in the hydrogenation of butyraldehyde to *n*-butanol compared to the activated oxide catalyst. The copper reduction takes place at the same time as the decomposition of the (hydroxy-) carbonate phases without the formation of (crystalline) copper oxide intermediates.

3.6 Synthesis of a copper-zinc catalyst via a design of experiments approach

As discussed in previous chapters, the influence of synthesis conditions, especially the precipitation conditions can have a strong influence on the properties and the catalytic activity of copper-zinc catalysts. Numerous parameters like the composition and concentration of metal precursors, the precipitation agent, aging conditions, the calcination, or activation and furthermore influence the properties and the catalytic activity of copper catalysts. Especially the precipitation conditions seem to have a strong influence. The variation and detailed evaluation of all parameters individually would lead not only to a countless number of experiments needed, but also very likely to misinterpretation or overlooking of interaction effects of different parameters.[191] Optimal synthesis conditions as well as structure activity relationships shall be gained for a highly active copper-zinc catalyst used in the hydrogenation of butyraldehyde. For this reason, a design of experiments was set to evaluate statistically a number of precipitation conditions. This design of experiments approach enables that conclusions regarding the importance and the interaction of precipitation parameters (factors) can be drawn. While a variety of important precipitation parameters was varied in a design of experiments approach, all other parameters (like the copper to zinc ratio, the precipitation agent or calcination and activation conditions) were fixed according to previous results or literature. After precipitation, drying and aging, the catalysts were characterized regarding there structure properties (elemental analysis, XRD, TPR, BET and copper surface area) and tested in the butyraldehyde hydrogenation. The importance as well as interaction of the individual synthesis conditions to each other shall be obtained regarding surface properties and the catalytic activity of the catalysts. Additionally, synthesis-structure-activity relationships shall be drawn.

3.6.1 Influence of synthesis parameters on the properties and the catalytic activity

The concentration of the copper-zinc and the soda solution were varied between 0.75 and 1.25 M. A lower concentration could lead to incomplete precipitation while a higher concentration could lead to incomplete dissolved solutions. The precipitation pH was varied between 7 and 9, lower values could lead to precipitation of undesired gerhardtite phase (see also chapter 3.3.2) while a pH above 9 could lead to the direct precipitation of tenorite (copper oxide) which reduces the catalytic activity significantly.[192] The aging time was varied between 30 and 90 minutes to allow at least a partial aging and recrystallization (see also chapter 3.3.2, Figure 21) while a too long synthesis time is not feasible regarding experiment efficiency. The aging temperature was varied between 55 and 85 °C regarding literature reports which claim an optimum aging temperature to be around 70 °C.[93]

A 2^{5-1} fractional factorial design was set with the aging temperature as product of the other four parameters. This could reduce the number of experiments from 32 to 16. Additionally, the center point (1 M copper-zinc solution, 1 M soda solution, pH = 8, 70 °C, 1 h aging) was measured three times. The experimental plan is summarized in Table 14.

Table 14: Experimentel plan for the synthesis of copper-zinc catalysts.

Experiment	**Run**	**C (Cu,Zn)**	**C (Na_2CO_3)**	**pH**	**Aging time**	**Aging temperature**
-	-	M	M	-	min	°C
DoE-13	2	0.75	0.75	9	90	85
DoE-14	3	1.25	0.75	9	90	55
DoE-6	4	1.25	0.75	9	30	85
DoE-9	5	0.75	0.75	7	90	55
DoE-5	6	0.75	0.75	9	30	55
DoE-10	7	1.25	0.75	7	90	85
DoE-2	8	1.25	0.75	7	30	55
DoE-1	9	0.75	0.75	7	30	85
DoE-8	11	1.25	1.25	9	30	55
DoE-16	12	1.25	1.25	9	90	85
DoE-12	13	1.25	1.25	7	90	55
DoE-4	14	1.25	1.25	7	30	85
DoE-11	15	0.75	1.25	7	90	85
DoE-7	16	0.75	1.25	9	30	85
DoE-15	17	0.75	1.25	9	90	55
DoE-3	18	0.75	1.25	7	30	55
Central-1	1	1	1	8	60	70
Central-2	10	1	1	8	60	70
Central-3	19	1	1	8	60	70

The calcined catalysts were characterized by various techniques and the catalytic activity was determined in the hydrogenation of butyraldehyde. The BET and the copper surface area, the mean reduction temperature, copper and zinc oxide crystallite size as well as the catalytic activity (calculated as T_{90}) were determined to be a statistically significant response factor and will be discussed in detail. The change to occur due to noise is below 5 % for this response factors and can be seen as statistically relevant (Table 15). These response factors for all experiments and the central points are listed in Table 16. The surface area was determined to be between 52 and 71 m^2g^{-1} (BET) respectively 12 to 17 m^2g^{-1} (active copper). The mean reduction temperature was found to be between 167 and 203 °C. The copper oxide crystallite size was determined to be between 3.9 and 7.4 nm and 6.5 to 9.5 nm for the zinc oxide crystallite size. The catalytic activity determined as T_{90} was found to range between 186 and 298 °C. Other response factors like the copper-zinc ratio, the reduction degree or the pore distribution are not affected significantly by the precipitation conditions and will not be discussed.

Table 15: Ananylsis of variance (ANOVA) of the design responce factors.

		BET-SA	Reduction temp.	Cu-SA	CuO-Cryst. Size	ZnO-Cryst. Size	Activity (T_{90})
Signal to noise ratio	-	3.23	2.32	2.6	20.48	3.08	14.26
Model F-value	-	6.05	4.02	16.4	4.56	5.46	4.46
Change to occur due to noise	%	0.88	2.65	0.1	4.85	1.21	1.93

Table 16: Response factor of the design DoE experiments.

Experiment	BET-SA	Red. temp.	Cu-SA	CuO-Cryst. Size	ZnO-Cryst. Size	Activity (T_{90})
-	m^2g^{-1}	°C	m^2g^{-1}	nm	nm	°C
DoE-13	61	198	15.1	6.2	8.3	208.5
DoE-14	58	182	13.8	7.4	8.9	203.2
DoE-6	63	196	15.6	5.4	8.4	192.4
DoE-9	71	191	14.8	5.9	8.2	185.5
DoE-5	63	178	16.7	5.3	6.5	205.7
DoE-10	52	175	14.2	5.2	7.7	240.0
DoE-2	64	167	12.6	5.3	7.4	205.2
DoE-1	57	203	12.6	4.7	8.0	220.1
DoE-8	64	181	16.4	7.3	7.4	253.0
DoE-16	62	173	15.4	5.1	8.4	216.0
DoE-12	58	179	12.0	5.8	9.2	214.9
DoE-4	56	178	14.1	5.7	8.8	233.7
DoE-11	53	180	14.3	5.5	8.6	195.8
DoE-7	62	169	15.6	5.1	7.7	202.0
DoE-15	64	188	15.4	7.4	8.4	202.6
DoE-3	62	169	14.5	6.4	9.0	298.2
Central-1	59	175	15.3	3.9	7.8	192.9
Central-2	56	n.d.	14.4	n.d.	8.0	197.0
Central-3	57	184	n.d.	4.0	8.3	193.3

While the copper surface area and the copper oxide crystallite size are only affected by one precipitation parameter (precipitation pH respectively the aging temperature), different main and interaction effects are found to be relevant for the BET surface area, the zinc oxide crystallite size, the main reduction temperature, and the activity. The relevant factors and the interaction effects were calculated as nominated value (Figure 36).

It could be shown that the BET surface area is mainly affected by the aging temperature and the interaction of the pH and the aging temperature. Additionally, the pH, the interaction of soda concentration and the pH and the interaction of aging time and the copper-zinc concentration play a minor roll. A higher aging temperature leads in general to a lower surface area, especially if the pH is set to its low level. At a high pH the aging temperature has only a minor influence. It can be assumed that a higher aging temperature increases slightly the solubility of the precipitates. This could lead to an increased mixing and the precipitation of precursor phases with smaller pores which have a lower surface area. This effect is minimized

if the pH is set to the high level where a fast precipitation due to a high hydroxide and carbonate concentration is obtained.

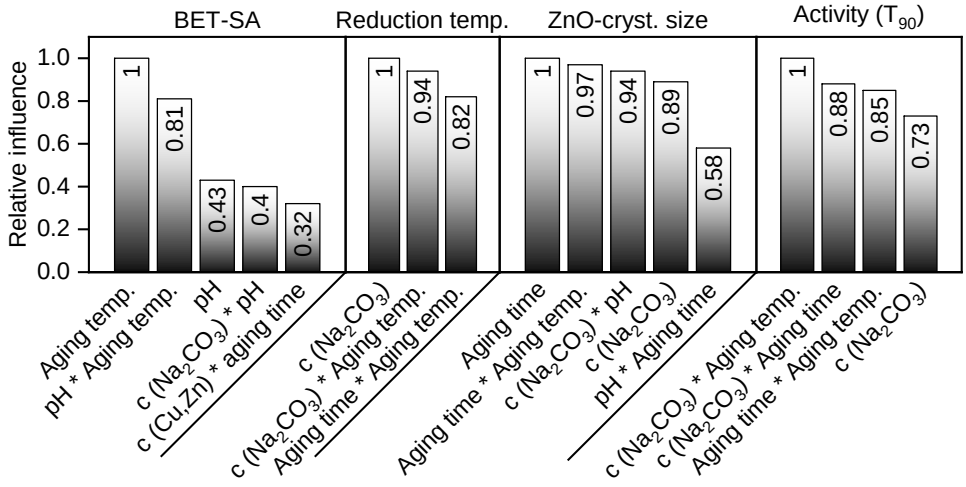

Figure 36: Relative influence of significant parameters and their interactions on the BET surface area, the mean reduction temperature, the zinc(II) oxide crystallite size (Scherrer) and the catalytic activity (T_{90}).

The reduction temperature is affected by the soda concentration as well as the interaction of soda concentration and aging temperature. Additionally, the interaction of aging temperature and time has an influence. In general, a higher soda concentration leads to a lower mean reduction temperature. This effect is strengthened at the high level of the aging temperature while the soda concentration has only a minor influence on the mean reduction temperature if the aging temperature is set to its low level. A longer aging time at the low level of the aging temperature increases the mean reduction temperature while there is no influence of the aging time if the aging temperature is set to its low level. A higher soda concentration leads in general to a faster precipitation and less copper-zinc interactions. A higher aging temperature increases the solubility which leads to larger particles which form larger copper oxide crystallites. This reduces the mean reduction temperature. A longer aging allows a better mixture between copper and zinc particles which leads to a higher copper-zinc interaction. It can be assumed that a stronger interaction leads to a slightly higher reduction temperature.

The copper surface area is only affected by the pH value, where a higher precipitation pH increases the copper surface area. It can be assumed that a higher precipitation pH leads to a higher concentration of hydroxide and carbonate ions in the precipitation solution. This leads to a faster formation of insoluble copper-zinc hydroxycarbonates which prevents sintering effects and leads to higher copper-zinc interaction. Smaller copper oxide particles are formed which lead (after activation) to a higher copper surface area.

A similar effect if found for the copper oxide crystallite size, where a higher aging temperature leads to smaller particles. A higher aging temperature increases the speed of precipitation and smaller particles are formed which have a stronger copper-zinc interaction. These particles lead to smaller copper oxide crystallites after calcination.

A variety of factors influence the zinc oxide crystallite size. Especially the aging time and the soda concentration as well as the interaction of aging time and temperature and pH and soda concentration have a significant influence. Also, the interaction of pH and aging time if found to have an influence but compared to the other factors this is only a minor influence. Both increasing soda concentration and a higher aging time lead to larger zinc oxide crystallites. The soda concentration has especially a significant influence it the pH is set to its low level. A high pH value decreases the effect of the soda concentration. The effect of the aging time is increased if the aging temperature is set to its low level while a high aging temperature decreases the influence of the aging time. A faster precipitation is obtained at a higher soda concentration which leads to less copper-zinc interactions. This effect is strengthened at a low hydroxide concentration. Additionally, it can be assumed that a high soda concentration at a low pH value leads to a high carbonate but a low hydroxide concentration in the precipitation solution. This would be beneficial for the precipitation of a copper free zinc carbonate, whereas a pure copper carbonate does not exist. Longer aging times allow the growth of larger precursor particles (sintering effects) which lead to an increased zinc oxide particle side.

The catalytic activity is influenced by the soda concentration and the interaction of soda with aging time and temperature as well as the interaction of aging time and aging temperature. A higher soda concentration leads to less active catalysts (higher T_{90}). This effect is strengthened if the aging temperature or the aging time are set to its low levels while the influence of soda concentration is minor if aging time or aging temperature are set to its high levels. A high aging time at the low level of the aging temperature increase the catalytic activity while at the high aging temperature level the aging time has only a minor influence on the catalytic activity. As previously discussed, a higher soda concentration leads to slightly increased particle size which yields in less active catalysts. Additionally, a low aging temperature can lead to larger particles (decreased catalytic activity). This effect is minimized at high aging temperatures where beneficial copper-zinc interactions are obtained (which are beneficial for copper-zinc catalysts). Additionally, a long aging decreases the influence of the soda concentration due to increased copper-zinc interactions. On the other hand, a high aging temperature leads to a faster precipitation so that the effect of the beneficial copper-zinc interactions due to a long aging time is decreased.

3.6.2 Structure-activity relationships in copper-zinc oxide catalysts

The obtained data allow additionally a discussion of the catalytic activity as a function of (surface-) properties of the catalysts. Two roughly linear trends could be identified: A higher reduction temperature as well as a higher BET surface area lead in general to an increased catalytic activity and lower T_{90} (Figure 37). A higher reduction temperature is obtained due to smaller particles and a better copper-zinc interaction. Smaller particles lead to beneficial

surface properties (not only the BET surface area but also the copper surface area) which are beneficial for a highly active catalysts due to a higher number of active sites.

A higher BET surface area is obtained due to a faster precipitation, a lower solubility and the precipitation of smaller particles. Smaller particles lead to a higher copper surface area and a higher number of active sites. Additionally, a higher copper-zinc interaction is found since the copper-zinc segregation is prevented during the precipitation. This is beneficial for the catalytic activity so that catalysts with a higher activity are obtained in the case of a higher BET surface area.

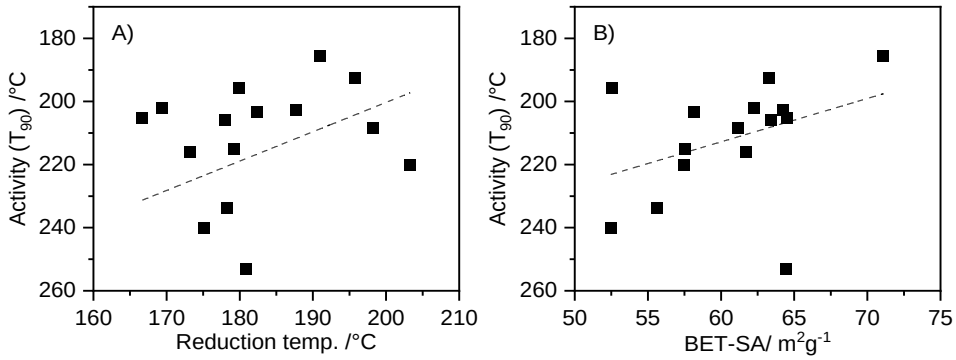

Figure 37: Influence of A) the mean reduction temperature and B) the BET surface area on the catalytic activity.

In general, the following properties lead to highly active copper-zinc catalysts for the hydrogenation of butyraldehyde: a) a high BET surface area, b) good copper-zinc interactions and c) the precipitation of smaller crystallites. This is obtained especially in the case of fast precipitation (e.g., due to a high hydroxide concentration) and the prevention of the segregation of copper and zinc particles (e.g., due to a lower soda concentration or a decreased aging time).

It is evident that a design of experiments approach is a highly effective tool for the optimization of synthesis conditions of a copper-zinc oxide hydrogenation catalyst. It was not only possible to optimize a variety of synthesis conditions with a handful of experiments and to gain a highly active catalyst, but also clear insights into the complex precipitation process could be presented and direct synthesis-structure-activity relationships could be drawn.

3.7 Conclusion

Copper-zinc oxide catalysts used for the aldehyde hydrogenation are synthesized by co-precipitation followed by thermal treatment of hydroxycarbonate precursors and subsequent activation. Aurichalcite was found to be the predominant precursor phase for copper-zinc oxide hydrogenation catalysts with a molar copper-to-zinc ratio of 1:2. A metastable high-temperature carbonate was found as an intermediate during the thermal decomposition. Activation conditions were optimized to allow a) a complete reduction of copper, b) a mild reduction process to form a high copper surface area and to prevent the catalyst from sintering and c) the reduction in a feasible time. This highly active catalyst can be used for the gas-phase hydrogenation of butyraldehyde.

A variety of precipitation conditions have a strong influence on the physical properties and the catalytic activity of the catalyst. The complex phase composition of the copper-zinc precursor obtained by co-precipitation under slightly alkaline conditions was resolved as a function of the copper-to-zinc ratio. Depending on that, hydrozincite, aurichalcite, or malachite were found to be the predominant precursor phase. Catalysts obtained from aurichalcite-rich precursors show beneficial properties regarding a) a high copper dispersion, b) a mild reduction behavior and c) a high catalytic activity. This can be attributed to higher copper-zinc interactions found for these catalysts which are transferred from the precursor through the whole process of precipitation, calcination and activation. A “chemical memory effect” is found for these catalysts. The synthesis of the catalysts under slightly acidic conditions leads to the precipitation of the undesired gerhardtite phase. Although the precipitation of gerhardtite as an additional precursor phase does not influence the decomposition process, the catalytic properties are strongly influenced. Larger copper oxide crystallites are obtained, which show a disadvantageous reduction behavior and a lower catalytic activity. A complex interplay between precursor phase composition, the decomposition during the calcination and the active catalyst occurs.

Copper aluminate spinel catalysts show similar activity to copper-zinc oxide catalysts. Comparable copper-(zinc-)aluminum oxide catalysts are slightly less active due to strong metal support interactions. The complex decomposition and reduction process of the copper aluminate spinel catalyst was resolved: Different decomposition steps take place and a metastable high-temperature carbonate is obtained for partially calcined copper-aluminum catalysts (similar to pure copper-zinc catalysts). The pure oxide is obtained in a second decomposition step while further temperature increase leads to the crystallization of the spinel. The synthesis of a phase pure copper aluminate spinel is not possible but a controlled leaching step can reduce the oxide residuals to a minimum. Two copper sites are found in the spinel, copper in the oxide and in the spinel lattice. To obtain a highly active catalyst both copper sites have to be reduced yielding metallic copper supported on an oxidic aluminum modification.

Precise thermal treatment allows the targeted synthesis of the high-temperature copper-zinc oxycarbonate. The direct reductive activation of the oxycarbonate and the hydroxycarbonate is possible and leads to beneficial surface properties: a higher copper dispersion, a milder reduction behavior and a slightly higher catalytic activity are obtained. Additionally, the complex reduction mechanism was resolved by *in situ* techniques and it could be shown that the decomposition of (hydroxy-) carbonates and the reduction of copper takes place simultaneously.

The complex interplay of various precipitation factors was investigated by a design of experiments approach. A variety of precipitation conditions influence the physical properties and the catalytic activity of copper-zinc catalysts, especially the precipitation agent and the aging are very important parameters. A higher surface area and a higher mean reduction temperature lead to an increased catalytic activity, which can be obtained by a fast precipitation process and the prevention of segregation of copper and zinc particles during aging.

New insights into the complex precipitation-calcination-activation process of copper-zinc catalysts could be presented.

4

Deactivation of Copper Catalysts

4.1 Introduction

Copper catalysts are used in a broad variety of hydrogenation reactions.[57, 124] On the one hand, high volume gas-phase reactions like the methanol synthesis, the reversed water gas shift reaction (RWGS) or the reduction of nitrous oxide are catalyzed by copper catalysts.[129-131, 133] On the other hand, copper catalysts are additionally used as hydrogenation catalysts in the field of organic synthesis. Especially due to the preferred hydrogenation of C-O bonds, copper catalysts can be used as cheaper alternative to palladium catalysts which generally prefer the hydrogenation of C-C bonds.[125-126, 146, 193-195]

Large scale gas-phase hydrogenation reactions – especially the methanol synthesis – are catalyzed by copper-zinc(-aluminum) oxide systems.[176] These catalysts are typically synthesized via co-precipitation.[154] A thermal treatment follows yielding the oxidic precatalysts. Subsequently, a reductive activation leads to the active form of the catalyst, which can be described as metallic copper on zinc oxide.[96] Huge scientific effort concentrates on structure activity relationships of the (pre-)catalyst in the field of methanol synthesis.[92, 160, 196] Additionally, numerous publications deal with the hydrogenation mechanism of the methanol synthesis catalyst.[197-198] In contrast, scientific work investigating these catalyst systems in other reactions, especially in the field of organic C-O bond hydrogenation is limited.[199] Especially detailed discussions of the mechanism are not reported.

Copper-aluminum catalysts are often used in the field of C-O bond hydrogenation.[128, 200] These catalysts are used in a broad range from the hydrogenation of aldehydes and ketones, the hydrogenolysis of esters or the reduction of amides to amines.[71, 85, 122, 201-202] They are also applied in dehydrogenation reactions including the dehydrogenation of alcohols.[203-204] Special attention should be paid to copper aluminate spinel systems which are often used as ecological alternative to chrome containing Adkins catalysts.[34, 205] In general, the preparation of these catalysts is done similarly to methanol synthesis catalysts via co-precipitation.[206-207] While copper-zinc oxide species are obtained after calcination of precipitated copper-zinc hydroxycarbonate precursors, the thermal treatment is more critical in the case of copper-aluminum catalysts. A calcination temperature below 500 °C yields copper-aluminum oxides, while a calcination temperature above 700 °C leads to formation of copper aluminate spinels.[208-209]

One particular reaction in the field of organic C-O bond hydrogenation is the aldehyde hydrogenation of butyraldehyde to *n*-butanol. Downstream applications are, inter alia, the use as plasticizers (especially 2-ethylhexanol, obtained after aldol condensation and subsequent hydrogenation) or flavors and paints.[152, 210] Additionally, butanol can be used as promising alternative to gasoline fuel as replacement for bioethanol for internal combustion engines.[211-212]

While several reports deal with copper-alumina used for the butyraldehyde hydrogenation, only a limited number of reports use copper-zinc oxide catalysts for this reaction.[71, 108] Mostly, this

reaction is done in the liquid-phase (especially over copper aluminate spinel catalysts). Nevertheless, the hydrogenation in the gas-phase is also possible and mostly done over copper-zinc oxide catalysts.[108, 144, 146] The long-term stability is a critical aspect for the gas-phase reaction. In case of the liquid-phase hydrogenation, the chemical and mechanical stability of these catalysts is of particular interest. Especially leaching effects can decrease the stability of the catalysts.[213]

Several reports deal with the mechanism of this reaction, both in the liquid and the gas-phase. While in general a Langmuir-Hinshelwood mechanism is accepted for the liquid-phase hydrogenation, an Eley-Rideal mechanism is assumed for the gas-phase hydrogenation. The Langmuir-Hinshelwood mechanism is based on the idea that the reaction takes place on the surface of the catalyst and involves the adsorption of all reactant molecules onto the catalyst surface. The Eley-Rideal mechanism, on the other hand, assumes that one of the reactants is in the gas-phase, while the other is adsorbed on the catalyst surface.[175, 214-215] It can be assumed that a longer free path way in the gas-phase allows an Eley-Rideal mechanism. Additionally, not only the reaction phase but also the catalyst influences the mechanism. Gudkov *et al.* reports that copper(0) sites are the active sites in the gas-phase hydrogenation of butyraldehyde over metallic copper catalysts. Also, the hydrogenation follows an Eley-Rideal mechanism. By isotope exchange reactions, they showed that dissociatively adsorbed hydrogen is formed on copper(0) sites.[175] At the same time, Hubaut *et al.* showed that the liquid-phase hydrogenation of allylic alcohols over copper aluminate and copper-chromite spinel catalysts lead to a broad variety of primary products. In the mixed oxides, two active sites are simultaneously present. While copper(I) sites catalyze the hydrogenation of C-C bonds, chromium and especially aluminum centers favor isomerization reactions.[85] Bechara *et al.* support the findings that copper(I) sites are active in C-C bond hydrogenation. Additionally, they claimed that reductive activation of a copper aluminate spinel leads to copper(0) centers on the surface and copper(I) sites in the octahedral positions.[216] Yurieva *et al.* showed that copper(0) sites are found after reductive activation on the surface of copper aluminate spinels. These centers can activate the acetone C-O bond while protons from the spinel lattice (which balance the negative charge caused by the reduction of copper) migrate to this bond, isopropanol is formed and desorbs from the surface. An oxidation of copper results and copper(II) migrates back in the spinel lattice.[217] Simentsova *et al.* showed that reductive activation of copper aluminate spinels leads to formation of copper(0) particles on the surface under evolution of water while bulk reduction of copper occurs over incorporation of protons in the lattice to balance the negative charge.[218] Plyasova *et al.* observed that different copper sites are present in copper aluminate spinels. By high temperature X-ray analysis, they showed that copper in tetrahedral sites can be reduced below 300 °C while the reduction of copper in octahedral sites needs temperatures above 300 °C. Above 400 °C, a partial dissolving of the oxygen framework takes place.[186] In comparison to findings by

Bechara *et al.*, Rodriguez *et al.* showed that a formation of copper(I) sites during the reductive activation in typical copper-oxide systems does not take place. Only a strongly limited hydrogen supply leads to formation of copper(I) sites.[219] Fierro *et al.* support this theory and claimed that promoting copper-oxide catalysts with zinc oxide leads to even lower reduction temperatures.[220]

Two drawbacks result from the presented studies: While most of them relate the catalytic activity with the structure and the morphology of the pre-catalyst or the activated catalyst, a detailed investigation of the used catalyst is missing. Additionally, the mechanism of the hydrogenation of aldehydes, in particular the hydrogenation of butyraldehyde is discussed either in the gas or the liquid-phase and concentrates mainly on copper-aluminum catalysts. Comparison between copper-aluminum and copper-zinc oxide systems are missing so far.

To overcome these drawbacks, a test setup for the gas-phase hydrogenation of butyraldehyde was developed which allows the inert handling of used catalysts. This enables detailed characterization of the structure and the morphology of used catalysts. These findings are related to the catalytic properties of the investigated catalysts. Copper-zinc oxide and copper aluminate spinel catalysts were synthesized by co-precipitation followed by thermal treatment and reductive activation. These catalysts were applied in the hydrogenation of butyraldehyde. The used catalysts were obtained after gas-phase hydrogenation and characterized by various techniques including elemental analysis (CHNS), powder and *in situ* XRD, BET surface area determination, thermogravimetric analysis and temperature-programmed desorption experiments (all under inert conditions). The obtained results were compared to the long-term stability of the catalysts and the deactivation mechanisms is discussed. The hydrogenation was performed additionally in the liquid-phase and leaching effects were determined. The catalytic performance of copper-zinc oxide and copper aluminate spinel catalysts were compared to the ones obtained from the gas-phase hydrogenation and a comparative mechanistic discussion is presented.

4.2 Gas-phase test unit for inert handling of used catalysts

An existing test unit (single test unit, STU) was modified to allow the inert handling of spent catalysts after their use in the gas-phase hydrogenation of aldehydes. Beforehand, the unit was used for the carbon dioxide methanation and the synthesis of methanol. The unit is described in detail by O. Thomys, the PI-diagram as well as an image of a) the unit itself and b) the reactor is given in Figure 38 and Figure 39.[221] The catalyst is loaded in a 4.5 mm inner diameter U-shaped stainless-steel reactor (fixed bed reactor) placed in a PC controlled oven. This reactor has a bypass and can be connected and disconnected from the unit under inert conditions which allows the inert handling of used catalysts. The outlet of the reactor is connected to an online gas chromatograph (GC) for the quantification of educt, product and side products to calculate the conversion and selectivity. The pipe connection between reactor and GC is electrically heated to prevent condensation of water or other liquids. The gas flow (He, CO_2 and H_2) is controlled by mass flow controllers installed before the reactor. The pressure in the reactor is maintained by a manually controlled back-pressure regulator installed downstream to the reactor.

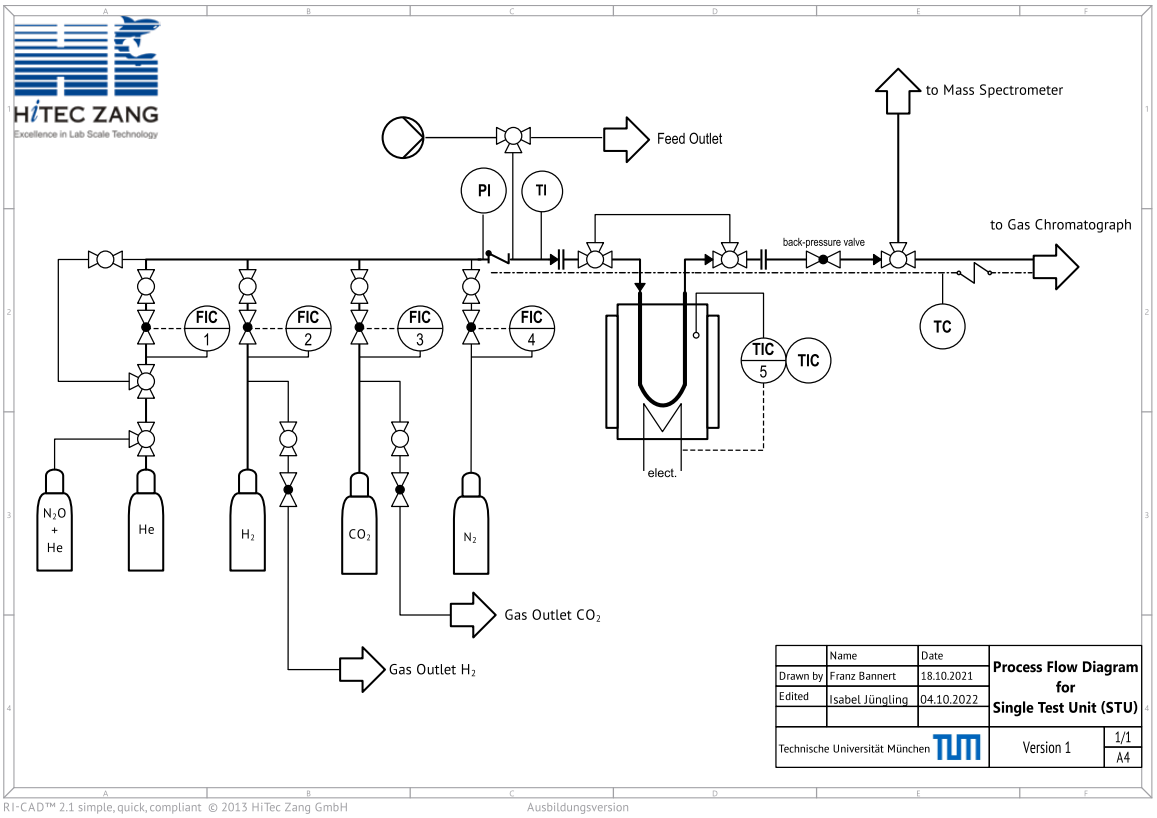

Figure 38: PI-diagram of the modifed single test unit.

To allow the gas-phase hydrogenation of aldehydes, a HPLC-pump was installed for feeding of these (liquid) aldehydes. A thin capillary is used as feed outlet and placed in a heated T-pipe installed upstream to the reactor. In this T-pipe, a) aldehyde and hydrogen are mixed and b) due to the increased temperature and the decreased aldehyde vapor pressure a continuous vaporization of the aldehyde takes place. The vaporization was monitored time resolved by a

mass spectrometer connected to the outlet of the reactor and a (nearly) fluctuation free and continuous vaporization can be guaranteed. The modification of the test unit and the preliminary tests are reported in detail in the thesis of I. Jüngling.[222]

Figure 39: A) Picture of the test unit and B) picture of the U-shaped reactor.

To compare both test units (ILS, chapter 2.1 and the modified single test unit), a stability test at 125 °C was performed with the copper-zinc benchmark catalyst (chapter 3.2). To allow characterization of used catalysts under inert conditions, the catalyst bed dilution was omitted in the modified single test unit. All other activation and catalysis parameters (GHSV, LHSV, ratio particle size to inner diameter of the reactor) were kept constant respectively adapted to the modified reactor geometry (see also chapter 6.5).

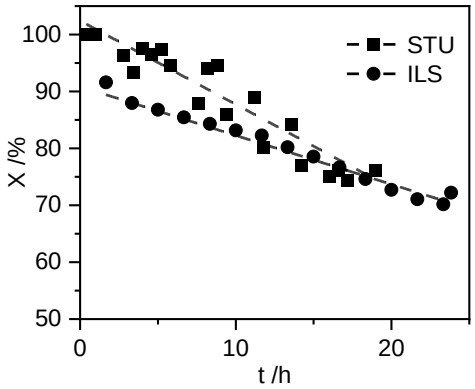

Figure 40: Catalytic activity as function of time of the Cu-Zn benchmark catalyst in both test units.

While an initial activity of around 90 % is reached at the ILS test unit, the modified STU shows an initial activity of nearly 100 %. In both test units a strong deactivation is found. The copper-zinc benchmark catalyst loses around 15 % conversion within one day in the ILS while slightly higher deactivation rates are found for the modified STU. The decreasing conversion proceeds roughly linear. It can be assumed that the temperature control is slightly more accurate in the ILS compared to the modified STU. In the ILS, a thermocouple is in direct contact to the catalyst bed so that a direct measurement of the catalyst temperature takes place. On the other hand,

the temperature in the modified STU is only controlled over a thermocouple placed in the oven. It can be assumed that a slightly higher reaction temperature in the modified STU leads to slightly higher initial activity. Another explanation could be that the omission of the catalyst bed dilution in the modified STU lead to hotspots. As seen previously (chapter 2.3), the dilution of the catalyst bed with an inert filling is necessary to prevent hotspots and to allow isothermal reaction control. Most likely, hotspots occur during the reaction which lead to a slightly overestimation of the conversion. These hotshots could lead in addition to sintering effects of copper crystallites which increases the observed deactivation rate of the copper catalyst.

To test if an inert handling of the catalyst is possible in the modified test unit, a p-XRD of the activated copper-zinc benchmark catalyst was taken under inert conditions. Therefore, the catalyst was activated in the test unit and transferred under inert conditions into the glovebox where a capillary for XRD measurements was prepared. Subsequently, the powder-XDR pattern were taken. The reduced catalyst shows only reflexes according to zinc oxide and copper(0) indicating that an inert handling of the catalyst is possible and no (bulk) copper oxidation takes place (Figure 41, B).

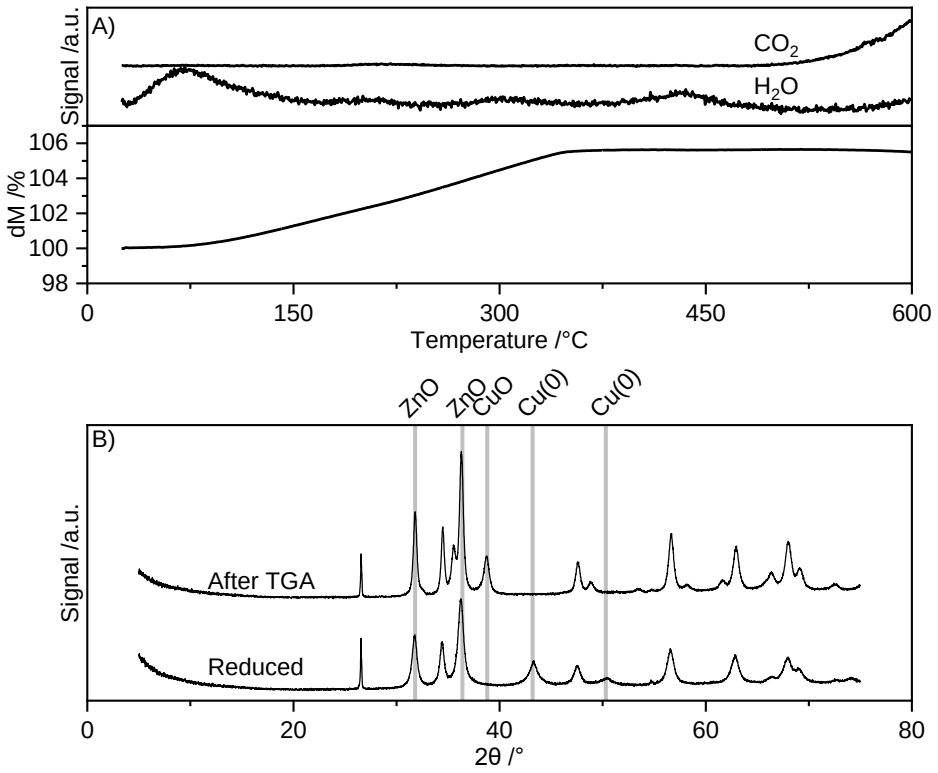

Figure 41: Method developement for the characterization of spent catalysts. A) TGA of reduced Cu-Zn oxide catalyst. B) p-XRD of reduced Cu-Zn oxide catalyst before and after TGA analysis. Reflexes according to the COD data base (CuO: 96-101-1149, Cu: 96-151-2505, ZnO: 96-900-4179). [153, 155, 158]

In addition, a thermogravimetric analysis was performed with the activated catalyst under nitrogen. Therefore, the catalyst was transferred under pseudo-inert conditions (argon sealed TGA pan) into the TGA and inserted in the nitrogen filled oven chamber. The catalyst was heated under nitrogen to 600 °C and the mass change and the MS signal for water and carbon dioxide were recorded (Figure 41, A). At around 100 °C a small water signal can be found in

the MS while no mass change takes place at this temperature. Between 150 and 350 °C a mass gain of around 6 % takes place while no water or carbon dioxide is released. Further temperature increase above 550 °C leads to evolution of carbon dioxide. The water signal is attributed to desorption of minor amounts of water from the catalyst surface (no measurable change in the mass). The mass gain of 6 % can be attributed to the oxidation of copper to copper(II) oxide. A theoretical value of 7 % mass gain can be calculated for the complete oxidation of the copper-zinc benchmark catalyst with a copper loading of 27 %. This indicated that a (nearly) complete oxidation of copper to copper(II) takes place during the thermogravimetric analysis under nitrogen. It can be assumed that minor oxygen residuals in the oven chamber in the TGA are enough to allow a complete copper oxidation. The evolution of CO_2 above 550 °C can be referred to release of minor high-temperature carbonate residuals. On the other hand, nearly no mass loss is found above 550 °C indicating that only marginal carbonate residuals are present in the activated (and beforehand calcined) copper-zinc benchmark catalyst.

Summarizing the results so far, it could be shown that the modified single test unit allows the catalytic test of copper catalysts in the gas-phase hydrogenation of aldehydes as well as the inert handling of used catalysts. Similar test results are obtained in the ILS and the modified STU, nevertheless, the omission of the catalyst bed dilution leads to a slight overestimation of initial activity and a slightly faster catalyst deactivation (probably due to hotspots). The inert handling of used catalysts is possible, no oxidation takes place during the handling. Nevertheless, also under a nitrogen atmosphere during the thermogravimetric analysis, oxidation of copper(0) to copper oxide takes place due to oxygen residuals in the oven chamber.

4.3 Deactivation behavior of copper catalysts

To investigate the deactivation of copper catalysts in detail, a variety of copper-zinc oxide and copper-aluminum oxide and spinel catalysts were synthesized, tested in their activity and stability in the butyraldehyde hydrogenation and characterized by various techniques after the catalysis test (powder and *in situ* XRD, BET, CHNS, TPD, TGA). A modified test unit was used which allows the inert handling of used catalysts. The deactivation behavior of the catalysts is linked to changes in their structural properties to get a deeper understanding of the deactivation mechanism. A detailed discussion of the synthesis and the characterization of the catalyst precursors is given previously in this thesis (chapter 3.4).

4.3.1 Comparison between copper oxide and copper spinel catalysts

Copper-zinc(-aluminum) oxide as well as copper-aluminum oxide catalysts were synthesized by coprecipitation and subsequent calcination at 350 or 450 °C. A copper aluminate spinel catalyst was synthesized by coprecipitation, calcination at 800 °C and leaching to get rid of copper oxide residuals.

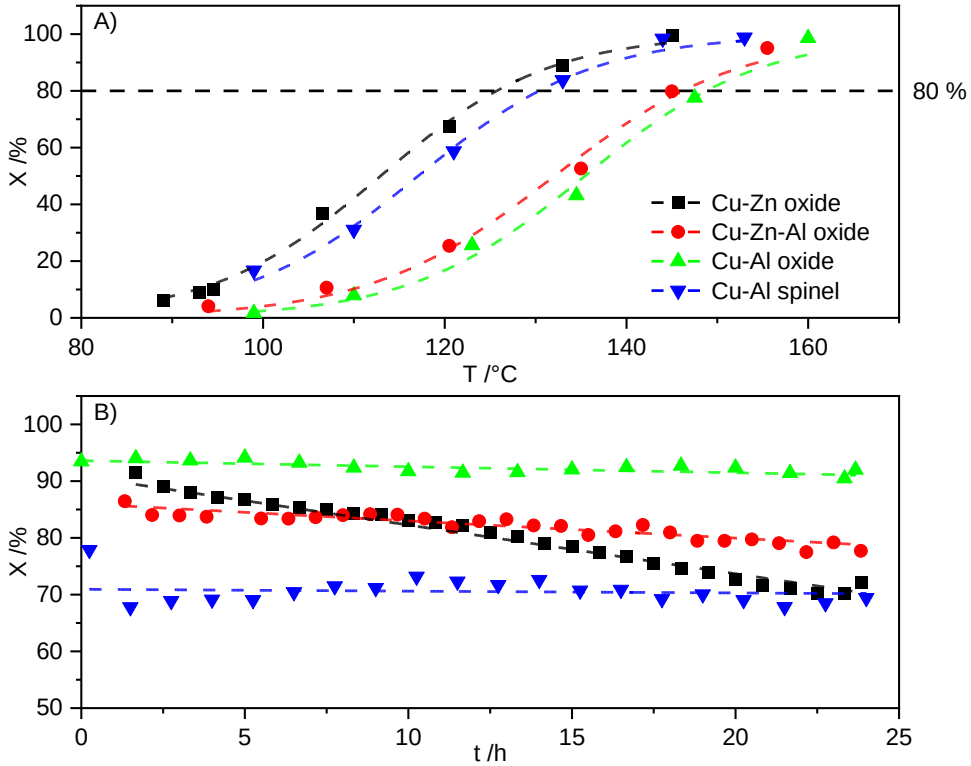

Figure 42: Catalytic performance of Cu-Zn and Cu-Al catalysts. A) Activity as function of temperature, B) actvity as function of time measured at 130 (Cu-Zn oxide; Cu-Al spinel) or 140 °C (the others).

The catalytic activity and the stability were tested in the hydrogenation of butyraldehyde. A similar activity in the temperature conversion relation for all catalysts was found (Figure 42, A). Initial activity is found at around 90-100 °C while full conversion is reached at around 150 °C. for all catalysts. The temperature conversion curve can be described by a sigmoidal fit. The pure copper-zinc oxide and the copper aluminate spinel catalysts are slightly more active compared to the copper-zinc-aluminum and the copper-aluminum oxide catalysts. The copper-

zinc oxide and the copper aluminate spinel catalysts have with around 120 °C a slightly lower T_{50} compared to the copper-zinc-aluminum and the copper-aluminum oxide catalysts (T_{50} around 130 °C).

To determine the chemical stability of these catalysts, the conversion was measured over one day at a fixed temperature. The temperature was set to 130 (copper-zinc oxide and copper aluminate spinel) respectively 140 °C (copper-zinc-aluminum oxide and copper-aluminum oxide) to reach around 80 % initial conversion to follow potential decrease in activity. All catalysts show an initial activity of around 70 to 90 % which agrees with the temperature conversion relation. While both zinc-free copper-aluminum oxide and copper aluminate spinel catalysts show nearly no decrease in conversion within one day, both copper-zinc and copper-zinc-aluminum oxide catalysts show deactivation within one day. A decrease of around 15 % conversion is found for the copper-zinc and 10 % for the copper-zinc-aluminum catalyst. The loss of activity can be described roughly linear (Figure 42, B).

To investigate the deactivation in detail, the used catalysts were characterized by various techniques after catalysis (mostly under inert conditions to prevent oxidation or further phase transformations).

4.3.2 Characterization of used oxide and spinel catalyst

A thermogravimetric analysis under nitrogen was performed with the used catalysts (Figure 43). Additionally, the evolution of carbon dioxide was recorded with a mass spectrometer. The evolution of hydrocarbons could not be determined. A mass loss of 28 % respectively 61 % was found for the copper-zinc and copper-zinc-aluminum oxide. This mass loss occurs between 250 to 300 °C under release of carbon dioxide. Only minor mass loss of 9 respectively below 1 % is found for the zinc-free copper-aluminum oxide and copper aluminate spinel catalyst. In addition, the carbon dioxide signal is smaller for both catalysts.

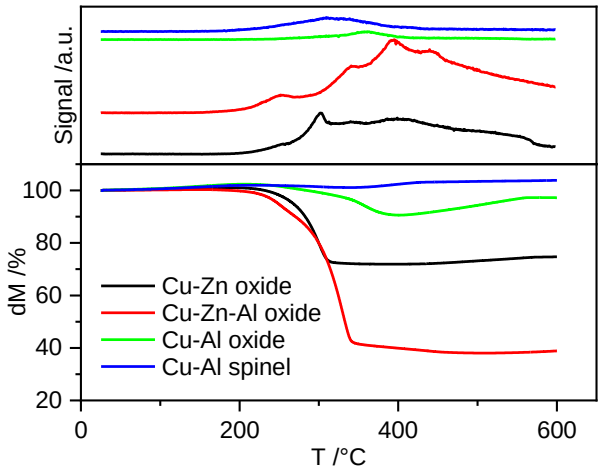

Figure 43: Themrogravimetric analysis of used Cu-catalysts under nitrogen. The mass change and the CO_2 signal from the MS are displayed.

It can be assumed that an organic species adsorbs during the catalysis on zinc-containing catalysts. Especially the copper-zinc-aluminum catalyst shows a significant amount of adsorbed species. Probably, this species leads to deactivation at low reaction temperatures. On the other hand, the thermogravimetric analysis shows that the adsorbed species can be removed at relative mild temperatures between 250 to 300 °C.

To prove the significant mass loss found for the zinc-containing catalysts, the carbon and hydrogen amount of the used catalysts was determined by CHNS analysis. It could be shown that the zinc-containing catalysts contain significant amounts of carbon and hydrogen. For the used copper-zinc oxide, 14 % carbon and 2 % hydrogen were found while 30 % carbon and 5 % hydrogen were found for the copper-zinc-aluminum oxide (Table 17). Interestingly, the molar hydrogen to carbon ratio fits with 1.6:1 (copper-zinc oxide) and 1.8:1 (copper-zinc-aluminum oxide) not to butyraldehyde (theoretical 2.0:1) or butanol (theoretical 2.5:1). For the zinc-free catalysts, much lower carbon and hydrogen residuals were found. Additionally, the hydrogen to carbon ratio of 2.0 found for the copper-aluminum oxide (C: 5 %, H: 1 %) fits quite well to adsorbed butyraldehyde while 2.6 is found for the copper aluminate spinel (C: 2 %, H: 0.5 %)) indicating adsorption of butanol. This is additionally in accordance to the slightly higher activity obtained for the spinel in comparison to the oxide.

Table 17: Physico-chemical of reduced and used Cu-Catalysts.

Sample	**C**	**H**	**n(H:C)**	**Δm TGA**	**$BET_{reduced}$**	**BET_{used}**	**$P.V._{reduced}$**	**$P.V._{used}$**
	%	%	-	%	m^2g^{-1}	m^2g^{-1}	cm^3g^{-1}	cm^3g^{-1}
Cu-Zn oxide	13.9	1.9	1.6	28	82	38	0.27	0.04
Cu-Zn-Al oxide	29.6	4.5	1.8	61	n.d.	n.d.	n.d.	n.d.
Cu-Al oxide	4.7	0.8	2.0	9	n.d.	n.d.	n.d.	n.d.
Cu-Al spinel	2.3	0.5	2.6	<1	96	65	0.35	0.24

Summarizing this, the zinc-containing oxides show a) a high amount of carbon and hydrogen (which explains the large mass loss found in the TGA experiments) and b) a quite low hydrogen to carbon ratio which does not fit either butyraldehyde or butanol.

To get further insight into the used catalysts, the total surface area (BET) as well as the pore volume (BJH) of the copper-zinc oxide and copper aluminate spinel was determined. The surface area and the pore volume of the reduced form were compared to the used form of the catalysts. While the total surface area and the pore volume of the used copper aluminate spinel catalyst decrease only around one third from the reduced to the used form, a higher decrease in the total surface area and especially the pore volume is found for the copper-zinc oxide catalyst. The BET surface area of the reduced copper aluminate spinel decreases from 96 m^2g^{-1} before catalysis (reduced state) to 65 m^2g^{-1} after catalysis (used state) and the pore volume decreases from 0.35 to 0.24 cm^3g^{-1}. For the copper-zinc oxide, a larger decrease is found. The BET surface area decreases from 82 to 38 m^2g^{-1} and the pore volume decreases from 0.27 to 0.04 cm^3g^{-1}. Especially the huge loss of pore volume is notable and indicates a

significant phase change during the catalysis which could explain the decreasing activity. A disintegration of the pore system or the complete blocking of the pores is possible.

To investigate the phase change during catalysis in detail, a temperature programmed desorption experiment of the used catalysts was performed. As seen from the thermogravimetric analysis, a significant mass loss with release of carbon dioxide was found to take place for the zinc-containing catalysts. Nevertheless, it has to be mentioned that the evolution of carbon dioxide is probably due to burning of adsorbed organic species during the thermogravimetric analysis as oxygen residuals are in the oven chamber.

To overcome this drawback, temperature programmed desorption experiments under complete inert atmosphere were performed after catalysis (Figure 44). The used catalysts were heated to 250 °C (2 K/min) and kept for four hours at this temperature. The temperature was kept at 250 °C to prevent the risk of complete decomposition of potentially desorbing species. Additionally, thermogravimetric analysis revealed that the desorption starts at around this temperature. Butyraldehyde, butanol and butyric acid were recorded by a mass spectrometer during the temperature programmed desorption. During the desorption, both zinc-containing catalysts show a significant butyraldehyde signal at around 200-250 °C indicating that larger amounts of butyraldehyde desorb at this temperature. Especially for the copper-zinc-aluminum oxide catalyst a huge signal is obtained which is in accordance with the huge mass loss and the high carbon and hydrogen residuals. Additionally, a minor butyric acid signal is found for this catalyst. On the other hand, no or nearly no signals of butyraldehyde, butanol or butyric acid can be found for the zinc-free catalysts. While no desorption is found to take place for the copper aluminate spinel catalyst, a minor butyraldehyde signal is found for the copper-aluminum oxide catalyst after around two hours at 250 °C. Maybe, the temperature control in the TPD oven is not that accurate and a slight temperature increase took place after two hours. This could lead to desorption of minor amounts of butyraldehyde (which is in accordance with the hydrogen to carbon ratio indicating that butyraldehyde absorbs during the catalysis).

Summarizing the results so far, the following conclusions can be drawn: copper-aluminum catalysts seem to be stable, while copper-zinc catalysts lose activity (10 to 20 % within one day). Additionally, the latter ones show a strong mass loss during thermogravimetric analysis under evolution of carbon dioxide. The strong mass loss is additionally confirmed by CHNS analysis of the used catalysts which revealed that up to 35 % of carbon and hydrogen were found on the used catalysts. This indicates that a significant change in morphology takes place during catalysis for the zinc-containing catalysts which causes the deactivation. In addition, this phase transformation could be confirmed by BET and BJH method. While the catalysis causes only a minor decrease of the surface area (BET) and the pore volume (BJH) for the copper aluminate spinel catalyst, a significant loss of surface area and especially pore volume takes place for the copper-zinc oxide catalyst. In addition, the hydrogen to carbon ratio found

for the zinc-containing catalysts is quite low and does not fit either butyraldehyde or butanol. Desorption experiments under inert conditions suggest that desorption of butyraldehyde takes place for the zinc-containing catalysts. Interestingly, minor amounts of desorbed butyric acid were found for the copper-zinc-aluminum catalyst.

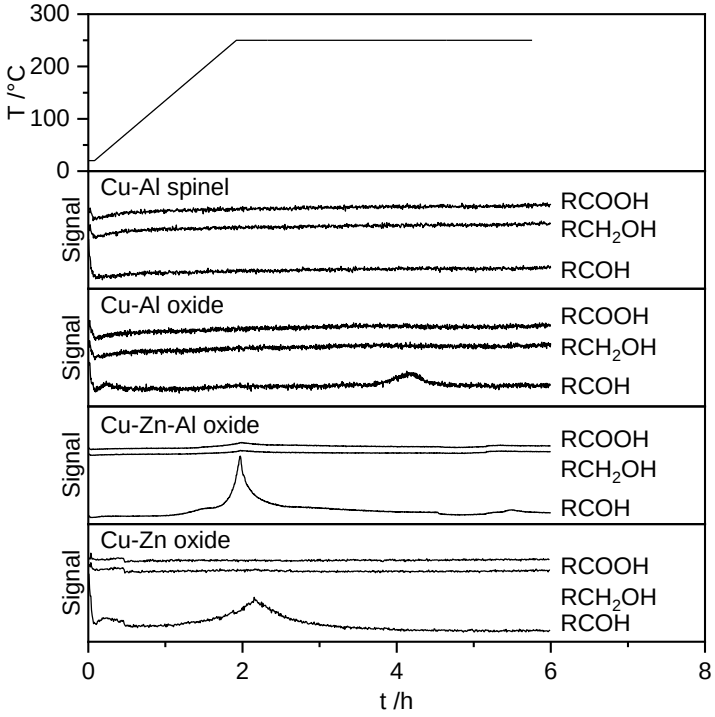

Figure 44: Temperature-programmed-desorption of used Cu-catalysts under inert conditions, temperature ramp = 2 $Kmin^{-1}$; R = $CH_3(CH_2)_2$.

In conclusion, it can be noted that a significant change in morphology takes place for the zinc-containing catalysts. This change is linked to the adsorption of organic species (likely butyraldehyde) during catalysis which causes a) a decrease in total (BET) surface area, b) a blocking of pores and c) strong deactivation of the catalysts. It seems that zinc supports this process.

4.3.3 Mechanism of deactivation of copper-zinc catalysts

For further investigation of the morphology change during catalysis, p-XRD pattern were taken of the reduced and used catalysts (Figure 45). While no notable phase transformation takes place for the copper-aluminum catalysts, a significant phase transformation takes place for the zinc-containing catalysts. Only reflexes according to copper(0) can be found for the reduced and used copper-aluminum catalyst while both forms of the spinel catalyst show additional reflexes according to γ-Al_2O_3 (it can be assumed that the high temperature reduction of the spinel leads to formation of copper an γ-alumina, Reaction scheme 22).[186] On the other hand, a new reflex appears in the used state for zinc-containing catalysts. While both catalysts show mainly reflexes according to copper(0) and zinc oxide in the reduced state, a new reflex at 7.5 °2θ appears in the used state and the reflexes according to copper and zinc oxide vanish nearly completely. This new reflex indicates the formation of zinc-butyrate,

$Zn(CH_3(CH_2)_2COO)_2$. It can be assumed that minor feed impurities of butyric acid cause the formation of zinc-butyrate. Purity analysis of the feed revealed up-to 0.5 % butyric acid. Presumably, the morphological change and the formation of a new phase, which occurs during the gas-phase hydrogenation of butyraldehyde, relates to the formation of zinc-butyrate.

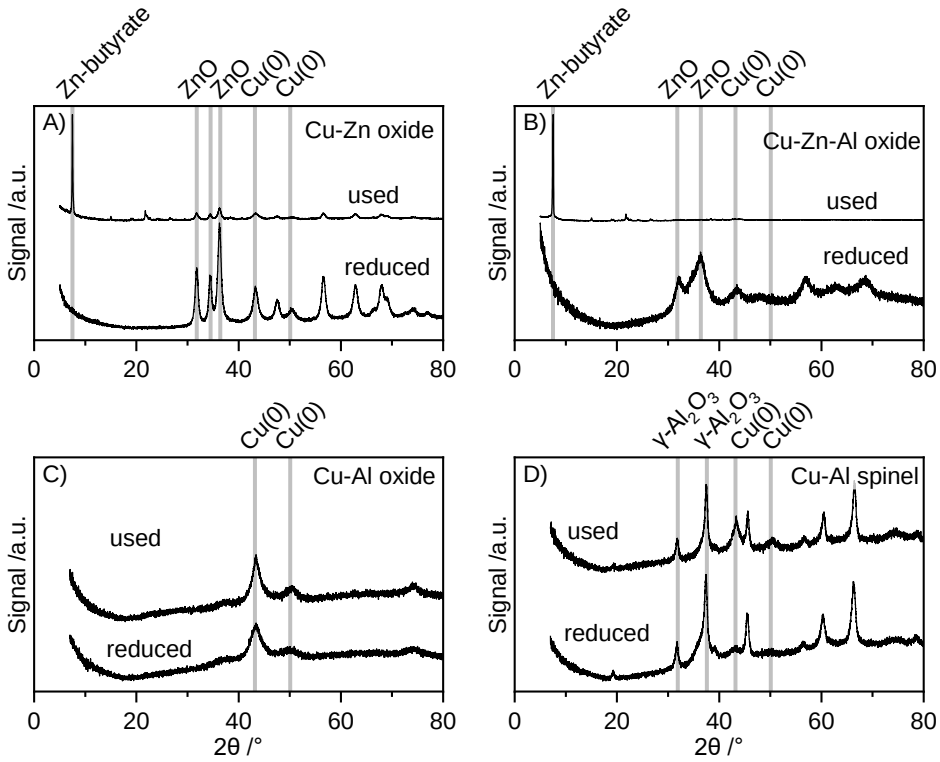

Figure 45: p-XRD of reduced and used Cu-catalysts. A) Cu-Zn oxide; B) Cu-Zn-Al oxide; C) Cu-Al oxide; D) Cu-Al spinel. Reflexes according to Reflexes according to the COD data base (Cu: 96-151-2505, ZnO: 96-900-4179, γ-Al_2O_3: 06-201-5531).[153, 158, 184]

Another possible option for the butyric acid impurities and the formation of the new phase could be the Cannizzaro reaction which yields a primary alcohol and a carboxylic acid under disproportionation of an aldehyde.[224] Nevertheless, it has to be mentioned that this reaction works mainly under strong basic aqueous conditions. Additionally, the Cannizzaro reaction is mainly found for aldehydes without protons in α-position to the aldehyde group. It seems more reasonable that the formation of zinc-butyrate is caused by feed impurities in the butyric acid. The formation of zinc-butyrate takes place only for the zinc-containing copper catalysts as the other once do not contain zinc. This indicates that zinc provides strong adsorption sites for butyric acid impurities causing the formation of this new phase. Additionally, the new phase can be attributed to the significant change in morphology found in previous experiments. The hydrogen to carbon ratio of 1.6 respectively 1.8 found for the copper-zinc and copper-zinc-aluminum oxide fits quite well to the butyrate species (theoretical: 1.75 hydrogen to carbon). It can be assumed that the formation of zinc-butyrate causes not only significant changes in the morphology of the catalyst (decreased surface area, blocking of pores) but leads in addition to the deactivation behavior of the zinc-containing catalysts. On the other hand, both

thermogravimetric analysis as well as temperature programmed desorption experiments revealed that the decomposition of zinc-butyrate takes place at relative mild temperatures.

To investigate the temperature stability of the zinc-butyrate phase, an *in situ* p-XRD of the used copper-zinc oxide catalyst was performed under increasing temperature and inert as well as reductive conditions (Figure 46).

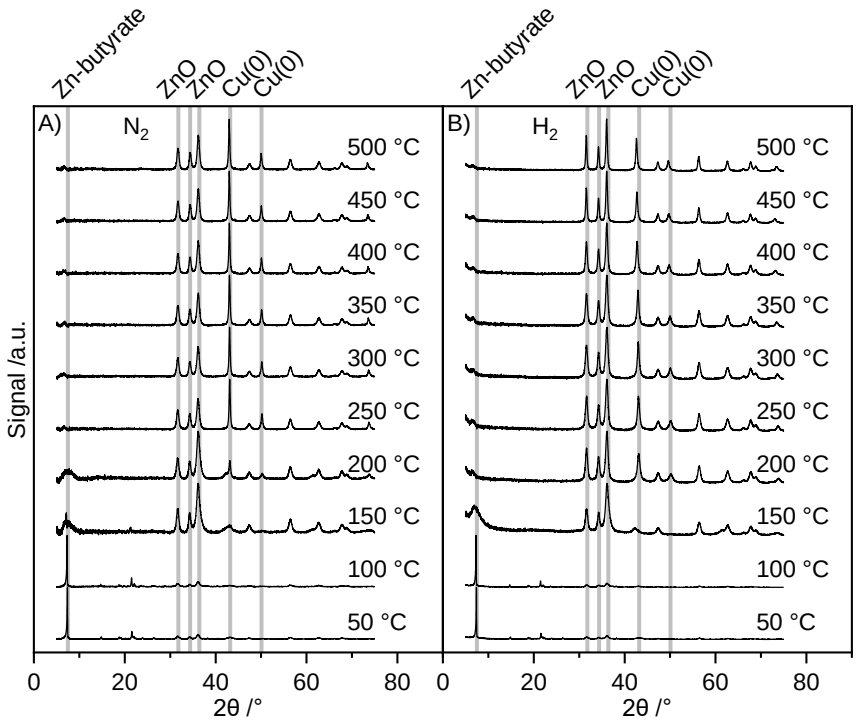

Figure 46: *In situ* XRD of used Cu-Zn oxide catalyst under A) N_2 and B) H_2.

Similar results are obtained both under inert (N_2) and reductive (H_2) conditions. The zinc-butyrate phase is stable up to around 100 °C, a further temperature increase leads to the decomposition of the phase. A complete decomposition of the phase is obtained at around 250 °C under nitrogen and 200 °C under hydrogen suggesting that hydrogen slightly supports the decomposition of the zinc-butyrate phase. In both cases a mixture of copper(0) and zinc oxide is obtained after decomposition of the butyrate phase and no formation of copper oxide takes place. Further temperature increase does not change the phase composition but leads to sintering of copper particles (sharper copper(0) reflexes).

Summarizing the results so far, it can be suggested that the zinc-butyrate phase found in used zinc-containing catalysts is formed during the gas-phase hydrogenation of butyraldehyde due to butyric acid impurities in the feed. The formation of this phase is a solid-state reaction which can be followed by XRD analysis. Additionally, a significant change in morphology of the catalyst takes place and causes strong deactivation in comparison to the copper-aluminum catalysts which does not form a zinc-butyrate phase. On the other hand, *in situ* XRD experiments revealed that the zinc-butyrate phase is not temperature stable and decomposes already at around 150 °C. To prove these findings, the catalytic stability of the copper-zinc oxide and the copper aluminate spinel (nearly similar catalytic activity in the temperature-conversion relation) was determined in two seven day long-term experiments

(Figure 47). Therefore, the catalytic stability was tested first at 150 °C and after a thermal treatment at 200 °C the catalytic stability was tested again one week at 130 °C.

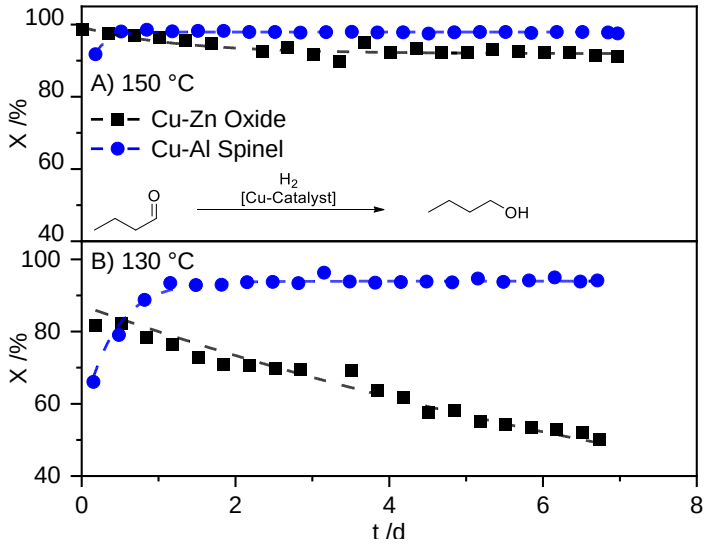

Figure 47: Long-term stability of Cu-Zn oxide and Cu-Al spinel catalyst at A) 150 and B) 130 °C.

The initial activity of nearly 100 % conversion is obtained at 150 °C for both copper-zinc oxide and copper aluminate spinel. While the spinel does not lose any activity within one week and stabilizes at around 95 % conversion, the copper-zinc oxide loses around 10 % conversion within one day and stabilizes at around 85 % conversion. Nevertheless, it has to be mentioned that both catalysts seem to be quite stable at 150 °C and do not lose activity. After thermal treatment, a second stability test was performed at 130 °C. The initial activity of both catalysts is slightly lower (70 % for the copper aluminate spinel and 85 % for the copper-zinc oxide) as expected due to the decreased reaction temperature. While the copper aluminate spinel catalyst reaches an activity of around 90 % in one day and stays constant at this conversion rate, a constant decrease in activity is obtained for the copper-zinc oxide catalyst. The activity decreases within one week by around 40 % and reaches after one week 50 %. The decrease in activity proceeds linear, it can be assumed that within two or three weeks of catalytic activity, a complete deactivation takes place and no conversion is obtained anymore.

These long-term experiments confirmed the assumptions. Zinc-butyrate forms during low-temperature hydrogenation of butyraldehyde (due to acidic feed impurities) and causes catalyst deactivation (Reaction scheme 26). The deactivation is caused due to a) a morphologic change in the active catalyst structure and b) blocking of active centers. It can be prevented by a) higher reaction temperatures above 150 °C or b) an impurities-free feed.

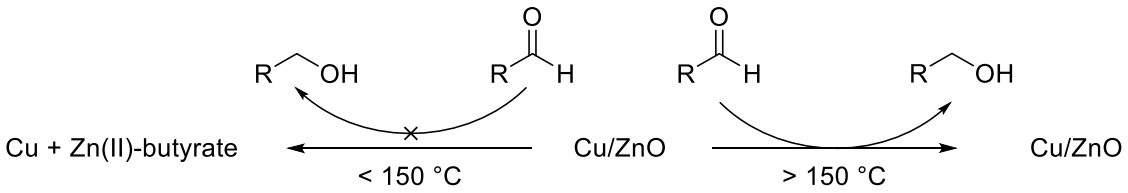

Reaction scheme 26: Deactivation of Cu-Zn oxide catalysts due to formation of Zn-butyrate below 150 °C.

4.4 Comparison between the gas and liquid-phase hydrogenation

As seen in chapter 4.3, both copper-zinc oxide and copper aluminate spinel catalysts are active in the gas-phase hydrogenation of butyraldehyde. For those catalysts which have a similar copper loading, a similar activity is obtained. Nevertheless, the copper-zinc oxide was found to be slightly more active in comparison with the copper aluminate spinel catalyst (Figure 42). The selectivity to *n*-butanol does not seem to be affected by the catalysts, both showed a high selectivity of above 99 %. On the other hand, the copper aluminate spinel catalysts show beneficial properties in the long-term catalysis regarding chemical stability. As previously discussed, copper-zinc oxide catalysts tend to form inactive species during the hydrogenation (zinc-butyrate) which leads to decreasing catalytic activity and deactivation of the catalyst. To investigate the similarities and differences of these catalysts in the hydrogenation of butyraldehyde and to investigate the properties of the catalysts further, the investigations were extended to the liquid-phase hydrogenation. Additionally, similarities and differences in the butyraldehyde hydrogenation mechanism between the gas and liquid-phase shall be examined. Therefore, the catalytic activity and selectivity of these catalysts was determined in a autoclave setup which is in detail described elsewhere.[215] The catalytic properties and the hydrogenation mechanism in the liquid-phase hydrogenation (slurry batch hydrogenation) is compared with the hydrogenation in the gas-phase (fixed bed continuous gas-phase hydrogenation). Additionally, as leaching effects can take place in slurry phase hydrogenation reactions and can cause a decreasing activity, the leaching of copper and zinc/ aluminum was determined during the liquid-phase butyraldehyde hydrogenation and compared with deactivation effects found in the gas-phase hydrogenation.[71]

The copper-zinc oxide catalyst reaches full conversion after around 2 h while a selectivity of around 80 % regarding *n*-butanol is reached at full conversion (Figure 48). A slightly lower activity is obtained for the copper aluminate spinel catalyst, full conversion is reached after around 4 h reaction time. Interestingly, a decreased selectivity of only 50 % regarding *n*-butanol is reached at full conversion. Unfortunately, the side products were not determined in the liquid-phase hydrogenation. Around 1.5 % zinc leaching is initially obtained for the copper-zinc oxide catalyst which decreases to around 0.5 % at full conversion. No copper is found to leach. For the copper aluminate spinel catalyst, a copper leaching of around 0.5 % is initially obtained which decreases below 0.1 %. The aluminum leaching was found to be below 0.2 % during the whole reaction period.

It could be shown that the copper-zinc oxide catalyst is more active compared to the copper aluminate spinel catalyst. Similar results were found for the gas-phase hydrogenation although the copper-zinc oxide catalyst was only slightly more active (Figure 42). It can be assumed that a higher copper dispersion and/ or a higher copper surface area leads in general to more active catalysts. For the gas-phase hydrogenation, it could be shown that for similar catalysts the highest activity is obtained for catalysts with the highest dispersion (Table 8). It seems that

similar trends are obtained in the liquid-phase hydrogenation and catalysts with a higher copper surface area are more active, too. In comparison to the gas-phase hydrogenation, in the liquid-phase hydrogenation is it necessary that hydrogen diffuses through the solvent to the copper nanoparticles before hydrogen is activated and available in the catalytic cycle. In the gas-phase hydrogenation, a direct activation of hydrogen takes place after (dissociative) adsorption from the gas-phase to the copper particles. Probably, catalysts with a higher copper surface area can adsorb more hydrogen which can overcome the rate-limiting effect of hydrogen diffusion through the solvent.

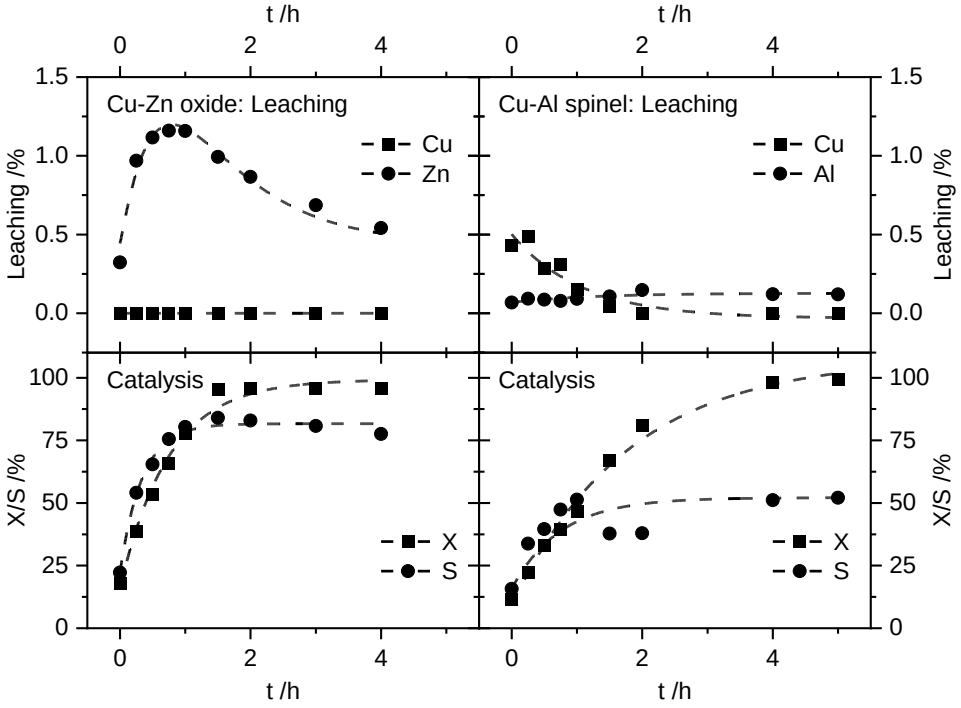

Figure 48: Hydrogenation of butyraldehyde over Cu-Zn oxide (left) and Cu-Al spinel (right) catalyst. Leachig of Cu and Zn/ Al given in % (top) and conversion/ selectivity in % (bottom).

In addition to the slightly increased activity, the copper-zinc oxide catalyst shows a significant higher selectivity to *n*-butanol compared to the spinel catalyst. Such trends could not be determined for the gas-phase hydrogenation of butyraldehyde. Here, a selectivity of over 99.5 % was determined for both copper-zinc oxide and copper aluminate spinel catalysts. Only for the copper-aluminum oxide system a slightly decreased selectivity of around 99.0 % was found.

It can be assumed that different reaction mechanisms take place in the liquid and the gas-phase reaction. Gudkov *et al.* claimed that the gas-phase hydrogenation of butyraldehyde over different copper catalysts follows a modified Eley-Rideal mechanism under dissociative adsorption of hydrogen while butyraldehyde is not adsorbed.[175] Under assumption of this, copper nanoparticles formed during the activation of the copper catalysts would be the active center for the hydrogenation. Hydrogen is dissociatively adsorbed and the C-O bond in the aldehyde is hydrogenated. Aluminum in the spinel lattice does not contribute to the catalytic cycle itself and does not affect the selectivity. On the other hand, especially in the methanol

literature, indications for adsorption of both, hydrogen and the C-O bond containing species are found. Especially zinc in copper-zinc oxide catalysts seems to have an important role regarding the adsorption of C-O bonds.[133, 225] Nakamura *et al.* claimed that copper-zinc surface alloys formed during the reductive activation of these catalysts are important for the adsorption of formates ($HCOO^-$).[226] Behrens *et al.* found out that especially CuZn (211) sites lead to an increased adsorption strengths for oxygen bonded intermediates during the methanol synthesis.[196] While a similar activity was found for the copper-zinc oxide and the copper aluminate spinel catalyst in the gas-phase butyraldehyde hydrogenation, the copper-aluminum catalyst showed a better long-term stability in comparison to the copper-zinc catalyst (Figure 42). It could be shown that copper-zinc catalysts tend to form an inactive zinc-butyrate species at low temperature, while on the other hand this species could not be detected for copper-aluminum oxide and spinel catalysts (Figure 45). Apparently, copper nanoparticles on the surface of both copper-zinc oxide and copper aluminate spinel catalysts are the predominant active centers. These centers lead to the selective hydrogenation of butyraldehyde to *n*-butanol without formation of significant amounts of side products (e.g., esters). On the other hand, it seems that zinc supports the formation of undesired and inactive zinc-butyrate species by strong adsorption of butyric acid impurities. Assumingly, butyric acid adsorbs strongly on zinc (oxide) sites and undergoes a solid-state reaction under formation of the inactive zinc-butyrate species.

The decreased long-term stability and the deactivation of the oxide catalyst in the gas-phase hydrogenation of butyraldehyde are caused by the formation of an inactive zinc-butyrate species. This species is formed in a solid-state reaction between zinc oxide and butyric acid due to minor butyric acid feed impurities. Proposed reasons for the deactivation are a) changes in the morphologic structure of the catalyst, b) the blocking of active centers, or c) the loss of synergetic copper-zinc oxide interactions.

The highest activity in the butyraldehyde hydrogenation is found for copper-zinc catalysts with the highest copper dispersion. This confirms findings by Gudkov *et al.* who claimed that mainly the activation of hydrogen on copper sites is important for the hydrogenation of butyraldehyde.[175] A high copper dispersion is found for catalysts with a medium copper loading of 20-30 % (Table 8). On the other hand, these catalysts have a high zinc loading which explains the strong deactivation due to strong adsorption of butyric acid impurities causing the solid-state reaction between zinc oxide particles and butyric acid under formation of zinc-butyrate. Additionally, it can be assumed that small copper particles undergo preferred this solid-state reaction. This explains that on the one hand, a high dispersion leads to highly active catalysts for the hydrogenation of butyraldehyde. On the other hand, these catalysts tend to form zinc-butyrate species causing deactivation. While highly active catalysts are obtained, these catalysts are less long-term stable.

Another reaction mechanism is proposed for the liquid-phase hydrogenation where a Langmuir-Hinshelwood mechanism is accepted as general mechanism for the butyraldehyde hydrogenation.[215] The adsorption of both hydrogen and the unsaturated C-O bond to an active site is necessary. A broad variety of literature deals with the active sites of copper-aluminum and copper-zinc catalysts used for the liquid-phase hydrogenation of C-O and C-C bonds. Bechara *et al.* found out that the reduction of spinel leads to copper(0) sites on the surface and additionally copper(I) sites in the octahedral position which are active for C-C bond hydrogenation reactions.[216] Krieger *et al.* claimed that after reductive activation different hydrogen species are available in copper aluminate spinel catalysts. Atomic hydrogen is found in octahedral positions while protons offset the negative charge caused by the reduction of copper. Metallic copper is found on the surface of the spinel while protons form hydroxides with lattice oxygen.[227] Simentsova *et al.* claimed that two different reduction steps are involved in the activation of copper spinel catalysts. Copper on the surface is reduced under evolution of water (hydrogen is oxidized and reacts with surface oxygen ions under formation of water, $2\ H^+ + O^{2-} \rightarrow H_2O$). Copper in the spinel lattice is also reduced by hydrogen which forms protons. On the other hand, these protons are incorporated in the spinel lattice to overcome the negative charge due to the reduction of the copper. No oxygen is involved in this reduction.[218] Yurieva *et al.* showed that mainly copper(0) centers are involved in the C-O bond hydrogenation of acetone. Copper(0) is formed during reductive activation on the surface of the spinel while protons in the spinel lattice stabilize the negative charge caused by copper reduction. The activation of the C-O bond takes place on the copper(0) center and two electrons are transferred in the C-O bond under oxidation of copper(0) to copper(II). These copper species are then transferred into the lattice while simultaneously two protons from the lattice migrate to the negatively charged adsorbed acetone species. The protons hydrogenate the C-O bond, isopropanol is formed and desorbs from the surface.[228] On the other hand, consecutive studies of this research group also discuss the importance of copper(I) sites as active sites for the hydrogenation of carbon monoxide (which are chemically similar to an aldehyde group).[217] Hubaut *et al.* showed that two active sites are involved in C-C bond hydrogenation and isomerization over copper aluminate and copper-chromite spinel catalysts. While copper(I) sites are involved in the hydrogenation of C-C bonds, the trivalent metal (aluminum/ chromium) is the active center for the isomerization. Especially aluminum favors the isomerization due to the higher acidity in comparison to chromium.[229]

As briefly discussed, the hydrogenation mechanism in the liquid-phase seems to be more complex in comparison to the gas-phase hydrogenation. Not only the activation of hydrogen is important but also the adsorption and activation of the C-O bond. As shown in Figure 48, both copper-zinc oxide and copper aluminate spinel catalysts are active in the liquid-phase butyraldehyde hydrogenation. A similar activity is obtained, although the copper-zinc oxide is slightly more active. On the other hand, the copper-zinc oxide catalyst showed an

advantageous selectivity to *n*-butanol in comparison to the copper aluminate spinel system. It can be assumed that both copper(0) and copper(I) sites are found in the spinel system which was reduced at 300 °C. This indicates that (at least) two different reaction sites are available in the spinel system. While the desired C-O bond hydrogenation of butyraldehyde is probably catalyzed by the copper(0) site, undesired side reactions could be catalyzed by copper(I) sites of the spinel (e.g., isomerization reactions). On the other hand, it can be assumed that the copper-zinc oxide system activated at 200 °C provides only copper(0) sites which explains the beneficial selectivity. Additionally, these catalysts do not provide aluminum sites. This could be also an explanation for the increased activity of the oxide: While only a part of the overall available copper sites of the spinel is activated to the desired copper(0) reaction sites, the whole amount of copper in the oxide is transferred to the catalytically active copper(0) sites.

Additionally, the adsorption and activation of the aldehyde C-O bond is more important in the liquid-phase hydrogenation in hexane. It can be assumed that aluminum provides acidic sides for the formation of butyl butyrate by the *Tishchenko* reaction. In this reaction, a disproportionation reaction takes place that allows the formation of esters from two equivalents of an aldehyde.[117] In comparison to zinc, aluminum has a significant stronger acidic character (pK_a ($Al(III)_{aq}$) = 4.85; $pK_a(Zn(II)_{aq})$ = 9.5).[230-231] This suggests that the choice of the metal oxide support (aluminum oxide/ zinc oxide) is more critical in the liquid-phase hydrogenation compared to the gas-phase reaction where mainly the copper(0) sites are the important characteristics of the catalysts. This is a further and important reason for the decreased selectivity of the copper aluminate spinel catalyst compared to the copper-zinc oxide.

Summarizing, it could be shown that copper-zinc oxide and copper aluminate spinel catalysts are active in the butyraldehyde hydrogenation. Both catalysts are active not only in the gas-phase hydrogenation but also in the liquid-phase hydrogenation. The activity of copper-zinc oxide and copper aluminate spinel is similar both in the liquid and the gas-phase hydrogenation, although in both cases the copper-zinc oxide catalyst is slightly more active. On the other hand, the catalyst strongly affects the selectivity in the liquid-phase hydrogenation while the long-term stability in the gas-phase hydrogenation is strongly affected by the choice of the catalyst. Different reactions mechanisms and active sites are involved in the investigated hydrogenation reaction and can explain the similarities and differences of the catalysts and their properties. The gas-phase reaction follows an Eley-Rideal mechanism where mainly the activation of hydrogen is the important step while the activation of the C-O bond is not that critical. The active centers for the dissociative hydrogen adsorption are mainly copper(0) sites. This explains the beneficial activity of the copper-zinc oxide catalyst due to a higher copper dispersion in comparison to the copper aluminate spinel catalyst. On the other hand, the drawback of the oxide catalyst is the high zinc loading which causes decreased long-term stability due to strong adsorption of butyric acid impurities causing formation of zinc-butyrate which leads to deactivation.

The liquid-phase hydrogenation follows a Langmuir-Hinshelwood mechanism where both the activation of hydrogen and the C-O bond are important steps in the catalytic cycle. Similar to the gas-phase hydrogenation, the activation of hydrogen and the favored C-O bond hydrogenation takes place on the copper(0) sites. Deponing on the reduction conditions, the formation of additional copper(1) sites during the activation is possible, especially for the spinel. These sites could lead to undesired side reactions like isomerization or esterification. A significant difference in the liquid-phase hydrogenation compared to the gas-phase hydrogenation of butyraldehyde are acid sites due to the leaching of aluminum. These acid sites catalyze undesired side reactions like *Tishchenko* reaction leading to undesired esters. This indicates that the choice of the metal oxide support is more important in the liquid-phase hydrogenation.

4.5 Conclusion

Copper-zinc oxide and copper aluminate spinel catalysts are highly active in the hydrogenation of butyraldehyde. A test setup was constructed to investigate the catalytic performance of these catalysts used in the gas-phase hydrogenation of butyraldehyde. Furthermore, this setup allows the handling and characterization of used copper catalysts after the gas-phase hydrogenation of aldehydes. It could be shown that the catalysts are active both in the liquid-phase (batch) hydrogenation as well as the gas-phase (continuous) hydrogenation. While, both catalysts showed similar activity in the liquid, as well as the gas-phase hydrogenation, the long-term stability in the gas-phase hydrogenation, is significantly influenced by the catalyst. Copper aluminate spinel catalysts showed superior long-term stability over days while strong deactivation was found to take place for copper-zinc oxide catalysts. Powder and *in situ* XRD experiments revealed that the strong deactivation of copper-zinc oxide catalysts is caused by the formation of an inactive butyrate species. This species is most likely zinc-butyrate which forms due to the strong adsorption of butyric acid impurities at the zinc sites and a solid-state reaction between zinc oxide and adsorbed butyrate. This causes the deactivation of the catalyst due to blocking of active sites and morphologic changes in the active catalyst species. Higher reaction temperatures above the decomposition temperature of zinc-butyrate can overcome the deactivation.

The selectivity of *n*-butanol is significantly influenced by the catalyst in the liquid-phase hydrogenation. While both catalysts showed nearly entire hydrogenation to *n*-butanol in the gas-phase, significant amounts of side products are formed during the liquid-phase hydrogenation. A much higher selectivity was obtained for the copper-zinc oxide catalyst in comparison to the copper aluminate spinel catalyst.

These findings, the decreased long-term stability of copper-zinc oxide in the gas-phase and the decreased selectivity of copper aluminate spinel in the liquid-phase can be explained by different hydrogenation mechanisms. The gas-phase hydrogenation follows an Eley-Rideal mechanism where mainly copper(0) nanoparticles are the active sites for the hydrogenation. Nevertheless, the zinc-rich oxide catalyst provides additional adsorption sites for butyric acid impurities leading to the formation of the inactive zinc-butyrate species.

The liquid-phase hydrogenation follows a Langmuir-Hinshelwood reaction mechanism where both the adsorptive activation of hydrogen and the adsorption (and activation) of the C-O bond are involved in the catalytic cycle. Despite the copper centers which are similar to the copper-zinc oxide and the copper aluminate spinel catalyst, the spinel catalyst provides additional acidic centers due to the leaching of aluminum. This allows the formation of butyl butyrate due to the *Tishchenko* reaction. Additionally, copper(I) sites in the spinel could negatively affect the selectivity in the liquid-phase hydrogenation.

5

Summary

Copper catalysts are used in a broad range of hydrogenation reactions. This thesis focuses on copper oxide and spinel catalysts used for the hydrogenation of butyraldehyde to n-butanol. Butanol is used as a plasticizer, in coatings, or as gasoline like biofuel. The investigated catalysts are copper-zinc oxides as well as copper-aluminum oxides and spinels. These were synthesized by co-precipitation followed by a thermal treatment (calcination) yielding the oxide or spinel structure. The active species is obtained after a reduction.

Chapter 2 describes the commissioning of a multipurpose test setup (ILS-601) used for the investigation of copper catalysts, which catalyze the gas-phase hydrogenation of butyraldehyde. Reliable test conditions were provided by preliminary experiments to exclude transport limitations and to guarantee for isothermal conditions. The latter one is obtained by dilution of the catalyst bed. Reproducible catalysis tests can be performed and the deviation of the conversion could be reduced below 3 %.

Chapter 3 focuses on the synthesis, characterization and catalytic test of copper oxide and copper spinel catalysts. A benchmark copper-zinc catalyst containing around 30 % copper synthesized by co-precipitation and thermal treatment is introduced as the reference system. This catalyst is in detail characterized and tested in the gas-phase hydrogenation of butyraldehyde. It could be shown that the hydroxycarbonate precursor of this catalyst consists mainly of aurichalcite. Two decomposition steps take place during the thermal treatment, a high-temperature oxycarbonate is obtained as a metastable intermediate. Complete calcination above 350 °C yields copper-zinc oxide. This catalyst is highly active and selective in the gas-phase hydrogenation of butyraldehyde, the T_{50} was determined to be around 115 °C. Copper-zinc oxide catalysts with a medium copper loading of 20-30 % copper show the highest copper dispersion of nearly 10 % leading to a superior catalytic activity in the butyraldehyde hydrogenation. A roughly linear trend is obtained for the dispersion-activity relationship. These beneficial properties are obtained for precursors consisting mainly of aurichalcite.

A neutral to slightly alkaline precipitation solution is beneficial to obtain highly active copper-zinc oxide catalysts. The precipitation of copper and zinc in an acidic solution leads to the precipitation of gerhardtite as an additional precursor phase besides aurichalcite and malachite. This undesired phase results in a lower BET surface area as well as larger aurichalcite crystallites. As a consequence of this, larger copper oxide crystallites are obtained after calcination. This leads to a lower mean reduction temperature causing a lower copper surface area and a decreased catalytic activity.

Copper-aluminum oxides and spinels with around 30 % copper loading show similar activity to the benchmark copper-zinc oxide. Especially the spinel system is as active as the reference system. The complex thermal decomposition of the copper-aluminum precursor was resolved: Initially, a high-temperature carbonate (similar to the copper-zinc oxide) is obtained which is subsequently transferred into a pure copper-alumina. Further temperature increase leads to the crystallization of the spinel structure. Residuals of around 10 % copper oxide are obtained

for the 800 °C calcined spinel which can be partially removed by leaching. On the other hand, the leached spinel shows copper both in the oxide and the spinel lattice. Both copper sites have to be reduced to gain a highly active catalyst. Copper oxide can be reduced below 200 °C while 300 °C leads to the reduction of copper in the spinel lattice. A higher reduction temperature above 350 °C leads to a partial dissolving of the oxygen framework.

The reductive activation of copper-zinc oxides yields the catalytically active species: metallic copper on zinc oxide. It could be shown that direct reductive activation of the hydroxycarbonate precursor as well as the high-temperature oxycarbonate is possible, too. In all three cases, a morphologically similar copper-zinc oxide species is obtained. Nevertheless, beneficial properties like a higher copper dispersion or a milder activation behavior are obtained in the case of direct reductive activation of the precursor or the oxycarbonate. It could be shown that the activation of the oxycarbonate and the oxide is exothermic while the simultaneous decomposition and activation of the hydroxycarbonate is endothermic. Higher catalytic activity is obtained in the case of the direct activation of precursor and oxycarbonate.

A design of experiments approach for the catalyst synthesis gave further insights into the complex precipitation and aging process of copper-zinc oxides. Beneficial properties like a higher copper dispersion or a smoother reduction as well as a higher catalytic activity can be obtained by faster precipitation (achieved by a high hydroxide concentration) and/or the prevention of copper-zinc particle segregating (achieved by a lower soda concentration).

Chapter 4 focuses on the stability and the reaction and deactivation mechanism of copper-zinc oxides and copper aluminate spinels. Therefore, long-term stability tests in the gas-phase and comparative experiments in the liquid-phase including leaching experiments were conducted. A test setup was modified to allow the inert handling of used catalysts obtained after the gas-phase hydrogenation. While the copper-zinc oxide and copper aluminate spinel catalysts are similarly active in the gas-phase hydrogenation, only copper-aluminum oxide and spinel catalysts show superior long-term stability. Detailed characterization of the used catalysts under inert conditions revealed that copper-zinc forms an inactive zinc-butyrate species during the butyraldehyde hydrogenation below 150 °C. Zinc oxide provides strong adsorption sites for butyric acid impurities. A solid-state reaction between zinc oxide and butyric acid causes the deactivation. *In situ* XRD experiments under inert and reductive conditions as well as detailed desorption experiments showed that these species decompose above 150 °C and no deactivation takes place.

A similar catalytic activity is obtained for the copper-zinc oxide and the copper aluminate spinel in the liquid-phase while the spinel shows a lower selectivity to *n*-butanol. Potential explanations are: a) aluminum leaching causing side reaction like the *Tishchenko* reaction b) a different reaction mechanism depending on the phase of hydrogenation (the gas-phase reaction follows an Eley-Rideal mechanism while the liquid-phase reaction follows a Langmuir-Hinshelwood mechanism) and c) additional copper(I) sites in the spinel.

6

Experimental

6.1 Materials

All solid and liquid chemicals were supplied through Sigma Aldrich or VWR (Germany) and were used without further purification. Gases were supplied by Westfalen AG (Germany) with a purity of 99.5 % (N_2O), 99.996 % (He), and 99.999 % (H_2, Ar, H_2/Ar, N_2 and syn. air). Detailed descriptions of gas mixtures are given with the respective experimental procedure. All chemicals were used without further purification.

6.2 Synthesis of catalysts

All catalysts were prepared by co-precipitation followed by aging, washing, drying and thermal treatment in air. Metal nitrates (copper, zinc, aluminum) were used as metal precursors and aqueous solutions with a total concentration of 1 $molL^{-1}$ (expect DoE approach) were prepared according the desired copper to zinc/aluminum ratio. Soda (Na_2CO_3) was used as precipitation agent with a concentration of 1 $molL^{-1}$ (expect DoE approach). The precipitation was performed in a double-walled *HWS* glass autoclave with a total volume of 2 l. 500 mL water were added before precipitation and heated by a *Lauda ecoline RE 306* thermostat to the desired precipitation temperature (70 °C if not other stated). The metal solution was added with a volumetric flow of 4 mLmin-1 by a *Medorex* peristaltic pump. A *Metrohm 736 GP Titrino* with a 20 mL dosing unit was used to measure and control the pH value by adding the proper amount of precipitation agent. Therefore, a *Mettler Toledo electrode plus* was calibrated with *VWR AVS Buffer* solutions beforehand. During precipitation and aging, the solution was stirred at a constant speed of 450 rpm by a *KPG* stirrer. If not other stated, the precipitates were aged for 1 h in their mother liquor. The aged precipitates were isolated by vacuum filtration of the hot reaction mixture and washed multiple times using distilled water, until the conductivity of the filtrate decreases below 0.5 $mScm^{-1}$. The standard synthesis procedure is summarized in Reaction scheme 15.

The precipitates were subsequently dried at 120 °C overnight. The precipitated precursors were calcined in air at 280 °C (HT-carbonate), 350/ 450 °C (oxide) or 800 °C (spinel). A heating ramp of 5 $Kmin^{-1}$ was applied, the temperature was kept for 4 hours (HT-carbonate, oxide) or 8 h (spinel).

Spinel catalysts were additionally leached in concentrated ammonium carbonate solution ($(NH_4)_2CO_3$) after calcination. Therefore, the samples (around 2 g) were treated in the leaching solution (around 5 mL) in an ultrasonic bath for 2 h and subsequently stirred for 30 minutes in this solution at 50 °C. The suspension was then filtered and washed with water and dried again overnight at 120 °C.

6.3 Characterization of catalysts

Elemental analysis

Elemental analysis was determined by an *Agilent 700* ICP-OES. Spinel containing catalysts were diluted in conc. phosphoric acid and stirred overnight at 90 °C. Oxidic catalysts were diluted with 6 M HCl and stirred 30 minutes at room temperature. A multiple element standard from Merck was used for calibration. Wavelengths 324 and 327 nm (Cu), 213 and 334 nm (Zn) and 394 and 396 nM (Al) were analyzed.

Carbon, hydrogen and nitrogen contents were determined by combustion analysis using an elemental analyzer (*Eurovector*). Inert sample preparation was carried out in a glovebox charging a tin foil mini weighing-boat with 5 – 10 mg of the sample, which was wrapped into another tin foil weighing boat.

X-Ray diffraction

Powder X-ray diffraction (p-XRD) was measured on a *Rigaku MiniFlex 600* diffractometer (5 – 75 °2 Theta, Cu Kα1, 0.01 °/step, 15 min) in reflection mode.

In situ measurements were performed on an Empyrean Panalytical instrument (5 – 95 °2 Theta, Cu Kα1, 0.013 °/step, 20 min). An *Anton Paar XRK-900* reaction chamber connected to the instrument was used. The gas flow (2.5 %H_2/Ar, pure H_2, syn. air or N_2) was set to 20 mLmin^{-1}, heating ramp to 5 Kmin^{-1}.

Particle sizes were determined by the Scherrer equation.[156] Phase identification was done with *Highscore* and reference pattern were obtained from the ICCD database. Rietveld refinement was performed with the *TOPAS* software package.

Raman

Raman spectra are recorded on an *InVia* Raman Microscope from *Renishaw* with a *Newton EMCCD* Camera (Spectroscopy EMCCD, width: 25.6 mm, 1600 pixel, 3 MHz) from *Andor*. For the measurements, a frequency-doubled Nd:YAG laser (λ = 532 nm) and an objective with 50x magnification (*Leica N PLAN EPI* 50x/0.75) are used. The standard laser intensity was 0.015 mW and the standard scanning time 5 sec with 10 repetitions.

Thermogravimetry

The samples were measured on a Mettler-Toledo *TGA/DSC 3+* coupled with a *Pfeiffer GSD 320T* gas analyzer. The samples were heated with 5 Kmin^{-1} to 600 °C (reductive and inert conditions) or 10 Kmin^{-1} to 1 000 °C (oxidative conditions). The gas flow was set to 20 mLmin^{-1} syn. air, N_2 or 2.5 % H_2/Ar. The m/z ratio was set to 1,2 (H_2), 4 (He), 14, 28 (N_2), 16, 32 (O_2), 17,18 (H_2O), 30 (NO), 40 (Ar), 44 (CO_2), 72 (butyraldehyde), 74 (butanol) and 88 (butyric acid).

Total surface area determination by Brunauer-Emmett-Teller (BET) method

BET-surface area was determined by N_2 adsorption/ desorption on a *Quantachrome 4XL* at -196 °C. Samples were degassed 3 h at 120 °C in vacuum before measurement. A 40 points N_2 isotherm was recorded and analyzed subsequently with the *Quantachrome TouchWin* software.

Temperature-programmed reactions

Temperature programmed reduction (TPR) was measured on a *Micromeritics Autochem II* analyzer equipped with a thermal conductivity detector (TCD). The samples were heated in 10 %H_2/Ar with 50 mLmin^{-1} to 400 °C for oxidic samples and 800 °C for spinel samples. The sample amount was calculated according to Monti *et al.*[232] An isopropanol/liquid nitrogen slurry was used to maintain cold trap temperatures of approximately -80 °C to freeze water.

Temperature programmed desorption (TPD) experiments were performed on a self-made oven system connected to an on-line *Pfeiffer GSD 320T* gas analysis system. The m/r ratio was adapted from the TGA-MS experiments. The samples (around 30 mg) were inserted under inert conditions and were heated to 250 °C at a rate of 2 K min^{-1} under Helium with a flow rate of 20 mLmin^{-1}.

Copper surface area determination by nitrous-oxide chemisorption

The copper surface area was determined by N_2O pulse chemisorption experiments. A *Micromeritics Autochem II* analyzer was used. The samples were pre-reduced for 1 h at 200 (oxide samples) or 350 °C (spinel samples). The heating ramp was set to 2 Kmin^{-1} and the reduction was performed at a GHSV of 6000 h^{-1} (10 mLmin^{-1}; 80 mg) in 10 % H_2/Ar. After reduction, the sample was flushed with helium (20 mLmin-1, 0.5 h) at the reduction temperature to get rid of adsorbed hydrogen. Pulses of defined amount (50µl) of pure N_2O were introduced to the helium gas stream (20 mLmin^{-1}) until no difference towards the baseline could be detected. A cooling trap filled with liquid nitrogen (-196 °C) was used to freeze residuals of N_2O. Formed nitrogen was detected with a thermal conductivity detector (TCD). The calculation of the surface area was adapted according to Hinrichsen *et al.*[159]

6.4 Design of experiments

A fractional factorial 2^{5-1} design with the aging temperature as product of the other four parameters (E = ABCD) was used to investigate the influence of a variety of parameters (factors) on the synthesis of copper-zinc catalysts used in the hydrogenation of butyraldehyde. Table 18 summarizes the factors with its low and high levels including the central point. The total (N_2-isotherm) and the copper surface area (N_2O pulse chemisorption), the copper oxide and zinc oxide crystallite size (Scherrer equation), the mean reduction temperature (temperature programmed reduction) as well as the catalytic activity (as T_{90}) were determined as response factors. The evaluation was performed with the *Design Expert 9* software by *Stat-Ease*.

Table 18: Design of experiments factors with their low and high level.

	Factor	low level	Center point	High level	
A	c (Cu-Zn)	0.75	1.0	1.25	$molL^{-1}$
B	c (Na_2CO_3)	0.75	1.0	1.25	$molL^{-1}$
C	pH	7	8	9	-
D	Aging time	30	60	90	min
E = ABCD	Aging temperature	55	70	85	°C

6.5 Catalytic hydrogenation of butyraldehyde

Commercial test setup (chapter 2.1)

The gas-phase hydrogenation of butyraldehyde to *n*-butanol was performed in an ½ inch stainless steel reactor with sieved catalyst (0.1-0.3 mm) placed in the isothermal zone of the reactor (Figure 4). The catalysts (1 g) were mixed with α-Al_2O_3 in the volumetric ratio of 1:6 to prevent hotspots. The catalysts were pre-reduced *in situ* before catalysis (20 % H_2/N_2, GHSV = 3 000 h^{-1}, 2 $Kmin^{-1}$, 200 °C (oxide) or 350 °C (spinel), 2 h). The hydrogenation was performed between 90 up to 250 °C and 3.4 bar g (Reaction scheme 13). The GHSV was set to 18 000 h^{-1}, LHSV to 6 h^{-1}. The temperature was increased in 10 to 20 K steps every 4 hours for the determination of the catalytic activity (temperature-conversion dependence). Long term stability experiments were performed for 24 h or 7 days at constant temperature. The temperature was controlled by a thermocouple in direct contact with the catalyst bed. Quantification was performed on an *Agilent 7890 B* equipped with an *CP-Sil 5* column (25m x 0.32mm x 5um). A sigmoidal curve-fit was used for the determination of the T_{50} and T_{90}. The butyraldehyde conversion and the *n*-butanol selectivity was calculated as follows:

$$Conversion\ (\%) = \frac{mol\ of\ butyraldehyde\ converted}{mol\ of\ butyraldehyde\ \ fed}$$

$$Selectivity\ (\%) = \frac{mol\ of\ product}{mol\ of\ butyraldehyde\ converted}$$

Modified Single test unit (chapter 4.2)

The gas-phase hydrogenation of butyraldehyde to n butanol was performed in a stainless-steel reactor with an inner diameter of 4.5 mm loaded with 333 mg sieved catalyst (0.02-0.1 mm). The reduction was performed *in situ* before catalysis, the reduction conditions were adapter according to the commercial test setup (GHSV = 3 000 h^{-1}). The hydrogenation was performed at 3 bar g, GHSV of 18 000 h^{-1} and LHSV of 6 h^{-1} (Reaction scheme 13). Hexane was used as internal standard and mixed 5:95 with butyraldehyde. Quantification was performed on an online connected *Perkin Elmer Clarus 590 GC* gas chromatograph with a *Stabilwax* column (30m, 0.32 mm, 0.5 µm) and a TDC detector. The conversion of butyraldehyde was referenced to hexane. Long term stability experiments were performed for 24 h at constant temperatures. The catalyst was removed under inert conditions and transferred to a glovebox for further analysis.

Liquid-phase hydrogenation (chapter 4.4)

A 300 mL stainless steel autoclave by *Parr* was used for the liquid-phase hydrogenation of butyraldehyde. Prior to the hydrogenation, the catalysts were activated under flowing hydrogen in a U-shaped glass reactor (spinel: 1 $Kmin^{-1}$, 300 °C, 1 h, 50 $mLmin^{-1}$ pure H_2, oxide: 2 $Kmin^{-1}$, 200 °C, 1 h, 50 $mLmin^{-1}$ 20 % H_2/He). The catalysts were transferred under inert conditions into a glovebox. Around 300 mg activated catalysts were transferred into the autoclave under Schlenk technique and loaded into the autoclave under a self-made argon chamber to allow the filling of the autoclave under exclusion of oxygen. The autoclave was loaded with the catalyst, 100 mL hexane as solvent, 1.2 g *n*-dodecane as internal standard (for the GC measurements) and 8 g butyraldehyde. The reactor was pressurized with hydrogen to 60 bar after closing. The reaction was performed at 120 °C and a propeller type impeller was used as stirrer (750 rpm). Samples of 2 mL were takes every 15 – 60 minutes and analyzed by GC (catalysis) and elemental analysis (by ICP-OES for the determination of the leaching). The complete procedure is reported in detail by C. Dörfelt.[215]

7

References

[1] in *The IUPAC Compendium of Chemical Terminology*, International Union of Pure and Applied Chemistry (IUPAC), Research Triangle Park, NC, **2011**.

[2] M. Beller, G. Centi, *Chemsuschem* **2009**, *2*, 459-460.

[3] F. Kapteijn, R. J. Berger, J. A. Moulijn, in *Handbook of Heterogeneous Catalysis*, **2008**, pp. 1693-1714.

[4] J. A. Dumesic, G. W. Huber, M. Boudart, in *Handbook of Heterogeneous Catalysis*, **2008**.

[5] U. Dingerdissen, A. Martin, D. Herein, H. J. Wernicke, in *Handbook of Heterogeneous Catalysis*, **2008**, pp. 37-56.

[6] B. Cornils, W. A. Herrmann, M. Rasch, *Angewandte Chemie International Edition in English* **1994**, *33*, 2144-2163.

[7] B. Cornils, in *Catalysis from A to Z*, **2020**.

[8] M. Boudart, *J. Mol. Catal.* **1985**, *30*, 27-38.

[9] J. C. Chadwick, R. Duchateau, Z. Freixa, P. W. N. M. van Leeuwen, *Homogeneous Catalysts: Activity - Stability - Deactivation*, Wiley, **2011**.

[10] R. Schlögl, *Angewandte Chemie International Edition* **2015**, *54*, 3465-3520.

[11] M. Appl, in *Ullmann's Encyclopedia of Industrial Chemistry*, **2006**.

[12] J. G. Reuvers, J. R. Brightling, D. T. Sheldon, in *Proceedings-International Fertiliser Society*, International Fertiliser Society, **2014**, pp. 1-28.

[13] E. L. Bell, W. Finnigan, S. P. France, A. P. Green, M. A. Hayes, L. J. Hepworth, S. L. Lovelock, H. Niikura, S. Osuna, E. Romero, *Nature Reviews Methods Primers* **2021**, *1*, 46.

[14] D. Yi, T. Bayer, C. P. Badenhorst, S. Wu, M. Doerr, M. Höhne, U. T. Bornscheuer, *Chemical Society Reviews* **2021**, *50*, 8003-8049.

[15] J. Hagen, *Industrial catalysis: a practical approach*, John Wiley & Sons, **2015**.

[16] K. P. de Jong, *Synthesis of solid catalysts*, John Wiley & Sons, **2009**.

[17] L. Liu, A. Corma, *Chemical Reviews* **2018**, *118*, 4981-5079.

[18] R. L. Augustine, *Heterogeneous catalysis for the synthetic chemist*, CRC Press, **1995**.

[19] C. H. Bartholomew, R. J. Farrauto, *Fundamentals of industrial catalytic processes*, John Wiley & Sons, **2011**.

[20] D. Borodin, I. Rahinov, O. Galparsoro, J. Fingerhut, M. Schwarzer, K. Golibrzuch, G. Skoulatakis, D. J. Auerbach, A. Kandratsenka, D. Schwarzer, *Journal of the American Chemical Society* **2021**, *143*, 18305-18316.

[21] T. Pu, H. Tian, M. E. Ford, S. Rangarajan, I. E. Wachs, *ACS catalysis* **2019**, *9*, 10727-10750.

[22] P. Munnik, P. E. De Jongh, K. P. De Jong, *Chemical reviews* **2015**, *115*, 6687-6718.

[23] J. A. Bergwerff, B. M. Weckhuysen, in *Handbook of Heterogeneous Catalysis*, **2008**, pp. 1188-1197.

[24] B. Leach, *Applied industrial catalysis*, Elsevier, **2012**.

[25] O. Beeck, *Discuss. Faraday Soc.* **1950**, *8*, 118-128.

[26] S. Nishimura, *Handbook of heterogeneous catalytic hydrogenation for organic synthesis*, Wiley New York, **2001**.

[27] G. Bond, P. Wells, in *Advances in Catalysis, Vol. 15*, Elsevier, **1965**, pp. 91-226.

[28] J. Scholten, A. Pijpers, A. Hustings, *Catalysis Reviews* **1985**, *27*, 151-206.

[29] H. B. Kagan, *Angew. Chem.* **2012**, *124*, 7490-7497.

[30] M. Che, *Catalysis Today* **2013**, *218-219*, 162-171.

[31] P. Sabatier, *Catalysis in organic chemistry*, D. Van Nostrand Company, **1922**.

[32] F. Haber, G. Van Oordt, *Zeitschrift für anorganische Chemie* **1905**, *44*, 341-378.

[33] T. P. Hughes, *Past & Present* **1969**, 106-132.

[34] H. Adkins, E. E. Burgoyne, H. J. Schneider, *Journal of the American Chemical Society* **1950**, *72*, 2626-2629.

[35] H. Adkins, R. Connor, *Journal of the American Chemical Society* **1931**, *53*, 1091-1095.

[36] I. Horiuti, M. Polanyi, *Transactions of the Faraday Society* **1934**, *30*, 1164-1172.

[37] A. J. Medford, A. Vojvodic, J. S. Hummelshøj, J. Voss, F. Abild-Pedersen, F. Studt, T. Bligaard, A. Nilsson, J. K. Nørskov, *Journal of Catalysis* **2015**, *328*, 36-42.

[38] J. K. Nørskov, F. Studt, F. Abild-Pedersen, T. Bligaard, *Fundamental concepts in heterogeneous catalysis*, John Wiley & Sons, **2014**.

[39] N. Wiberg, (Ed.: A. F. Holleman), De Gruyter, **2008**, pp. 1433-1482.

[40] S. Pietrzyk, B. Tora, in *IOP conference series: materials science and engineering, Vol. 427*, IOP Publishing, **2018**, p. 012002.

[41] A. Lossin, in *Ullmann's Encyclopedia of Industrial Chemistry*, **2001**.

[42] D. Dreisinger, N. Verbaan, M. Canizares, in *Proceedings of the 61st Conference of Metallurgists, COM 2022*, Springer, **2023**, pp. 753-772.

[43] K. Daehn, A. Allanore, *Current Opinion in Electrochemistry* **2020**, *22*, 110-119.

[44] M. Li, S. J. Zinkle, **2012**.

[45] M. P. Sibi, G. R. Cook, in *Lewis Acids in Organic Synthesis*, **2000**, pp. 543-574.

[46] T. Punniyamurthy, L. Rout, *Coord. Chem. Rev.* **2008**, *252*, 134-154.

[47] V. Imandi, P. Puri, V. Korde, in *Journal of Physics: Conference Series, Vol. 1913*, IOP Publishing, **2021**, p. 012083.

[48] P. A. Jacobs, in *Handbook of Heterogeneous Catalysis*, **2008**, pp. 3684-3700.

[49] S. D. McCann, S. S. Stahl, *Acc. Chem. Res.* **2015**, *48*, 1756-1766.

[50] I. P. Beletskaya, A. V. Cheprakov, *Coord. Chem. Rev.* **2004**, *248*, 2337-2364.

[51] H. Rao, H. Fu, *Synlett* **2011**, *2011*, 745-769.

[52] A. De Meijere, F. Diederich, A. de Meijere, *Metal-catalyzed cross-coupling reactions, Vol. 1*, Wiley-VCH Weinheim, **2004**.

[53] F. Ullmann, J. Bielecki, *Berichte der deutschen chemischen Gesellschaft* **1901**, *34*, 2174-2185.

[54] H. Lin, D. Sun, *Org. Prep. Proced. Int.* **2013**, *45*, 341-394.

[55] I. Goldberg, *Berichte der deutschen chemischen Gesellschaft* **1906**, *39*, 1691-1692.

[56] W. R. H. Hurtley, *Journal of the Chemical Society (Resumed)* **1929**, 1870-1873.

[57] R.-P. Ye, L. Lin, Q. Li, Z. Zhou, T. Wang, C. K. Russell, H. Adidharma, Z. Xu, Y.-G. Yao, M. Fan, *Catalysis Science & Technology* **2018**, *8*, 3428-3449.

[58] S. Sá, H. Silva, L. Brandão, J. M. Sousa, A. Mendes, *Applied Catalysis B: Environmental* **2010**, *99*, 43-57.

[59] J. B. Hansen, P. E. Højlund Nielsen, in *Handbook of Heterogeneous Catalysis*, **2008**, pp. 2920-2949.

[60] S. Dang, H. Yang, P. Gao, H. Wang, X. Li, W. Wei, Y. Sun, *Catalysis Today* **2019**, *330*, 61-75.

[61] R. Guil-López, N. Mota, J. Llorente, E. Millán, B. Pawelec, J. L. G. Fierro, R. Navarro, *Materials* **2019**, *12*, 3902.

[62] W.-H. Cheng, *Methanol production and use*, CRC Press, **1994**.

[63] H. Adkins, B. Wojcik, L. W. Covert, *Journal of the American Chemical Society* **1933**, *55*, 1669-1676.

[64] H.-J. Alfort, *IST International Surface Technology* **2017**, *10*, 48-51.

[65] V. Pospelova, J. Aubrecht, O. Kikhtyanin, K. Pacultova, D. Kubicka, *Chemcatchem* **2019**, *11*, 2169-2178.

[66] M. B. Gawande, A. Goswami, F. X. Felpin, T. Asefa, X. X. Huang, R. Silva, X. X. Zou, R. Zboril, R. S. Varma, *Chemical Reviews* **2016**, *116*, 3722-3811.

[67] X. Yang, Q. Meng, G. Ding, Y. Wang, H. Chen, Y. lei Zhu, Y. W. Li, *Applied Catalysis A: General* **2018**, *561*, 78-86.

[68] X. Wang, M. Chen, X. Chen, R. Lin, H. Zhu, C. Huang, W. Yang, Y. Tan, S. Wang, Z. Du, *Journal of Catalysis* **2020**, *383*, 254-263.

[69] S. Valange, A. Derouault, S. Pronier, J. Barrault, Z. Gabelica, in *Stud. Surf. Sci. Catal., Vol. 158*, Elsevier, **2005**, pp. 1557-1564.

[70] V. Gutierrez, M. Alvarez, M. A. Volpe, *Applied Catalysis A: General* **2012**, *413*, 358-365.

[71] C. Dorfelt, M. Hammerton, D. Martin, A. Wellmann, C. C. Aletsee, M. Tromp, K. Kohler, *Journal of Catalysis* **2021**, *395*, 80-90.

[72] R. W. Wegman, D. R. Bryant, Google Patents, **1991**.

[73] Y. Kadono, Y. Hattori, M. Horio, F. Nakamura, Google Patents, **1998**.

[74] M. Paulus, F. Grossmann, O. Wegner, Google Patents, **2020**.

[75] P. Claus, Y. Önal, in *Handbook of Heterogeneous Catalysis*, **2008**, pp. 3308-3329.

[76] R. Watari, Y. Kayaki, *Asian Journal of Organic Chemistry* **2018**, *7*, 2005-2014.

[77] P. Gallezot, D. Richard, *Catalysis Reviews* **1998**, *40*, 81-126.

[78] D. Sokolskii, N. Anisimova, A. Zharmagambetova, S. Mukhamedzhanova, L. Edygenova, *Reaction Kinetics and Catalysis Letters* **1987**, *33*, 399-403.

[79] H. Arnold, F. Döbert, J. Gaube, in *Handbook of Heterogeneous Catalysis*, **2008**, pp. 3266-3284.

[80] F. Jiang, J. Cai, B. Liu, Y. Xu, X. Liu, *RSC Advances* **2016**, *6*, 75541-75551.

[81] B. C. Campo, M. A. Volpe, C. E. Gigola, *Ind. Eng. Chem. Res.* **2009**, *48*, 10234-10239.

[82] K. Christmann, G. Ertl, T. Pignet, *Surface Science* **1976**, *54*, 365-392.

[83] R. A. Beebe, G. W. Low, Jr., E. L. Wildner, S. Goldwasser, *J. Am. Chem. Soc.* **1935**, *57*, 2527-2532.

[84] C.-C. Chang, M.-S. Ku, *The Journal of Physical Chemistry C* **2021**, *125*, 10919-10925.

[85] R. Hubaut, J. P. Bonnelle, *Reaction Kinetics & Catalysis Letters* **1992**, *47*, 73-81.

[86] M. Holena, M. Baerns, in *Handbook of Heterogeneous Catalysis*, **2008**, pp. 66-81.

[87] M. I. Din, R. Rehan, *Analytical Letters* **2017**, *50*, 50-62.

[88] J. W. Geus, A. J. van Dillen, in *Handbook of Heterogeneous Catalysis*, **2008**, pp. 428-467.

[89] M. Behrens, D. Brennecke, F. Girgsdies, S. Kissner, A. Trunschke, N. Nasrudin, S. Zakaria, N. F. Idris, S. B. Abd Hamid, B. Kniep, R. Fischer, W. Busser, M. Muhler, R. Schlogl, *Appl Catal a-Gen* **2011**, *392*, 93-102.

[90] F. Schüth, M. Hesse, K. K. Unger, in *Handbook of Heterogeneous Catalysis*, **2008**, pp. 100-119.

[91] B. Delmon, in *Handbook of Heterogeneous Catalysis*, **2008**, pp. 655-676.

[92] C. Baltes, S. Vukojevic, F. Schuth, *Journal of Catalysis* **2008**, *258*, 334-344.

[93] J. L. Li, T. Inui, *Appl Catal a-Gen* **1996**, *137*, 105-117.

[94] P. Porta, S. Derossi, G. Ferraris, F. Pompa, *Solid State Ionics* **1991**, *45*, 35-41.

[95] S. Gusi, F. Trifiro, A. Vaccari, *React Solid* **1986**, *2*, 59-71.

[96] A. Tarasov, J. Schumann, F. Girgsdies, N. Thomas, M. Behrens, *Thermochimica Acta* **2014**, *591*, 1-9.

[97] H. Bahrmann, H. Bach, G. D. Frey, in *Ullmann's Encyclopedia of Industrial Chemistry*, **2013**.

[98] I. Wender, H. W. Sternberg, M. Orchin, *Journal of the American Chemical Society* **1953**, *75*, 3041-3042.

[99] D. Evans, J. Osborn, G. Wilkinson, *Journal of the Chemical Society A: Inorganic, Physical, Theoretical* **1968**, 3133-3142.

[100] T. Kégl, *RSC advances* **2015**, *5*, 4304-4327.

[101] J. Falbe, H. Bahrmann, W. Lipps, D. Mayer, G. D. Frey, in *Ullmann's Encyclopedia of Industrial Chemistry*, **2013**.

[102] D. K. Raff, in *Ullmann's Encyclopedia of Industrial Chemistry*, **2013**.

[103] P. Walters, D. F. Cadogan, C. J. Howick, in *Ullmann's Encyclopedia of Industrial Chemistry*, **2020**, pp. 1-27.

[104] H. Bahrmann, H.-D. Hahn, D. Mayer, G. D. Frey, in *Ullmann's Encyclopedia of Industrial Chemistry*, **2013**.

[105] J. Cropley, *Encyclopedia of Chemical Processing and Design: Volume 46-Pumps: Bypass to Reboilers* **1993**, 408.

[106] H. Noller, *Journal of Catalysis* **1984**, *85*, 25-30.

[107] M. Englisch, V. S. Ranade, J. A. Lercher, *Applied Catalysis A: General* **1997**, *163*, 111-122.

[108] A. N. Subbotin, B. S. Gudkov, N. V. Nekrasov, V. I. Yakerson, S. L. Kiperman, *Kinetics and Catalysis* **1988**, *29*, 984-988.

[109] Z. Wu, Y.-H. C. Chin, *Journal of Catalysis* **2021**, *394*, 429-443.

[110] T. Burger, F. Koschany, O. Thomys, K. Köhler, O. Hinrichsen, *Applied Catalysis A: General* **2018**, *558*, 44-54.

[111] T. Burger, H. M. S. Augenstein, F. Hnyk, M. Döblinger, K. Köhler, O. Hinrichsen, *ChemCatChem* **2020**, *12*, 649-662.

[112] M. Zhang, M. Wang, B. Xu, D. Ma, *Joule* **2019**, *3*, 2876-2883.

[113] C. De Bellefon, in *Principles and Methods for Accelerated Catalyst Design and Testing* (Eds.: E. G. Derouane, V. Parmon, F. Lemos, F. R. Ribeiro), Springer Netherlands, Dordrecht, **2002**, pp. 71-83.

[114] F. H. M. Dekker, A. Bliek, F. Kapteijn, J. A. Moulijn, *Chemical Engineering Science* **1995**, *50*, 3573-3580.

[115] H. A. Skinner, A. Snelson, *Transactions of the Faraday Society* **1960**, *56*, 1776-1783.

[116] K. B. Wiberg, L. S. Crocker, K. M. Morgan, *Journal of the American Chemical Society* **1991**, *113*, 3447-3450.

[117] A. M. P. Koskinen, A. O. Kataja, in *Organic Reactions*, **2015**, pp. 105-410.

[118] A. T. Nielsen, W. J. Houlihan, in *Organic Reactions*, **2011**, pp. 1-438.

[119] R. Kaur, B. Pal, *Appl Catal a-Gen* **2015**, *491*, 28-36.

[120] Y. Ahn, Y. Jeong, D. Lee, Y. Lee, *Acs Nano* **2015**, *9*, 3125-3133.

[121] S. S. Dang, H. Y. Yang, P. Gao, H. Wang, X. P. Li, W. Wei, Y. H. Sun, *Catalysis Today* **2019**, *330*, 61-75.

[122] S. Thongratkaew, C. Luadthong, S. Kiatphuengporn, P. Khemthong, P. Hirunsit, K. Faungnawakij, *Catalysis Today* **2021**, *367*, 177-188.

[123] R. P. Ye, L. Lin, Q. H. Li, Z. F. Zhou, T. T. Wang, C. K. Russell, H. Adidharma, Z. H. Xu, Y. G. Yao, M. H. Fan, *Catalysis Science & Technology* **2018**, *8*, 3428-3449.

[124] B. C. Ranu, R. Dey, T. Chatterjee, S. Ahammed, *Chemsuschem* **2012**, *5*, 22-44.

[125] S. E. Allen, R. R. Walvoord, R. Padilla-Salinas, M. C. Kozlowski, *Chemical Reviews* **2013**, *113*, 6234-6458.

[126] S. Adhikari, J. Y. Zhang, K. Unocic, E. C. Wegener, P. Kunal, D. J. Deka, T. Toops, S. S. Majumdar, T. R. Krause, D. X. Liu, Z. L. Li, *Acs Sustain Chem Eng* **2022**, *10*, 1664-1674.

[127] E. L. Rodrigues, A. J. Marchi, C. R. Apesteguia, J. M. C. Bueno, *Applied Catalysis A: General* **2005**, *294*, 197-207.

[128] V. Pospelova, J. Aubrecht, O. Kikhtyanin, D. Kubicka, *Appl Catal a-Gen* **2021**, *624*.

[129] D. Kopac, B. Likozar, M. Hus, *Acs Catalysis* **2020**, *10*, 4092-4102.

[130] J. Vassallo, E. Miro, J. Petunchi, *Appl Catal B-Environ* **1995**, *7*, 65-78.

[131] S. T. Yong, C. W. Ooi, S. P. Chai, X. S. Wu, *International Journal of Hydrogen Energy* **2013**, *38*, 9541-9552.

[132] R. V. Goncalves, R. Wojcieszak, H. Wender, C. S. B. Dias, L. L. R. Vono, D. Eberhardt, S. R. Teixeira, L. M. Rossi, *Acs Appl Mater Inter* **2015**, *7*, 7987-7994.

[133] R. Burch, S. E. Golunski, M. S. Spencer, *J Chem Soc Faraday T* **1990**, *86*, 2683-2691.

[134] T. Y. Yan, K. A. Fichthorn, *Journal of Physical Chemistry B* **2021**, *125*, 4178-4186.

[135] A. X. Guan, Z. Chen, Y. L. Quan, C. Peng, Z. Q. Wang, S. K. Sham, C. Yang, Y. L. Ji, L. P. Qian, X. Xu, G. F. Zheng, *Acs Energy Lett* **2020**, *5*, 1044-1053.

[136] A. Ghosh, R. W. Huang, B. Alamer, E. Abou-Hamad, M. N. Hedhili, O. F. Mohammed, O. M. Bakr, *Acs Mater Lett* **2019**, *1*, 297-302.

[137] C. Bertram, W. Fang, P. Pedevilla, A. Michaelides, K. Morgenstern, *Nano Letters* **2019**, *19*, 3049-3056.

[138] J. Singh, M. Rawat, *Journal of Bioelectronics and Nanotechnology* **2016**, *1*.

[139] A. Baiker, W. L. Holstein, *Journal of Catalysis* **1983**, *84*, 178-188.

[140] G. Behrendt, B. Mockenhaupt, N. Prinz, M. Zobel, E. J. Ras, M. Behrens, *Chemcatchem* **2022**, *14*.

[141] M. Behrens, R. Schlogl, *Zeitschrift Fur Anorganische Und Allgemeine Chemie* **2013**, *639*, 2683-2695.

[142] M. Behrens, F. Girgsdies, A. Trunschke, R. Schlogl, *European Journal of Inorganic Chemistry* **2009**, 1347-1357.

[143] L. L. Wang, W. Ding, Y. W. Liu, W. P. Fang, Y. Q. Yang, *J Nat Gas Chem* **2010**, *19*, 487-492.

[144] M. Hiller, K. Köhler, *Chemie Ingenieur Technik* **2022**, *94*, 1720-1726.

[145] J. Schumann, A. Tarasov, N. Thomas, R. Schlogl, M. Behrens, *Appl Catal a-Gen* **2016**, *516*, 117-126.

[146] E. L. Rodrigues, A. Marchi, C. R. Apesteguia, J. M. C. Bueno, *Appl Catal a-Gen* **2005**, *294*, 197-207.

[147] X. H. Yang, Q. W. Meng, G. Q. Ding, Y. Q. Wang, H. M. Chen, Y. L. Zhu, Y. W. Li, *Appl Catal a-Gen* **2018**, *561*, 78-86.

[148] S. Ghose, *Acta Crystallographica* **1964**, *17*, 1051-&.

[149] M. M. Harding, B. M. Kariuki, R. Cernik, G. Cressey, *Acta Crystallogr B* **1994**, *50*, 673-676.

[150] P. Susse, *Acta Crystallographica* **1967**, *22*, 146-&.

[151] R. L. Frost, M. C. Hales, B. J. Reddy, *Polyhedron* **2007**, *26*, 3291-3300.

[152] S. Jansen, M. Palmieri, M. Gomez, S. Lawrence, *Journal of Catalysis* **1996**, *163*, 262-270.

[153] K. Kihara, G. Donnay, *Canadian Mineralogist* **1985**, *23*, 647-654.

[154] J. Schumann, T. Lunkenbein, A. Tarasov, N. Thomas, R. Schlogl, M. Behrens, *Chemcatchem* **2014**, *6*, 2889-2897.

[155] G. Tunell, E. Posnjak, C. J. Ksanda, *Zeitschrift für Kristallographie - Crystalline Materials* **1935**, *90*, 120-142.

[156] A. L. Patterson, *Physical Review* **1939**, *56*, 978-982.

[157] D. D. Li, F. Xu, X. Tang, S. Dai, T. C. Pu, X. L. Liu, P. F. Tian, F. Z. Xuan, Z. Xu, I. E. Wachs, M. H. Zhu, *Nat Catal* **2022**, *5*, 99-108.

[158] K. Lejaeghere, V. Van Speybroeck, G. Van Oost, S. Cottenier, *Critical Reviews in Solid State and Materials Sciences* **2014**, *39*, 1-24.

[159] O. Hinrichsen, T. Genger, M. Muhler, *Chem Eng Technol* **2000**, *23*, 956-959.

[160] B. Bems, M. Schur, A. Dassenoy, H. Junkes, D. Herein, R. Schlogl, *Chem-Eur J* **2003**, *9*, 2039-2052.

[161] F. S. Stone, D. Waller, *Topics in Catalysis* **2003**, *22*, 305-318.

[162] D. Stoilova, V. Koleva, V. Vassileva, *Spectrochim Acta A* **2002**, *58*, 2051-2059.

[163] I. W. M. Brown, K. J. D. Mackenzie, G. J. Gainsford, *Thermochimica Acta* **1984**, *75*, 23-32.

[164] A. Sinhamahapatra, A. K. Giri, P. Pal, S. K. Pahari, H. C. Bajaj, A. B. Panda, *Journal of Materials Chemistry* **2012**, *22*, 17227-17235.

[165] B. J. Reddy, R. L. Frost, A. Locke, *Transition Metal Chemistry* **2008**, *33*, 331-339.

[166] G. Fierro, M. LoJacono, M. Inversi, P. Porta, F. Cioci, R. Lavecchia, *Appl Catal a-Gen* **1996**, *137*, 327-348.

[167] M. Boaro, M. Vicario, C. de Leitenburg, G. Dolcetti, A. Trovarelli, *Catalysis Today* **2003**, *77*, 407-417.

[168] S. Kuhl, A. Tarasov, S. Zander, I. Kasatkin, M. Behrens, *Chem-Eur J* **2014**, *20*, 3782-3792.

[169] D. Guse, S. Polierer, S. Wild, S. Pitter, M. Kind, *Chemie Ingenieur Technik* **2022**, *94*, 314-327.

[170] I. Schildermans, J. Mullens, B. J. Vanderveken, J. Yperman, D. Franco, L. C. Vanpoucke, *Thermochimica Acta* **1993**, *224*, 227-232.

[171] C. H. Yoder, E. Bushong, X. Liu, V. Weidner, P. McWilliams, K. Martin, J. Lorgunpai, J. Haller, R. W. Schaeffer, *Mineralogical Magazine* **2010**, *74*, 433-440.

[172] B. Bovio, S. Locchi, *J Cryst Spectrosc* **1982**, *12*, 507-517.

[173] C. J. G. Vandergrift, A. Mulder, J. W. Geus, *Appl Catal* **1990**, *60*, 181-192.

[174] S. J. Gentry, P. T. Walsh, *J Chem Soc Farad T 1* **1982**, *78*, 1515-1523.

[175] B. S. Gudkov, V. I. Yakerson, A. N. Subbotin, V. M. Kogan, *Mendeleev Communications* **1994**, 143-144.

[176] K. A. Ali, A. Z. Abdullah, A. R. Mohamed, *Renew Sust Energ Rev* **2015**, *44*, 508-518.

[177] R. Guil-Lopez, N. Mota, J. Llorente, E. Millan, B. Pawelec, J. L. G. Fierro, R. M. Navarro, *Materials* **2019**, *12*.

[178] G. Ertl, R. Hierl, H. Knözinger, N. Thiele, H. P. Urbach, *Applications of Surface Science* **1980**, *5*, 49-64.

[179] H. S. C. O'Neill, M. James, W. A. Dollase, S. A. T. Redfern, *European Journal of Mineralogy* **2005**, *17*, 581-586.

[180] H. S. Oneill, W. A. Dollase, *Physics and Chemistry of Minerals* **1994**, *20*, 541-555.

[181] V. Munoz, F. M. Z. Zotin, L. A. Palacio, *Catalysis Today* **2015**, *250*, 173-179.

[182] F. Marino, G. Baronetti, M. Jobbagy, M. Laborde, *Appl Catal a-Gen* **2003**, *238*, 41-54.

[183] D. L. Li, Y. Y. Fan, Y. Y. Ding, X. F. Wei, Y. H. Xiao, *Catalysis Communications* **2017**, *88*, 60-63.

[184] L. Smrcok, V. Langer, J. Krestan, *Acta Crystallogr C* **2006**, *62*, I83-I84.

[185] M. Chase, American Institute of Physics, -1, **1998**.

[186] L. M. Plyasova, T. M. Yur'eva, I. Y. Molina, T. A. Kriger, A. M. Balagurov, L. P. Davydova, V. I. Zaikovskii, G. N. Kustova, V. V. Malakhov, L. S. Dovlitova, *Kinetics and Catalysis* **2000**, *41*, 429-436.

[187] W. Preis, H. Gamsjager, *Journal of Chemical Thermodynamics* **2001**, *33*, 803-819.

[188] J. Yang, H.-Y. Zheng, Y.-L. Zhu, G.-W. Zhao, C.-H. Zhang, B.-T. Teng, H.-W. Xiang, Y. Li, *Catalysis Communications* **2004**, *5*, 505-510.

[189] F. Jiang, Y. Yang, L. Wang, Y. Li, Z. Fang, Y. Xu, B. Liu, X. Liu, *Catalysis Science & Technology* **2022**, *12*, 551-564.

[190] L. Nuñez, G. Pilcher, H. A. Skinner, *The Journal of Chemical Thermodynamics* **1969**, *1*, 31-43.

[191] M. J. Anderson, P. J. Whitcomb, *DOE simplified*, 3 ed., Apple Academic Press, Oakville, MO, **2015**.

[192] D. Marani, J. W. Patterson, P. R. Anderson, *Water Research* **1995**, *29*, 1317-1326.

[193] M. Cui, W.-K. Wong, W. Wisetsri, F. Mabrouk, I. Muda, Z. Li, M. Hassan, *Resources Policy* **2023**, *80*, 103133.

[194] Y. Zhang, H. chang, C. Saliba, A. Hasnaoui, *Resources Policy* **2022**, *78*, 102924.

[195] D. Teschner, Z. Révay, J. Borsodi, M. Hävecker, A. Knop-Gericke, R. Schlögl, D. Milroy, S. D. Jackson, D. Torres, P. Sautet, *Angewandte Chemie International Edition* **2008**, *47*, 9274-9278.

[196] M. Behrens, F. Studt, I. Kasatkin, S. Kuhl, M. Havecker, F. Abild-Pedersen, S. Zander, F. Girgsdies, P. Kurr, B. L. Kniep, M. Tovar, R. W. Fischer, J. K. Norskov, R. Schlogl, *Science* **2012**, *336*, 893-897.

[197] R. van den Berg, G. Prieto, G. Korpershoek, L. I. van der Wal, A. J. van Bunningen, S. Laegsgaard-Jorgensen, P. E. de Jongh, K. P. de Jong, *Nat Commun* **2016**, *7*, 13057.

[198] W. R. A. M. Robinson, J. C. Mol, *Appl Catal* **1988**, *44*, 165-177.

[199] V. Pospelova, J. Aubrecht, D. Kubicka, in *6th International Conference on Chemical Technology (ICCT)*, Czech Soc Industrial Chemistry, Mikulov, CZECH REPUBLIC, **2018**, pp. 348-352.

[200] K. T. V. Rao, Y. L. Hu, Z. S. Yuan, Y. S. Zhang, C. B. C. Xu, *Appl Catal a-Gen* **2021**, *609*, 12.

[201] M. N. Barroso, M. F. Gomez, L. A. Arrúa, M. C. Abello, *Catalysis Letters* **2006**, *109*, 13-19.

[202] B. K. Kwak, D. S. Park, Y. S. Yun, J. Yi, *Catalysis Communications* **2012**, *24*, 90-95.

[203] H. Adkins, P. P. Perkins, *Journal of the American Chemical Society* **1925**, *47*, 1163-1167.

[204] D. Damodara, R. Arundhathi, P. R. Likhar, *Advanced Synthesis & Catalysis* **2014**, *356*, 189-198.

[205] in *Comprehensive Organic Name Reactions and Reagents*, **2010**, pp. 21-24.

[206] L. Patron, V. Pocol, O. Carp, E. Modrogan, M. Brezeanu, *Materials Research Bulletin* **2001**, *36*, 1269-1276.

[207] V. Patrick, G. Gavalas, *J. Am. Ceram. Soc.* **1990**, *73*, 358-369.

[208] N. Kanjanasoontorn, T. Permsirivanich, T. Numpilai, T. Witoon, N. Chanlek, M. Niamlaem, C. Warakulwit, J. Limtrakul, *Catalysis Letters* **2016**, *146*, 1943-1955.

[209] D. W. Susnitzky, C. B. Carter, *Journal of Materials Research* **2011**, *6*, 1958-1963.

[210] R. Tsurumi, S. Shiraishi, Y. Ando, M. Yanagida, K. Takeda, *Journal of the Japanese Society for Food Science and Technology (Japan)* **2001**.

[211] W. R. d. S. Trindade, R. G. d. Santos, *Renewable and Sustainable Energy Reviews* **2017**, *69*, 642-651.

[212] S. M. N. Rahaju, I. Veza, N. Tamaldin, A. Sule, A. C. Opia, M. B. Abdulrahman, D. W. Djamari, *Automotive Experiences* **2022**, *5*, 251-260.

[213] J. Ladebeck, T. Regula, *Catalysis of Organic Reactions* **2000**, 403.

[214] L. Jalowiecki, *Journal of Catalysis* **1987**, *107*, 375-392.

[215] C. Dörfelt, Technische Universität München **2018**.

[216] R. Bechara, A. Aboukaïs, J.-P. Bonnelle, *Journal of the Chemical Society, Faraday Transactions* **1993**, *89*, 1257-1262.

[217] T. M. Yurieva, *Catalysis Today* **1999**, *51*, 457-467.

[218] I. I. Simentsova, A. V. Khasin, T. M. Yurieva, *Reaction Kinetics and Catalysis Letters* **1996**, *58*, 49-56.

[219] J. A. Rodriguez, J. Y. Kim, J. C. Hanson, M. Pérez, A. I. Frenkel, *Catalysis Letters* **2003**, *85*, 247-254.

[220] G. Fierro, M. Lo Jacono, M. Inversi, P. Porta, F. Cioci, R. Lavecchia, *Applied Catalysis A: General* **1996**, *137*, 327-348.

[221] O. D. Thomys, Technische Universität München **2015**.

[222] I. Jüngling, Technische Universität München **2022**.

[223] M. Levan, G. Perinet, P. Bianco, *Bulletin De La Societe Chimique De France* **1966**, 3104-&.

[224] S. Cannizzaro, *Justus Liebigs Annalen der Chemie* **1853**, *88*, 129-130.

[225] T. Bruhm, Technische Universität München **2021**.

[226] J. Nakamura, Y. Choi, T. Fujitani, *Topics in Catalysis* **2003**, *22*, 277-285.

[227] T. A. Krieger, L. M. Plyasova, L. P. Solovyeva, T. M. Yur'eva, O. V. Makarova, *Materials Science Forum* **1996**, *228-231*, 627-632.

[228] T. M. Yurieva, L. M. Plyasova, O. V. Makarova, T. A. Krieger, *Journal of Molecular Catalysis A: Chemical* **1996**, *113*, 455-468.

[229] R. Hubaut, J. P. Bonnelle, *Reaction Kinetics and Catalysis Letters* **1992**, *47*, 73-81.

[230] R. Gilson, M. C. Durrant, *Dalton Transactions* **2009**, 10223-10230.

[231] (Ed.: A. F. Holleman), De Gruyter, **2017**, pp. 1216-1428.

[232] D. A. M. Monti, A. Baiker, *Journal of Catalysis* **1983**, *83*, 323-335.

8

Appendix

8.1 List of publications

- Hiller, M.; Köhler, K., Copper-Zinc Oxide Catalysts for Aldehyde Hydrogenation by Direct Reductive Activation of Precursors. Chemie Ingenieur Technik **2022**, 94, 1720-1726.

8.2 Conference contributions

- Room Temperature Reactivity of Nitrous Oxide with Cerium Oxides Catalyzed by Transition Metals
  Max Hiller, Klaus Köhler
  - 53. Jahrestreffen Deutscher Katalytiker, Germany, 11 – 13 March 2020, transferred to online, Poster
  - 54. Jahrestreffen Deutscher Katalytiker, Germany, 16 – 19 March 2021, transferred to online, Poster

- Influence of activation conditions and precursor phase on copper zinc oxide catalysts for gas phase hydrogenation of aldehydes
  Max Hiller, Klaus Köhler
  - 55. Jahrestreffen Deutscher Katalytiker, Weimar, Germany, 27 – 29 June 2022, Poster

- Characterization of spent copper oxide and spinel catalysts used in butanal hydrogenation
  Max Hiller, Klaus Köhler
  - 56. Jahrestreffen Deutscher Katalytiker, Weimar, Germany, 15 – 17 March 2023, Poster